Chemistry Climate Model Simulations of Polar Stratospheric Ozone

by

Matthias Brakebusch

M.Sc., Leibniz Universität Hannover, 2007

M.Sc., University of Colorado at Boulder, 2011

A thesis submitted to the

Faculty of the Graduate School of the

University of Colorado in partial fulfillment

of the requirements for the degree of

Doctor of Philosophy

Department of Atmospheric and Oceanic Sciences

2013

This thesis entitled:
Chemistry Climate Model Simulations of Polar Stratospheric Ozone
written by Matthias Brakebusch
has been approved for the Department of Atmospheric and Oceanic Sciences

Prof. Cora E. Randall

Dr. V. Lynn Harvey

Date

The final copy of this thesis has been examined by the signatories, and we find that both the content and the form meet acceptable presentation standards of scholarly work in the above mentioned discipline.

Brakebusch, Matthias (Ph.D., Atmospheric Science)

Chemistry Climate Model Simulations of Polar Stratospheric Ozone

Thesis directed by Prof. Cora E. Randall

Stratospheric ozone (O_3) plays a crucial role in protecting organisms on Earth from lethal shortwave solar radiation. Because it is radiatively active, O_3 also determines the temperature structure of the stratosphere, so its distribution affects the circulation. For these reasons, understanding polar stratospheric O_3 has been a high priority of the scientific community for decades. Of primary interest in recent years is explaining and predicting variations in O_3 in a changing climate. Stratospheric O_3 distributions are affected by both chemistry and transport, which in turn are controlled by temperature, circulation, and dynamics. Hence, investigations of polar stratospheric O_3 require the separation of these intertwined processes, and an understanding of the relevant feedbacks. Investigations of these processes require global observations as well as coupled chemistry climate model simulations. This thesis focuses on chemical O_3 loss due to halogen and odd nitrogen (NO_X) catalytic cycles, and utilizes satellite measurements from several instruments and the Specified Dynamics Whole Atmosphere Community Climate Model (SD-WACCM).

The science questions are: (1) Is SD-WACCM a tool sophisticated enough for quantitative O_3 evolution investigations? (2) How much O_3 loss can be accurately attributed to the stratospheric O_3 loss processes induced by halogens, energetic particle precipitation, and NO_X individually? (3) Why is the observed O_3 in the Arctic 2010/2011 winter exceptionally low, despite high dynamical variability, which is usually associated with less O_3 loss?

The questions are addressed by: (1) iteratively evaluating and improving SD-WACCM simulations of the Arctic 2004/2005 winter through comparisons with satellite observations; (2) comparing multiple experimental SD-WACCM simulations of the Antarctic 2005 winter omitting individual O_3 loss processes to a reference simulation; (3) testing a hypothesis by means of a comprehensive model simulation of the Arctic 2010/11 winter season.

Conclusions of this thesis are: (1) SD-WACCM is a useful tool to quantify polar stratospheric O_3 evolution after including several model improvements; (2) 74% of total column O_3 loss can be attributed robustly to halogen chemistry preceded by heterogeneous chemistry; (3) severe O_3 loss in Arctic 2010/11 results in part from enhanced chlorine activation due to the high dynamical variability.

The work of this thesis improved SD-WACCM and adds an unprecedented evaluation regarding O_3 variability and O_3 loss in the stratosphere. Exact quantification of individual O_3 loss processes became possible even for extreme seasons. Hence this thesis enables analyses of polar stratospheric winter seasons on a level of detail that was not possible before.

Acknowledgements

I gratefully acknowledge my advisor Cora Randall. In addition to financial support, she made this thesis possible through numerous meetings, discussions, suggestions, language corrections, and personal advice. Many thanks also go to my committee members, who were always available for discussions and suggestions. In particular I thank Doug Kinnison who took me on the long and winding road through the modeling world. From a distance, Michelle Santee and Gloria Manney were a tremendous help with their invaluable feedback on my work.

Everyone in the middle atmosphere group was available for discussions, chat, and coffee which made the work on my PhD project quite a bit more interactive. I thank Bodil Karlsson in particular for bringing a new perspective into my view and planting a seed called Stockholm. I especially have to express my gratitude to Laura Holt as a group member but mostly as a friend and for sharing thoughts on many levels.

For clearing my mind in my spare time I'd like to thank Sam Stevenson and Steve Davis, especially for dragging me along into the beauty of Colorado. For reminding me of the Gemütlichkeit "back home" and being wonderful friends I'm grateful to Simone Stahringer and Jochen Wendel. Although far away, thank you to Benjamin Ruprecht who is always there for listening, thinking along, second opinions, and whole new insights.

I'm grateful for my understanding and loving family who all of a sudden saw me around Christmas time only. Above all I express my gratitude to my partner Susanne Benze who was always on my side during the sunniest and darkest moments of this entire journey; and who taught me to always look forward to our next joint chapter.

Contents

Chapter

Tables

Table

Figures

Figure

Chapter 1

Introduction

Polar stratospheric ozone (O_3) research is a complex and highly interesting subject. Its significance is based on O_3's role to protect organisms on Earth from lethal solar radiation. At the same time O_3 is a radiatively active gas that controls the temperature structure of the stratosphere. While remarkable advances in the understanding of polar stratospheric O_3 were made during the last decades, the projection of future O_3 remains challenging [*Charlton-Perez et al.*, 2010; *SPARC CCMVal*, 2010; *WMO*, 2011a]. The difficulties in simulating polar stratospheric O_3 are identified as numerous feedback processes in which O_3 directly or indirectly participates. In order to improve capabilities to simulate O_3, in-depth model evaluations are required. The subsequent quantification of individual feedback processes then enables their evaluation. Only if O_3, related species, and all feedback processes are implemented correctly, the projection of future O_3 gains robustness.

In this thesis, the performance of Community Earth System Model (CESM)/Whole Atmosphere Community Climate Model (WACCM), a representative state-of-the-art chemistry climate model (CCM), is evaluated and improved with respect to O_3 and related processes. In this chapter, the significance of this topic is described in detail and unanswered questions are summarized. Chapter 2 gives an overview of the most important dynamical and chemical processes affecting ozone. At the end of Chapter 2, science questions addressed in this thesis are posed. In Chapter 3, Chapter 4, and Chapter 5 the results necessary to answer these science questions are presented. Chapter 6 formulates conclusions and identifies the contribution of this thesis to science. Future

plans are described in an outlook at the end of Chapter 6.

Significance The Sun is the most important energy source for the Earth's atmosphere. Most of this energy is transported through space by electromagnetic radiation with a spectrum close to a Planck distribution corresponding to the solar temperature [1] . In the Earth's atmosphere this radiation is absorbed, reflected, and scattered by atmospheric gases and aerosols. Absorption of electromagnetic radiation can lead to ionization and photodissociation, depending on the wavelength of the radiation and the absorbing molecule. These processes cause particular wavelengths to be extinguished before they reach the Earth's surface.

Of the wavelengths reaching the Earth's surface, the most harmful ones for life on Earth are in the ultra violet (UV) regime and shorter since photons of that energy level can dissociate organic molecules. For example, plants show inhibited growth, exposed human skin exhibits an erythemal response [*Leaf*, 1993], and deoxyribonucleic acid (DNA) is dissociated. Reparation functions in the skin can produce recombination errors in the DNA molecule which can result in skin cancer [*Abarca and Casiccia*, 2002; *van Dijk et al.*, 2013]. Organisms on the Earth's surface and in the troposphere are largely protected from this high energy radiation since molecular nitrogen (N_2), molecular oxygen (O_2), and O_3 are strong absorbers in the UV and shorter wavelength regime. While the abundance of N_2 and O_2 throughout the atmosphere by far exceeds densities necessary to prevent most of the harmful part of the solar radiation to reach the Earth's surface (see Chapter 2), the attenuation of UV wavelengths by O_3 (see Figure 1.1) is more variable. This makes O_3 one of the most crucial atmospheric constituents for life on Earth. As an example, a 10% decrease in the ozone column leads to an increase in DNA-damaging radiation at the surface of 22% [*Newman*, 2010].

[1] The temperature referred to here is the temperature of the Sun's photosphere which is around 5800 K.

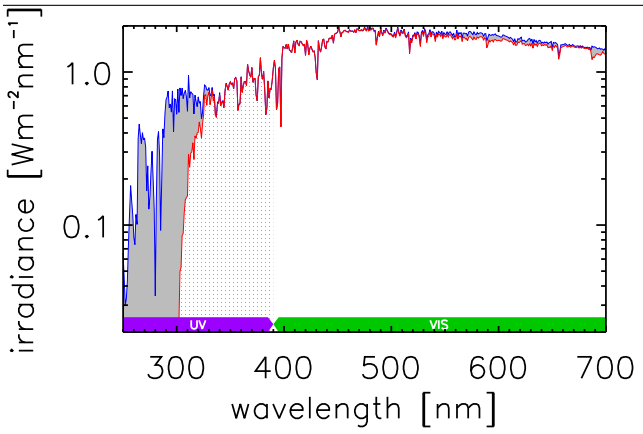

Figure 1.1: Solar spectral irradiance at the top of the Earth's atmosphere (blue) and the Earth's surface (red). The absorbed shortwave part of UV irradiance (solid gray) and the transmitted longwave part of the UV irradiance (dotted gray). Data provided by Sebastian Schmidt using libradtran/uvspec for a cloud and aerosol free atmosphere with low surface albedo.

At the same time, because O_3 is a radiatively active gas, the O_3 abundance determines the temperature structure in the stratosphere and mesosphere. O_3 absorbs solar radiation as well as longwave radiation emitted by the warm Earth surface and atmosphere, leading to heating. It also emits longwave radiation, which under some conditions leads to cooling. The temperature changes can influence atmospheric dynamics and temperature-sensitive chemistry. Recovery of the ozone layer thus changes the temperature structure in the stratosphere, which feeds back on dynamics. This feedback is particularly important when O_3 variability and long-term O_3 recovery are investigated.

Unanswered Questions The Scientific Assessment of Ozone Depletion is compiled by the World Meteorological Organization (WMO) in intervals of about four years; each assessment summarizes recent advances in atmospheric O_3 research. These reports also indicate which O_3 related processes lack understanding. There are other reports about research relevant to O_3 variability, e.g., the Intergovernmental Panel on Climate Change (IPCC) assessment reports. Atmospheric model development and evaluation is addressed in separate reports, e.g., the Stratospheric Processes And Their Role in Climate (SPARC) Chemistry-Climate Model Validation (CCMVal), now Chemistry-Climate Model Initiative (CCMI). Identified areas that require further research regarding O_3 can be subdivided into three fields:

(1) Monitoring O_3

After the identification of chlorofluorocarbons (CFCs) as the culprit of massive O_3 destruc-

tion, the emission of CFCs and subsequent replacements were regulated by the Montreal Protocol in 1987 and subsequent amendments. Questions of whether the regulations from the Montreal Protocol and its amendments are effective [*van Dijk et al.*, 2013, e.g.,] and are being realized remain valid and require the close monitoring of interannual O_3 variations.[2] Diagnostic model simulations can evaluate our current understanding of past O_3 loss seasons.

(2) Influence of climate change on O_3

Estimating the long-term evolution of O_3 requires consideration of climate change in addition to the decreasing anthropogenic chlorine (Cl) loading of the stratosphere. Climate change in the stratosphere is largely due to cooling by anthropogenic carbon dioxide (CO_2) [*Clough and Iacono*, 1995], which substantially affects dynamics, chemistry and microphysics. The diagnosis of climate effects is complicated by the long time scale needed to detect even small trends in, e.g., temperature, compared to the length of available observational records. Here models including the whole atmosphere can be used to compensate for the insufficient observational records.

(3) Feedback of O_3 recovery on climate

O_3, CFCs, and CFC-replacements are radiatively active gases and thus contribute to climate change. While O_3 recovery mitigates CO_2-induced cooling of the stratosphere by increased absorption of solar shortwave radiation, O_3 acts like other greenhouse gases (GHGs) in the longwave regime. Decreases in stratospheric temperatures result in increases in the large-scale atmospheric circulation, which masks chemical O_3 loss [*WMO*, 2011a]. At the same time the radiative forcing effects of the long-term reductions in CFCs and CFC-replacements compensate for a small part of the CO_2-induced cooling [*WMO*, 2011b]. As for the previous point, model simulations can support observations by adding temporal and spatial coverage of the temperature and GHG distributions.

[2] One example of the ongoing monitoring effort is National Aeronautics and Space Administration (NASA)'s Ozone hole watch at the Goddard Space Flight center

All of these three fields benefit strongly from the application of state of the art Earth System Models (ESMs). Models represent our current understanding of atmospheric processes as well as our ability to implement our understanding correctly. For instance, the big picture of processes affecting stratospheric O_3, explained in Chapter 2, is at least qualitatively understood [*WMO*, 2011a]. The quantitative diagnosis, however, requires a precise implementation of the processes involving O_3 and related species. The most significant driver behind this requirement is that climate change occurs gradually, and thus investigations require long time series with high accuracy to draw robust conclusions. Current model evaluation efforts (e.g., SPARC CCMI) indicate that comparisons of stratospheric O_3 simulations still show a range of results from different models [*SPARC CCMVal* [2010], Figure 6.36; *Charlton-Perez et al.* [2010]], complicating long-term trend analyses. WMO suggests that interactions between the middle atmosphere and the ocean are a possible source of the variability in the results, but these interactions are currently not realized in atmospheric models. The ultimate goal of further model development is the improvement of prognostic capabilities. In order to gain the necessary robustness for prognostic simulations, hindcast capabilities based on diagnostic simulations have to be improved first.

This chapter motivates the tasks *model evaluation* and subsequent *model improvements* using diagnostic simulations. These tasks describe the first central part of this thesis. The impact of individual processes is quantified which is the second central part of this work. Both parts are tested for robustness by an additional case study.

Chapter 2

Polar Stratospheric Ozone

Contents

O_3 is a molecule consisting of three oxygen atoms. The average bond order in the molecule is 1.5, which makes the O_3 molecule very reactive as an oxidant. O_3 has spectral absorption features in the UV (Hartley band at 200 nm - 300 nm and Huggins band at 310 nm - 350 nm), visible (VIS) (Chappuis band at 410 nm - 750 nm), and near infrared (NIR) ($\approx 9.5\,\mu$m) (see Figure 2.1). In the atmosphere O_3 appears as a trace gas with a total abundance of 7×10^{-6} % and highest concentra-

tions in the lower stratosphere of $\approx 60 \times 10^9\,\mathrm{cm}^3$ ($\approx 5\,\mathrm{ppmv}$).

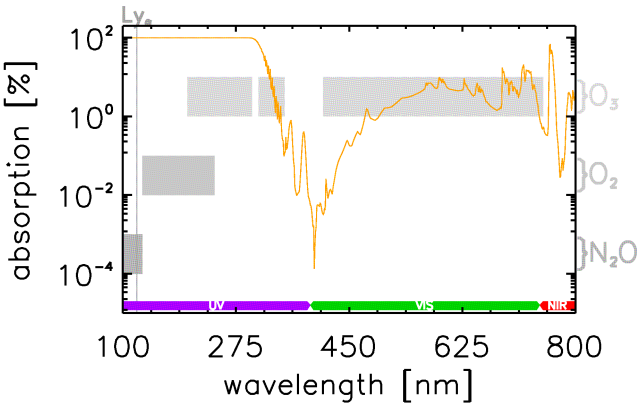

Figure 2.1: Relative absorption of solar spectral irradiance between top of the Earth's atmosphere and Earth's surface. Absorption bands of O_3, O_2, and N_2 are depicted by gray bars. The Lyman-α line is shown for reference. Wavelengths shorter than 100 nm cause ionization of dominant atmospheric constituents and are thus fully absorbed in the upper atmosphere. Data provided by Sebastian Schmidt using libradtran/uvspec for a cloud and aerosol free atmosphere with low surface albedo.

Due to these characteristics, O_3 fulfills different roles in the atmosphere. In the lower troposphere O_3 is a pollutant indirectly generated by combustion of fossil fuels. Due to its oxidizing capability tropospheric O_3 causes respiratory and plant damage. In the mid troposphere O_3 cleans air of pollutants, again due to its oxidizing capability. In the upper troposphere O_3 absorbs longwave radiation (heat) and emits some longwave radiation downward towards the Earth's surface, thus acting as a GHG. In the stratosphere, O_3 absorbs solar shortwave radiation, altering the solar spectrum in the UV region that reaches the Earth's surface; this is also the main process that controls stratospheric lapse rates in sunlit conditions.

O_3 is produced by UV photolysis of O_2 (more details in Section 2.2), which attenuates solar UV radiation penetrating the Earth's atmosphere. Based only on this attenuation, O_3 concentration would be expected to increase with increasing altitude. Atmospheric O_2 density, however, decreases with altitude. These two parts complement each other and create a maximum in O_3 concentration in the lower stratosphere (see dashed line in Figure 2.2).

In order to change the O_3 abundance in the atmosphere, O_3 either has to be (1) transported towards or from the area of interest or (2) created or destroyed. This fundamental statement is

described by the continuity equation:

$$\frac{d[O_3]}{dt} = \underbrace{\frac{\partial[O_3]}{\partial t} + \mathbf{v}\cdot\nabla[O_3]}_{(1)} + \underbrace{S}_{(2)} \tag{2.1}$$

where $[O_3]$ is the concentration of O_3, $\mathbf{v}$ is the wind vector, and S represents chemical sources and sinks of O_3. The first two terms on the right (1) represent the transport of O_3, which is controlled by atmospheric dynamics (see Section 2.1). The third term on the right (2) represents the creation or destruction of O_3 (source/sink), which is controlled by atmospheric chemistry (see Section 2.2). When investigating and quantifying O_3 loss the distinction between these two contributors to O_3 change is crucial since they can mimic or mask each other. At the same time, observations of O_3 can only provide the total change in O_3 with time, e.g., comparing the two curves in Figure 2.2. The distinction between dynamics and chemistry requires either observations that are taken by in-situ Lagrangian instruments (e.g., balloons) or meteorological observations of transport parameters (e.g., winds). This challenge must be addressed by any study investigating atmospheric O_3 loss; the approach taken here is explained in Chapter 3 [*Brakebusch et al.*, 2013].

The dramatic decrease of the O_3 layer shown in Figure 2.2 is known as the O_3 hole and occurs during spring time in the polar regions. The O_3 hole is defined as the area in which the total column abundance of O_3 is less than 220 Dobson Units (DU). In order to understand the formation, evolution, hemispheric differences, interannual variability, and impact of severe O_3 loss events, all involved processes must be explained. As described before, these processes can be categorized as dynamical and chemical processes. In the next two sections the relevant polar stratospheric dynamical mechanisms are characterized, followed by a description of the most important polar stratospheric chemical processes. This chapter then concludes with a compilation of requirements for investigating polar stratospheric O_3 and, based on that, develops remaining science questions that are answered in the subsequent chapters.

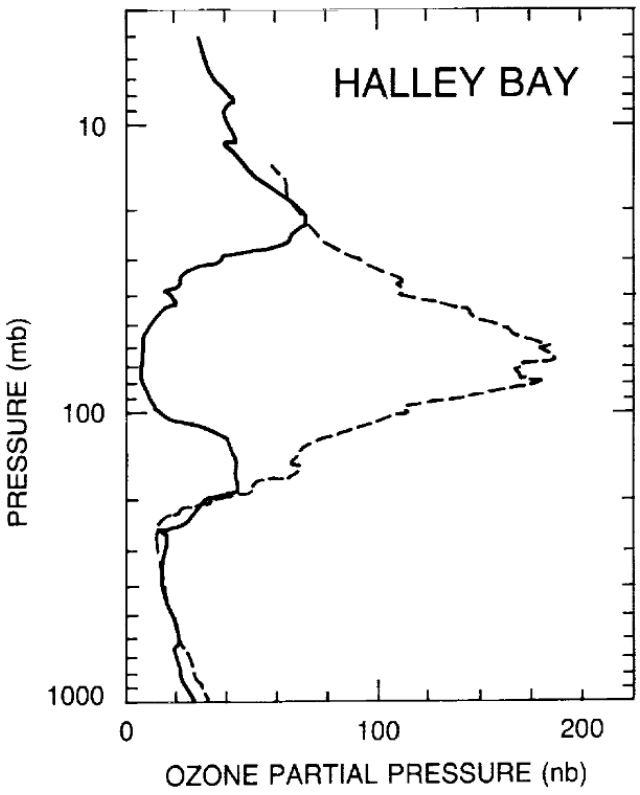

Figure 2.2: "Vertical distribution of the ozone partial pressure (nbar) observed at Halley Bay Station on August 15, 1987 (high values), and October 15, 1987 (low values), respectively. (Farman, personal communication, 1987)".[1]

2.1 Polar Stratospheric Dynamics

As described in Chapter 2, O_3 abundances are in part controlled by transport. Thus atmospheric dynamics are essential to explain the distribution of O_3. In the following paragraphs the main dynamical features affecting O_3 in the winter polar region, the Brewer Dobson circulation (BDC) and the polar vortex, are described; the section concludes with an explanation of hemispheric differences.

2.1.1 Brewer Dobson Circulation

Strongest O_3 production occurs in the equatorial stratosphere due to maximized solar insolation, while highest O_3 abundances are observed in the polar lower stratosphere [*WMO*, 2003]. This

[1] Reproduced from WMO (World Meteorological Organization) (1990), Report of the International Ozone Trends Panel: 1988, Global Ozone Research and Monitoring Project, Report No. 18.

apparent contradiction was first explained by *Brewer* [1949] and *Dobson* [1956], who proposed a tropical convective motion into the stratosphere followed by advection towards the winter pole and subsequent adiabatic descent at high latitudes. This circulation pattern is known as the BDC. The meridional gradient in solar insolation caused by the difference in mean solar zenith angle (SZA) between the equator and the winter polar region results in a meridional temperature gradient near the Earth's surface and thus a meridional pressure gradient. This pressure gradient creates a meridional tropospheric wind that is deflected by the Coriolis force. Once geostrophic balance is established, this wind is purely westerly at about mid-latitudes. Flow over large topographic features stretches and compresses the vertical extent of the flow (a thermal forcing due to land-sea contrast is also possible). In order to preserve potential vorticity (PV) this deformation is balanced by a change in relative vorticity, which results in a horizontally oscillating planetary wave (PW) also called a Rossby wave. *Charney and Drazin* [1961] showed that PWs have an easterly phase velocity and that they can propagate upward only if the background mean wind speed is westerly. While on average this background mean wind in the troposphere is westerly the entire year, the stratospheric mean winds change direction semiannually [*Reed*, 1966]. In the stratosphere the summer pole is heated due to solar UV absorption by O_3 while the winter pole is radiatively cooled, resulting in a temperature gradient spanning both hemispheres. Thus the geostrophic balance creates an easterly flow in the stratospheric summer hemisphere and a westerly flow in the stratospheric winter hemisphere, called the stratospheric polar night jet (PNJ). Thus PWs cannot propagate into the stratosphere in the summer hemisphere. *Charney and Drazin* [1961] also showed that even if the stratospheric winds are westerly, the phase speed of the PW must not exceed a critical value in order to allow upward propagation. This critical wind speed depends on the wavelength of the PW, effectively filtering higher wavenumbers. In fact only PWs with wavenumbers 1-3 are observed in the stratosphere. A stable PW is only maintained when non-linear components can be neglected. Since the amplitude of PWs increases with altitude, non-linear effects[2] increase in magnitude as

[2] Conservation of PV is given when the wave motion can be described with the quasi-geostrophic PV equation which is a linearized equation [*Holton*, 2004]. When PV is conserved, any deformation of material contours is reversible. If the amplitude becomes larger, non-linear terms are not negligible anymore and the flow cannot be approximated

well and the PW becomes unstable [*Holton*, 2004]. When the PW breaks its easterly phase speed results in an easterly momentum deposition, which slows or even reverses the zonal mean flow. Since the meridional component of the Coriolis force is proportional to the zonal wind speed, a poleward motion is induced when the geostrophic balance is reestablished. The breaking of PWs thus results in a net poleward movement, which is the driver of the BDC. This convergence of air masses in the polar region causes downward transport to preserve mass continuity. Downward motion then subsequently leads to adiabatic compression, thereby heating the winter stratosphere to temperatures above the radiative equilibrium temperature calculated by diabatic radiative cooling alone.

2.1.2 Polar Vortex

The stratospheric PNJ forms a strong cyclone that is present in the stratosphere and sometimes extends into the mesosphere. This cyclone is commonly referred to as the polar vortex. The distinct feature of the polar vortex is that it represents a barrier to horizontal transport. It can be shown that under the assumption of horizontal transport being purely adiabatic and the PNJ being purely geostrophic that PV is conserved for air parcels in the PNJ and that the meridional gradient of PV is very steep across the PNJ [e.g., *Brasseur and Solomon*, 2005]. Thus PV is a restoring force for air parcels in the PNJ while it has a repulsive effect on air parcels with higher or lower PV. For practical purposes a PV threshold can be used to define the edge of the polar vortex. When the previously discussed PWs break due to the PNJ, they deposit westward angular momentum, which slows the zonal wind speed of the PNJ. In order to conserve PV of the flow, the PNJ is deformed and locally gains meridional wind components [e.g., *Shepherd*, 2000]. The net poleward motion described in Section 2.1.1 causes increased descent after breaking PWs due to mass conservation. This increased descent leads to adiabatic warming; such events are called sudden stratospheric warming (SSW)s [*Matsuno*, 1971]. These warmings are classified into three

with the quasi-geostrophic PV equation. In that case PV is not conserved which results into *ir*reversible deformation of material contours, also called wave-breaking.

categories: (1) minor warming[3] , (2) major warming[4] , and (3) final warming[5] [*McInturff*, 1978; *Andrews et al.*, 1987]. Observations show that the polar vortex is deformed and displaced from the pole when PWs with wavenumber 1 break and the vortex is split into two cyclones when PWs with wavenumber 2 break [*Shepherd*, 2000]. The disturbance of PV due to wave breaking is usually accompanied by horizontal mixing or intrusion and extrusion of filaments. If the PW-breaking is too strong for the weak late season westerly PNJ, the winds are permanently reversed until the next winter season and air masses inside and outside the polar vortex are not isolated from each other anymore. This PW-breaking event is called final warming. In addition to the large-scale PWs that oscillate in a horizontal plane due to the restoring Coriolis force, another type of wave exists that oscillates in a vertical plane due to gravity as the restoring force. Hence these waves are called gravity wave (GW)s. Similar to PWs, the initial creation of GWs can be due to tropospheric flow over topography; but other sharp boundaries such as convection or frontal processes give rise to GWs as well [*Fritts and Alexander*, 2003]. GWs can have phase speeds that are westward or eastward and their wavelength of 10 km - 1000 km is much shorter than that of PWs. Also they are more frequent but carry less energy than PWs. The polar, upward propagation of GWs is also affected by the PNJ, which filters GWs that have phase speeds that are slower than but in the same direction as the PNJ [*Andrews et al.*, 1987]. Deposition of angular momentum from filtered GWs into the PNJ is small compared to PW breaking and can cause not more than a small amount of mixing across the polar vortex edge. Aside from the filtering, the reason for GW-breaking is their growth in amplitude as they propagate vertically. At a critical level the amplitude becomes too large to be convectively stable; this usually occurs in the mesosphere. Breaking GWs in the mesosphere are connected to descent in the upper atmosphere [*Andrews et al.*, 1987] and thus become important for the stratosphere due to transport of, e.g., reactive nitrogen species generated in the upper atmosphere by energetic particle precipitation (EPP) (see Section 2.2.4).

[3] Minor warmings are defined as a reversal of the zonal mean temperature gradient without a reversal of the zonal mean zonal wind to easterly direction.

[4] Major warmings are defined as a zonal mean temperature increase at $\geq$10 hPa poleward from 60° latitude and reversal of the zonal mean zonal wind to easterly.

[5] The final warming is defined as a reversal of the mean zonal wind to easterly direction without recovery.

2.1.3 Hemispheric Differences (Dynamics)

Dynamics in both hemispheres differ significantly. The primary reason for this difference is the distribution of land mass and oceans, which results in a zonal asymmetry. In the northern hemisphere (NH) more large scale wave-creating features, e.g., the Rocky Mountains or the Tibetian Plateau, disturb the zonal mean flow. Thus more PW activity is observed in the NH, which causes more disturbances due to deposition of westward angular momentum. This results in a stronger BDC in the NH and a much more variable polar vortex compared to the southern hemisphere (SH). A stronger BDC entails warmer NH temperatures inside the polar vortex due to stronger down-welling transport and subsequent adiabatic heating (see Figure 2.3). The NH vortex is also warmer because the Arctic ocean surface cools less than the Antarctic continent surface. A more variable polar vortex often results in a shorter lifetime of winter conditions limited by the final warming in the NH while the semiannual wind reversal dissolves the polar vortex in the SH (except the unusual SH 2002 winter [e.g., *WMO*, 2003]). At the same time the SH polar vortex is much more symmetric and provides a stronger confinement of air inside the polar vortex. Disturbances of the SH polar vortex are sometimes attributed to GWs which are excited by, e.g., the Andes [*Fritts and Alexander*, 2003].

Although these differences look purely dynamical at first sight, implications for chemistry are huge. In the next section, the impact of hemispheric temperature differences on chemistry in the form of gas-phase reaction rates, heterogeneous chemistry reaction rates, formation of clouds, and removal of solidified species by sedimentation are described.

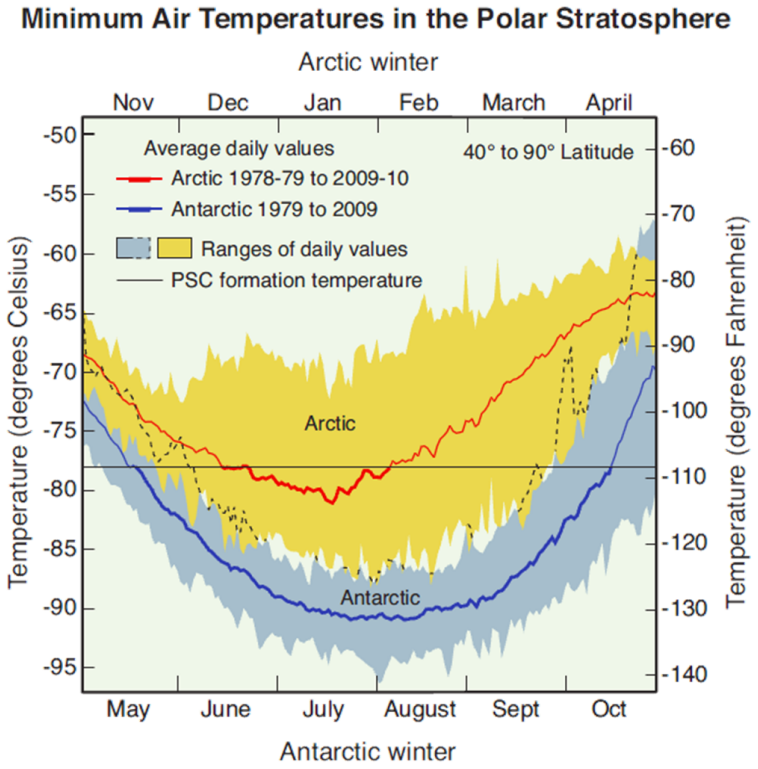

Figure 2.3: Evolution of minimum temperature in the polar stratosphere. While the Arctic temperatures are warmer, also the variability in the Arctic is larger than in the Antarctic.[6]

2.2 Polar Stratospheric Chemistry

Sources and sinks of O_3 in the Earth's atmosphere are determined by photochemistry (Section 2.2.1) and gas-phase chemistry (Section 2.2.2). The latter is in part preceded by heterogeneous chemistry (Section 2.2.3) that mostly occurs on polar stratospheric cloud (PSC) surfaces in low-temperature polar winter conditions. In this section, all of these types of chemistry are explained. EPP, which is a highly variable source of reactive nitrogen oxide (NO_X), is introduced as well (Section 2.2.4). This section concludes with the description of hemispheric differences in polar stratospheric chemistry (Section 2.2.5).

[6] Reproduced from WMO (World Meteorological Organization) (2011), Twenty Questions and Answers About the Ozone Layer: 2010 Update, D. W. Fahey and Hegglin, M. I. (Coordinating Lead Authors), Scientific Assessment of Ozone Depletion: 2010.

2.2.1 Photochemistry

The formation of O_3 is preceded by the photolysis of O_2, which forms atomic oxygen (O) (Reaction 2.2). In an exothermal three body reaction O and O_2 then combine to form O_3 (Reaction 2.3). Because fast photolysis of O_3 also forms O (Reaction 2.4), O and O_3 are interchanged rapidly. Also, O and O_3 can recombine (Reaction 2.5) to form O_2.

$$O_2 + h\nu \xrightarrow{J_{O_2}} O + O \qquad [\lambda \leq 242.4\,nm] \tag{2.2}$$

$$O + O_2 + M \xrightarrow{k_{O_2}} O_3 + M \qquad [\text{exothermal}] \tag{2.3}$$

$$O_3 + h\nu \xrightarrow{J_{O_3}} O_2 + O \qquad [200\,nm \leq \lambda \leq 350\,nm] \tag{2.4}$$

$$O + O_3 \xrightarrow{k_{O_3}} O_2 + O_2 \tag{2.5}$$

Here, the letters J and k are the reaction rate constants and M represents a third body necessary for momentum and energy deposition; thus M can be any atmospheric constituent. Stratospheric reactions requiring a third body depend highly on atmospheric density, making them more likely in the lower stratosphere. Because of the rapid interchange between O_3 and O, they are often treated together as the odd oxygen (O_X) family (Figure 2.4).

Note that Reaction 2.3 and Reaction 2.4 do not change the concentration of O_X ($[O_x]$) but have to be considered nevertheless since reaction Reaction 2.5 equally depends on O and O_3. Thus the source term in the continuity equation is given as

$$\frac{\partial[O_x]}{\partial t} = 2J_{O_2}[O_2] - \frac{2k_{O_3}J_{O_3}[O_3]^2}{k_{O_2}M[O_2]}. \tag{2.6}$$

The O_X chemistry described above was found by *Chapman* [1930] and it applies to a stationary atmosphere with oxygen-only chemistry. Global observations show, however, that column densities of equatorial O_3 are overestimated and O_3 in the polar region is underestimated, if only Chapman chemistry is considered (see Figure 2.5). Gas-phase catalytic chemistry as well as the BDC must be taken into account in order to describe the real O_3 distribution.

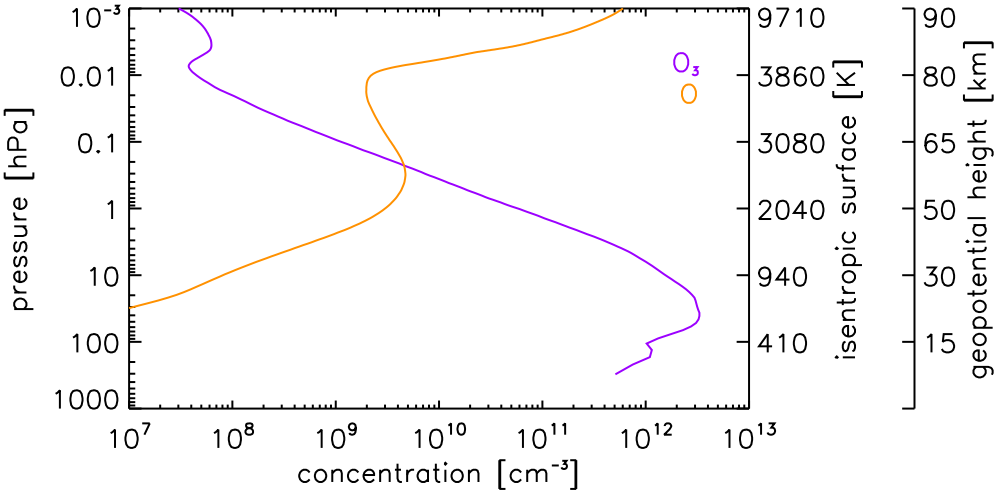

Figure 2.4: Modeled summer profiles of O_3 and O (Antarctic polar cap average on December 1). O_3 is the dominant O_X species in the stratosphere and below; above the stratopause, O becomes the dominant species due to the photochemically controlled upper atmosphere (see Section 2.3).

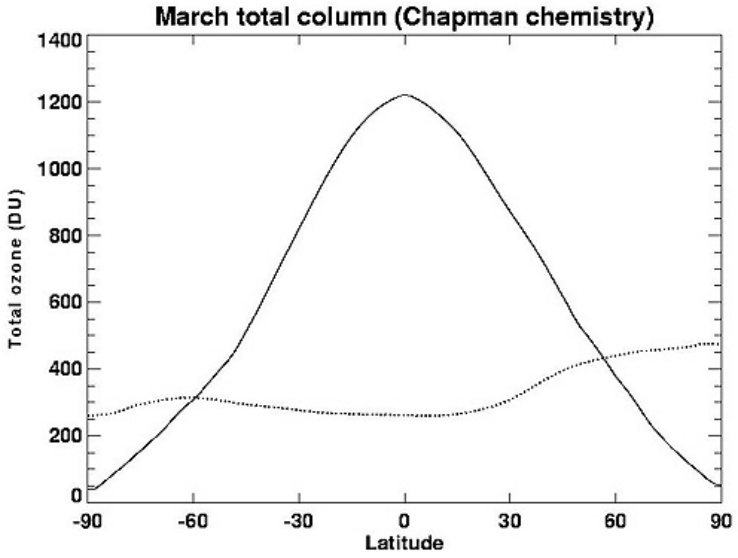

Figure 2.5: Chapman chemistry (solid) and Total Ozone Mapping Spectrometer (TOMS) observations (dotted) on March 21.[7]

[7] Reproduced with permission from Paul A. Newman. Newman, P. et al., Todaro, R. M. (Ed.) (2010), Stratospheric Ozone - An Electronic Textbook Goddard Space Flight Center Atmospheric Chemistry and Dynamics Branch

2.2.2 Gas-Phase Catalytic Chemistry

In addition to Chapman's pure-oxygen chemistry described above, the equilibrium amount of O_3 is controlled by catalytic reactions with a catalyst X according to the general scheme:

$$O_3 + X \longrightarrow XO + O_2 \tag{2.7}$$

$$XO + O \longrightarrow X + O_2 \tag{2.8}$$

$$\text{net} : O_3 + O \longrightarrow 2O_2. \tag{2.9}$$

Species that can most efficiently fulfill the role of catalyst X are hydroxyl radical (OH), nitrogen oxide (NO), and inorganic halogens. The following section summarizes gas-phase destruction of O_3 for these catalysts, their atmospheric abundance and relevance. The section will conclude with coupling reactions between catalysts.

Reactive Odd Hydrogen The O_3 chemistry related to odd hydrogen (HO_X), which consists of atomic hydrogen (H), OH, and peroxyl radical (HO_2), was first investigated by *Bates and Nicolet* [1950]. The dominant sources of polar HO_X in the middle and upper stratosphere are the oxidation of water vapor (H_2O) and methane (CH_4) transported from the tropical troposphere via the BDC:

$$OH + CH_4 \longrightarrow H_2O + CH_3 \tag{2.10}$$

$$H_2O + O(^1D) \longrightarrow 2OH. \tag{2.11}$$

Since the second step requires singlet D oxygen ($O(^1D)$), OH is primarily formed in the upper stratosphere where O_X is dominated by $O(^1D)$ due to UV photolysis. This dependence on UV radiation also causes a strong diurnal variation, with HO_X abundances being highest around local noon. Although H_2O is abundant in the troposphere, transport of H_2O from the the troposphere into the stratosphere is limited because of the low tropopause temperature [*Kley et al.*, 1982;

(Code 916).

Jackson et al., 1998; *Salby et al.*, 2003]. HO_X is also created sporadically in the stratosphere by precipitating solar protons or relativistic electrons (see Section 2.2.4). Additional anthropogenic sources of O_X in the stratosphere are indirectly present in the form of additional CH_4 production by livestock farming and growing swamps caused by melting of tundra regions. The sink for HO_X in the stratosphere is the sedimentation of the reservoir species H_2O, nitric acid (HNO_3), and peroxynitric acid (HNO_4). Depending on altitude several catalytic O_3 destruction cycles are possible. In the upper stratosphere the following two cycles are possible due to the abundance of O:

$$\mathrm{OH} + \mathrm{O_3} \longrightarrow \mathrm{HO_2} + \mathrm{O_2} \tag{2.12}$$

$$\mathrm{HO_2} + \mathrm{O} \longrightarrow \mathrm{OH} + \mathrm{O_2} \tag{2.13}$$

$$\mathrm{net}: \mathrm{O_3} + \mathrm{O} \longrightarrow 2\mathrm{O_2}, \tag{2.14}$$

$$\mathrm{H} + \mathrm{O_2} + \mathrm{M} \longrightarrow \mathrm{HO_2} + \mathrm{M} \tag{2.15}$$

$$\mathrm{HO_2} + \mathrm{O} \longrightarrow \mathrm{OH} + \mathrm{O_2} \tag{2.16}$$

$$\mathrm{OH} + \mathrm{O} \longrightarrow \mathrm{H} + \mathrm{O_2} \tag{2.17}$$

$$\mathrm{net}: 2\mathrm{O} \longrightarrow \mathrm{O_2}. \tag{2.18}$$

The following cycle is possible throughout the stratosphere:

$$\mathrm{OH} + \mathrm{O_3} \longrightarrow \mathrm{HO_2} + \mathrm{O_2} \tag{2.19}$$

$$\mathrm{HO_2} + \mathrm{O_3} \longrightarrow \mathrm{OH} + 2\mathrm{O_2} \tag{2.20}$$

$$\mathrm{net}: 2\mathrm{O_3} \longrightarrow 3\mathrm{O_2}. \tag{2.21}$$

Since the lifetime of HO_X is short compared to other catalysts that destroy O_3, the relevance for long-term O_3 loss is low [*Brasseur and Solomon*, 2005]. However, because of the short lifetime,

HO_X is a good indicator of energetic particle precipitation into the stratosphere, since this creates a transient increase in HO_X (see Section 2.2.4).

Reactive Odd Nitrogen *Crutzen* [1970] found that NO_X, which consists of NO and NO2 in the stratosphere, has a significant impact on O_3 destruction. NO_X in the stratosphere originates primarily from nitrous oxide (N_2O) via the following reactions:

$$N_2O + h\nu \longrightarrow NO + N(^4S) \qquad [\lambda \leq 200\,\text{nm}] \tag{2.22}$$

$$N(^4S) + O_2 \longrightarrow NO + O \tag{2.23}$$

$$N_2O + O(^1D) \longrightarrow 2NO. \tag{2.24}$$

The stratospheric source of N_2O is transport from the troposphere via the BDC, where N_2O naturally comes from soils in the tropical forest and the oceans. This source is anthropogenically enhanced by soil cultivation using common fertilizers and biomass burning [*WMO*, 1995]. Since the production of NO_X from N_2O depends on UV radiation and the abundance of $O(^1D)$, NO_X is primarily created in the upper stratosphere. Another stratospheric NO_X source is NO_X produced in the mesosphere by EPP that subsequently descends into the polar stratosphere (see Section 2.2.4). The primary O_3 destruction due to NO_X is described by the following catalytic cycle

$$NO + O_3 \longrightarrow NO_2 + O_2 \tag{2.25}$$

$$NO_2 + O \longrightarrow NO + O_2 \tag{2.26}$$

$$\text{net} : O_3 + O \longrightarrow 2O_2. \tag{2.27}$$

Many chemical reactions compete with this cycle, notably the deposition of NO_X into the night time reservoir nitrogen pentoxide (N_2O_5) via

$$NO_2 + O_3 \longrightarrow NO_3 + O_2 \tag{2.28}$$

$$NO_3 + NO_2 + M \longrightarrow N_2O_5 + M, \tag{2.29}$$

and the release from the reservoir via

$$N_2O_5 + h\nu \longrightarrow NO_3 + NO_2 \qquad [\lambda \leq 380\,\text{nm}] \tag{2.30}$$

$$NO_3 + h\nu \longrightarrow NO_2 + O \qquad [\lambda \leq 620\,\text{nm}]. \tag{2.31}$$

The above reactions result in a strong diurnal variation of the nitrogen partitioning. NO_X also interferes with other O_3 destroying catalysts, typically forming reservoir species like peroxinitric acid (HO_2NO_2), HNO_3, chlorine nirate ($ClONO_2$), and bromine nirate ($BrONO_2$). If NO_X is incorporated into the HNO_3 reservoir, it can permanently be removed from the stratosphere. This occurs via the formation of HNO_3-containing PSCs, followed by sedimentation of the PSCs (see Section 2.2.3). The formation of PSCs, however, can amplify chlorine chemistry (see Section 2.2.3). Thus nitrogen species, summarized as total reactive odd nitrogen (NO_Y), fulfill several roles in the picture of polar stratospheric O_3 loss both destroying O_3 and reducing O_3 loss by forming the $ClONO_2$ reservoir which effectively reduces total reactive chlorine (ClO_X) (see Section 2.2.3).

Inorganic Halogens Although the list of primordial halogens includes fluorine (F), Cl, bromine (Br), and iodine (I), only Cl and Br are of importance for stratospheric O_3 loss. This is due to the rapid irreversible formation of hydrogen fluoride (HF), which does not participate in O_3 chemistry [*Stolarski and Rundel*, 1975]. I is more efficient in destroying O_3 than Cl and Br due to a higher fraction of I being in reactive forms; but nevertheless the I abundance in the stratosphere is negligible [*Wennberg et al.*, 1997; *Pundt et al.*, 1998; *Cox et al.*, 1999]. Since Cl and Br participate in very similar chemical reactions [e.g., *Yung et al.*, 1980; *Poulet et al.*, 1992] both are summarized in this section. A natural source of halogens in the stratosphere is the convection of the insoluble methyl chloride (CH_3Cl) and methyl bromide (CH_3Br), which are photolyzed in the upper stratosphere. The halogen abundance, however, is dramatically altered by the vast use of CFCs. These stable molecules were invented in the late 19th century and have no natural occurrence. Around 1928 CFCs were recognized as non-toxic and non-reactive replacements for refrigerants, solvents, aerosol propellants, and fire retardants [e.g., *Sneader*, 2005]. Shortly after, CFCs were produced

on commercial scales and after about 1960 their atmospheric abundance increased dramatically [*Lovelock*, 1971; *Walker et al.*, 2000]. Once CFCs are transported to the upper stratosphere they are photolyzed, producing Cl and Br radicals. Thus the halogen abundance in the stratosphere was increased by $\approx 500\,\%$ of the natural abundance by the mid-1990s. *Molina and Rowland* [1974] as well as *Stolarski and Cicerone* [1974] investigated the dramatic O_3 destruction potential of CFCs. After *Farman et al.* [1985] reported dramatic decreases in Antarctic O_3 due to chlorine chemistry (see Figure 2.2), CFCs were soon confirmed as the primary source of polar stratospheric Cl leading to the substantial O_3 loss. In an unprecedented international collaboration the Montreal Protocol was signed in 1987 regulating the phase-out of CFCs; subsequent amendments regulate the phase-out of the less harmful immediate replacements. Nowadays, substances like R-410A[8] are used as refrigerants that have no O_3 depletion potential. *Molina and Rowland* [1974] proposed that the following catalytic cycle is responsible for Cl-induced catalytic O_3 destruction:

$$\mathrm{Cl} + \mathrm{O_3} \longrightarrow \mathrm{ClO} + \mathrm{O_2} \tag{2.32}$$

$$\mathrm{ClO} + \mathrm{O} \longrightarrow \mathrm{Cl} + \mathrm{O_2} \tag{2.33}$$

$$\mathrm{net}: \mathrm{O_3} + \mathrm{O} \longrightarrow 2\mathrm{O_2}. \tag{2.34}$$

Since this cycle requires the abundance of O it can only happen in the upper stratosphere and thus cannot sufficiently explain the O_3 loss observed. Accordingly, *Molina and Molina* [1987] proposed the termolecular self-reaction of chlorine monoxide (ClO) to replace Reaction 2.33, followed by photolysis and further reaction of the products:

$$2\mathrm{ClO} + \mathrm{M} \longrightarrow \mathrm{ClOOCl} + \mathrm{M} \tag{2.35}$$

$$\mathrm{ClOOCl} + \mathrm{h}\nu \longrightarrow \mathrm{ClOO} + \mathrm{Cl} \qquad [200\,\mathrm{nm} \leq \lambda \leq 420\,\mathrm{nm}] \tag{2.36}$$

$$\mathrm{ClOO} + \mathrm{M} \longrightarrow \mathrm{Cl} + \mathrm{O2} + \mathrm{M}. \tag{2.37}$$

[8] R-410A is a difluoromethane (CH_2F_2) and pentafluoroethane (CHF_2CF_3) mix.

Note that this cycle does not require O, and thus considering this cycle increases reaction rates for Cl-induced O_3 loss in the lower stratosphere. Also *McElroy et al.* [1986] and *Tung et al.* [1986] proposed a Cl/Br coupled reaction scheme to replace Reaction 2.33:

$$\mathrm{ClO} + \mathrm{BrO} \longrightarrow \mathrm{BrCl} + \mathrm{O_2} \tag{2.38}$$

$$\mathrm{BrCl} + \mathrm{h}\nu \longrightarrow \mathrm{Br} + \mathrm{Cl}. \tag{2.39}$$

The cycles here strongly depend on ClO and bromine monoxide (BrO) abundances and can only explain the observed O_3 depletion if the release of Cl and Br from the reservoir species hydrogen chloride (HCl), $ClONO_2$, hydrogen bromide (HBr), and $BrONO_2$ does not occur by photolysis alone. This finding marked the onset of research investigating the activation of Cl and Br via heterogeneous chemistry on PSC surfaces during polar night [*Crutzen and Arnold*, 1986; *McElroy et al.*, 1986; *Solomon et al.*, 1986].

Gas-Phase Coupling Reactions The catalysts and corresponding reservoir species participate in chemical reactions that couple HO_X, NO_X, ClO_X and reactive bromine (BrO_X) species. Aside from the ClO/BrO cycle (Reaction 2.38 and Reaction 2.39) presented in the previous paragraph, those coupling reactions often hamper the O_3 loss cycles and/or result in production of reservoir species. For instance, essential coupling reactions between ClO_X and NO_X are

$$\mathrm{ClO} + \mathrm{NO} \longrightarrow \mathrm{Cl} + \mathrm{NO_2} \tag{2.40}$$

$$\mathrm{ClO} + \mathrm{NO_2} + \mathrm{M} \longrightarrow \mathrm{ClONO_2} + \mathrm{M} \tag{2.41}$$

$$\mathrm{ClONO_2} + \mathrm{h}\nu \longrightarrow \mathrm{Cl} + \mathrm{NO_3} \tag{2.42}$$

$$\mathrm{NO_3} + \mathrm{h}\nu \longrightarrow \mathrm{NO_2} + \mathrm{O}. \tag{2.43}$$

While the Reaction 2.40 is beneficial for the Cl-induced O_3 loss cycle by reforming Cl without requiring O, it reduces the reaction rate of NO-induced O_3 loss (Reaction 2.25). Reaction 2.41 slows both Cl-induced and NO-induced O_3 loss by forming the reservoir $ClONO_2$. Since $ClONO_2$ needs to

be photolyzed (Reaction 2.42) in order to provide Cl and nitrogen dioxide (NO_2) (after subsequent photolysis of nitrate radical (NO_3)), O_3 loss is slowed down during night time periods.

This section illustrates that the three major catalysts Cl, Br, and NO cannot be considered separately from each other. Thus it is pointed out that in order to understand O_3 loss cycles all processes have to be considered simultaneously. In particular, the simultaneous presence of NO_X and ClO_X results in formation of the $ClONO_2$ reservoir, reducing the lifetime and abundance of ClO_X and NO_X, and thus hampering O_3 destruction cycles.

2.2.3 Polar Stratospheric Clouds

In Section 2.2.2, heterogeneous chemistry on PSC surfaces was pointed out as a crucial process for activation of halogens from their reservoir species. Counter-intuitively, low abundances of NO_2 before and during O_3 loss periods were observed [*Noxon et al.*, 1978; *Fahey et al.*, 1989] when PSCs were present. Condensation nuclei for PSCs originate from sulfate emission in the troposphere. Dominant natural sources are the oceans, volcanic eruptions, and biomass burning [*Bates et al.*, 1992]. These sources are by far exceeded by anthropogenic sources primarily due to the combustion of coal. Although most of the sulfates are removed in the troposphere via dry and wet deposition [*Brasseur and Solomon*, 2005], they can reach the tropical stratosphere in the form of the stable carbonyl sulfide (COS) molecule [*Crutzen*, 1976]. Volcanic eruptions are capable of direct sulfur (S) deposition into the stratosphere and thus represent a sporadic source of stratospheric COS [*IPCC*, 2007]. In the stratosphere COS gets photolyzed and ultimately forms sulfuric acid (H_2SO_4) via the chain:

$$\mathrm{COS} + \mathrm{h}\nu \longrightarrow \mathrm{CO} + \mathrm{S} \tag{2.44}$$

$$\mathrm{S} + \mathrm{O_2} \longrightarrow \mathrm{SO} + \mathrm{O} \tag{2.45}$$

$$\mathrm{SO} + \mathrm{O_2} \longrightarrow \mathrm{SO_2} + \mathrm{O} \tag{2.46}$$

$$\mathrm{SO_2} + \mathrm{OH} + \mathrm{M} \longrightarrow \mathrm{HSO_3} + \mathrm{M} \tag{2.47}$$

$$\mathrm{HSO_3} + \mathrm{O_2} \longrightarrow \mathrm{HO_2} + \mathrm{SO3} \tag{2.48}$$

$$\mathrm{SO_3} + \mathrm{H_2O} \longrightarrow \mathrm{H_2SO_4}. \tag{2.49}$$

Of the species in this chain, sulfur monoxide (SO), hydrogen sulfite (HSO_3^-), and H_2SO_4 are soluble in ambient H_2O and form sulfate aerosols that provide surface area density (SAD) for heterogeneous chemistry. Sinks for stratospheric sulfate aerosols (SSAs) are downwelling transport and sedimentation with subsequent wet deposition [*Turco et al.*, 1982]. SSAs with radii greater than 0.1 μm accumulate several kilometers above the tropopause, forming the stratospheric aerosol layer [*Junge et al.*, 1961; *Junge and Manson*, 1961].

The saturation vapor pressure for ambient H_2O decreases when stratospheric temperature declines during the polar night. Thus SSAs take up more H_2O by condensational growth, forming a binary solution of H_2SO_4/H_2O. At temperatures below ≈200 K all H_2SO_4 is assumed to be part of this binary solution. Since the H_2O uptake continues below ≈200 K the mass fraction of H_2SO_4 decreases.

At temperatures from ≈193 K to ≈191 K the saturation vapor pressure for HNO_3 is sufficiently low that the binary aerosol particles described previously gradually change to a binary composition of $H_2SO_4/HNO_3/H_2O$, with the H_2SO_4 fraction becoming very small. In this transition region particles are called supercooled ternary solution (STS) [*Lowe and MacKenzie*, 2008]. The STS particles (or Type Ib) are liquid, have typical radii of 0.5 μm, and are too small to sediment [*Toon et al.*, 1990]. In addition to providing SAD via uptake of HNO_3, STS particles also take up gas-phase HCl and HBr, making them unavailable for halogen activation [*Carslaw et al.*, 1995]. The temperature regime in which STS particles exist occurs regularly in average and cold Arctic winters

and thus STS particles are the dominant source of SAD in the NH.

In addition to liquid PSC particles, solid particles containing HNO_3 are also important for O_3 loss. The temperature threshold for the formation of these solid PSC particles is as high as ≈195 K in the lower stratosphere [*Hanson and Mauersberger*, 1988]. Observations show, however, that in addition to low temperatures, supersaturation is needed for these particles to nucleate [*Dye et al.*, 1990, 1992]. These particles consist of nitric acid trihydrate (NAT) or Type Ia) [e.g., *Fahey et al.*, 1989; *Toon et al.*, 1990; *Voigt et al.*, 2000]. Although NAT particle radii are typically between 1 μm and 5 μm, particles with larger radii of 10 μm to 20 μm also exist [*Fahey et al.*, 2001]. Large particles can sediment out of the stratosphere, with rates on the order of 60 m/h for particles with radii of 14 μm, removing HNO_3 in a process known as denitrification [e.g., *Toon et al.*, 1986]. This occurs more often in the SH due to hemispheric temperature differences (see Section 2.1.3 and Section 2.2.5).

The second type of solid PSC particles, which is primarily made of ice, is formed when the temperature drops below ≈188 K. These ice particles were proposed by *Steele et al.* [1983] and confirmed with observations by *Poole and McCormick* [1988] and *Fahey et al.* [1990] for the SH and by *Carslaw et al.* [1998a,b] for the NH. Ice particles are also known as Type II. Radii of ice particles range from ≈1 μm to 30 μm; sedimentation rates are about 100 m/h for a particle radius of 20 μm [e.g., *Brasseur and Solomon*, 2005]. The sedimentation causes dehydration of the lower stratosphere [*Kelly et al.*, 1989] and appears commonly in the SH, but is very unusual for the NH due to higher temperatures there.

The magnitude of O_3 loss can only be explained when Cl from both reservoir species HCl and $ClONO_2$ is made available in reactive form. Gas-phase reactions and O_2 photolysis alone cannot reproduce observed O_3 loss during polar night conditions. *Solomon et al.* [1986] proposed heterogeneous chemistry reactions on the surface of PSCs that produce molecular chlorine (Cl_2) and suppress the formation of NO_2 [*Toon et al.*, 1986]:

$$ClONO_2 + HCl \longrightarrow HNO_3 + Cl_2 \tag{2.50}$$

Subsequent photolysis of Cl_2 produces Cl which participates in O_3 destruction reactions. Over time more heterogeneous reactions on PSC surfaces were confirmed [*Solomon*, 1999, and references therein]:

$$N_2O_5 + H_2O \longrightarrow 2HNO_3 \tag{2.51}$$

$$ClONO_2 + H_2O \longrightarrow HNO_3 + HOCl \tag{2.52}$$

$$HCl + HOCl \longrightarrow H_2O + Cl_2 \tag{2.53}$$

$$BrONO_2 + HCl \longrightarrow HNO_3 + BrCl \tag{2.54}$$

$$BrONO_2 + H_2O \longrightarrow HNO_3 + HOBr \tag{2.55}$$

$$HCl + HOBr \longrightarrow H_2O + BrCl. \tag{2.56}$$

Note that these reactions do not produce ClO_X directly but require subsequent photolysis of Cl_2 or bromine chloride (BrCl). Also, all NO_Y produced is in the form of stable HNO_3, thus concentrations of $ClONO_2$ and $BrONO_2$ are substantially reduced. In summary, PSCs play two essential roles in large scale polar stratospheric O_3 destruction: they provide SAD for heterogeneous chemistry and at the same time denitrify and dehydrate the atmosphere as described earlier.

Heterogeneous chemistry is extremely sensitive to small temperature variations. This is reflected by the strong dependence of the uptake coefficient on temperature [*Carslaw et al.*, 1997]. This causes even small temperature changes to result in dramatic changes in heterogeneous chemistry reaction rate coefficients. The uptake coefficient γ is defined as the ratio of the number of collisions on a surface that lead to a reaction to the total number of collisions on a surface; thus the uptake coefficient represents a reaction probability which can also be expressed in values between 0 % and 100 %. Figure 2.6 shows the temperature dependence of uptake coefficients for the major heterogeneous reactions $ClONO_2$ + HCl (Reaction 2.50), $ClONO_2$ + H_2O (Reaction 2.52), and HCl + hypochlorous acid (HOCl) (Reaction 2.53) on STS particles [*Lowe and MacKenzie*, 2008].

Figure 2.6 illustrates that the reaction probability of the dominant $ClONO_2$ + HCl reaction (2.50) on STS increases from $\approx$0.1 % at 200 K to $\approx$100 % at 192 K. The resulting rate for

heterogeneous production of Cl_2 is described as

$$\frac{d[Cl_2]}{dt} = \frac{\bar{v}}{4}[ClONO_2][HCl]SAD(T)\gamma(T) \tag{2.57}$$

with $\bar{v}$ describing the mean molecular velocity [e.g., *Moore*, 1962]. For typical lower stratospheric conditions Reaction 2.50 leads to a change in reaction rate from 2×10^{-7} mol/s at 198 K to 1×10^{-3} mol/s at 190 K [e.g., *Wegner*, 2012]. This example illustrates that for investigations of heterogeneous chemistry in the lower stratosphere the accurate knowledge of temperature is a crucial requirement.

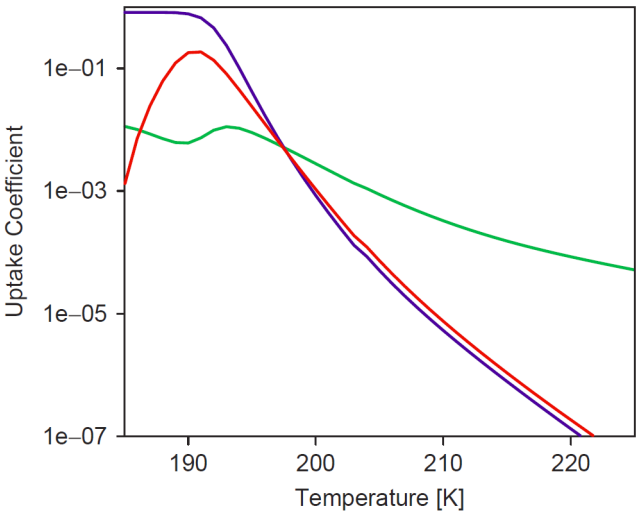

Figure 2.6: "Reactive uptake coefficients as a function of temperature for heterogeneous reactions occurring in liquid sulphuric acid aerosols. Reaction $ClONO_2$ + H_2O is represented by the green line, $ClONO_2$ + HCl by the blue line, and HOCl + HCl by the red line. The uptake coefficients are calculated using the parameterization of *Shi et al.* [2001], which takes into account the couplings of these reactions."[9]

2.2.4 Energetic Particle Precipitation

While the dominant source of NO_X in the stratosphere is the oxidation of N_2O (see Section 2.2.2), EPP represents an additional source of NO_X. Precipitating electrons and protons cause ionization and dissociation reactions that lead to NO production at different altitudes depending on the energy of the precipitating particle [*Thorne*, 1980]. *Crutzen et al.* [1975] showed that production of NO_X due to solar proton precipitation can be on the order of the production via oxidation of N_2O and is thus not negligible. In addition to the solar emission of low energy

[9] Reproduced with permission from Elsevier. Lowe, D. and A. R. MacKenzie (2008), Polar stratospheric cloud microphysics and chemistry, *J. Atmos. Terr. Phy.*, 70, 13-40, doi:10.1016/j.jastp.2007.09.011. Copyright [2008] Elsevier.

(auroral) electrons that occurs all the time, additional particles are emitted during solar flares and solar coronal mass ejections with unpredictable occurrence, intensity, and energy. Guided by the Earth's magnetic field lines, energetic particles (EPs) enter the Earth's atmosphere primarily in the polar regions. The penetration depth into the Earth's atmosphere is determined by the EPs' kinetic energy spectrum [e.g., *Jackman*, 1991] (see Figure 2.7).

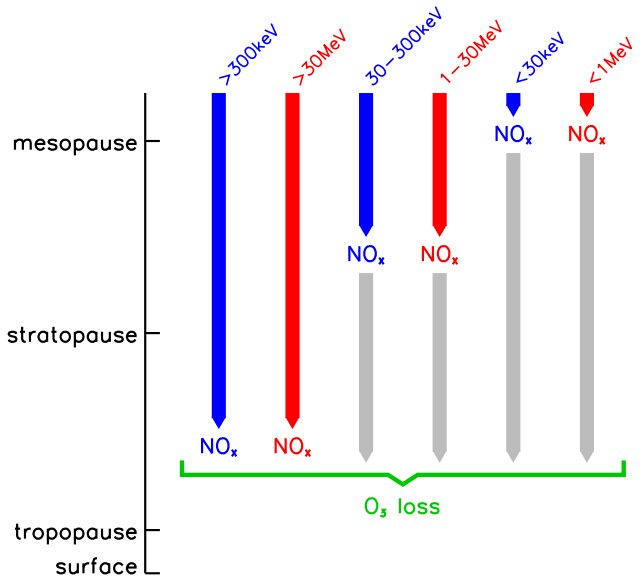

Figure 2.7: Maximum penetration depths into the Earth's atmosphere for electrons (blue) and solar protons (red). Subsequent descent into the stratosphere is shown in gray. Only EPs with high energy can produce NO_X directly in the stratosphere where it participates in O_3 loss reactions; NO_X created by lower energy EPP reaches the atmosphere after subsequent descent.

Electrons with energies smaller than ≈30 keV and protons with energies smaller than ≈1 MeV reach the thermosphere only, electrons with energies from ≈30 keV to ≈300 keV and protons with energies from ≈1 MeV to ≈30 MeV reach the mesosphere, and electrons with energies greater than ≈300 keV and protons with energies greater than ≈30 MeV reach the stratosphere and below. While these are direct penetration depths, secondary electrons produced by the initial ionization are also involved in subsequent reactions. There are two pathways for NO_X created by EPP to reach the stratosphere: NO_X can be created immediately in the stratosphere (direct effect) via ionization and dissociation of N_2 and O_2 [*Rusch et al.*, 1981], or it can be produced above the stratosphere and then descend into the stratosphere (indirect effect) [*Randall et al.*, 2006]. Characteristic for the indirect effect is that there is a time lag between the actual EPP event and the EPP-NO_X reaching the stratosphere [*Solomon et al.*, 1982].

2.2.5 Hemispheric Differences (Chemistry)

As described in Section 2.1.3, because of hemispheric differences in dynamics, specifically PW activity, the SH has a colder and more stable, longer-lasting polar vortex. This has big implications for chemistry and microphysics. Compared to the NH, the SH polar vortex is usually positioned more symmetrically over the pole, with fewer excursions to the sunlit mid-latitudes. This suppresses photochemistry inside the polar vortex and reduces mixing between air masses inside and outside the vortex [*Brasseur and Solomon*, 2005]. The most important implication of the longer and colder SH vortex season is more O_3 loss, which creates the Antarctic O_3 hole (see Figure 2.2). Specifically, the colder vortex leads to more PSCs, increasing the removal of HNO_3 from the lower stratosphere by PSC sedimentation. By denitrifying the lower stratosphere, this hampers Cl deactivation via Reaction 2.41. Less efficient Cl deactivation and the longer-lasting vortex combine to prolong O_3 loss in the SH relative to the NH. NO_X generated by EPP can affect this situation since additional NO_X can react with Cl to form the $ClONO_2$ reservoir (see Section 2.2.2). The stronger BDC in the NH compared to the SH leads to a higher abundance of O_3 in the NH than in the SH, as shown in Figure 2.8; the same figure also illustrates higher variability in O_3 loss in the NH compared to the SH due to PW activity.

2.3 Investigation of Polar Stratospheric Ozone

The previous sections illustrated that in order to investigate stratospheric O_3, dynamical transport and chemical processes must be included in the analysis. In this section requirements for observations and model simulations are explained. The first paragraph summarizes requirements for the lower stratosphere. The second paragraph does the same for the upper stratosphere. The third paragraph describes the necessity to include the Cl partitioning in the analysis, explains why this is problematic, and how model simulations can assist in the analysis. The fourth paragraph summarizes model requirements to correctly simulate NO_Y and related processes.

[10] Reproduced from WMO (World Meteorological Organization) (2011), Twenty Questions and Answers About the Ozone Layer: 2010 Update, D. W. Fahey and Hegglin, M. I. (Coordinating Lead Authors), Scientific Assessment of Ozone Depletion: 2010.

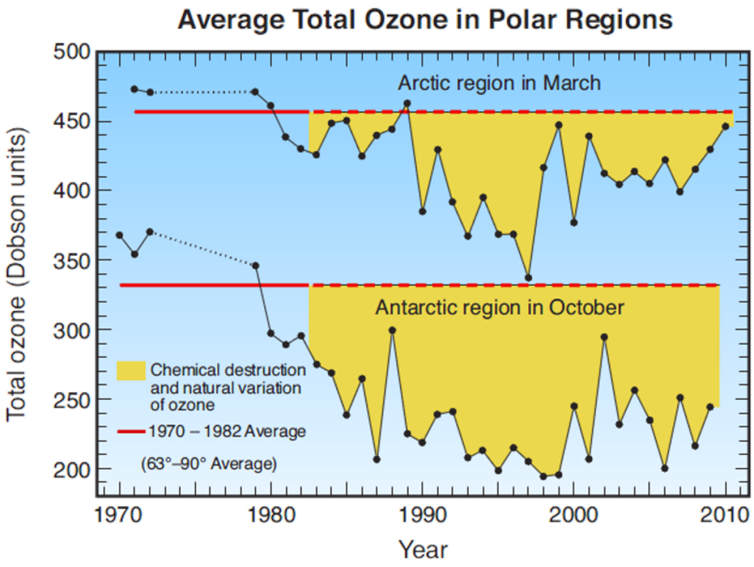

Figure 2.8: "History of the total averaged O_3 column from pre-CFC conditions through present. While there are exceptions, the Antarctic O_3 column is consistently lower than the Arctic O_3 column. The yellow area shows total O_3 loss due to chemical destruction and natural variation, e.g., dynamics."[10].

For the investigation of O_3 changes in the polar lower stratosphere (from the tropopause to 700 K / 17 hPa / 28 km), the partitioning of inorganic chlorine (Cl_Y), inorganic bromine (Br_Y), and NO_Y is of primary concern for gas-phase chemistry, while the formation of PSCs and thus the uptake of HNO_3 and H_2O is essential for heterogeneous halogen activation. Since the halogen activation is very sensitive to small temperature changes as shown in Section 2.2.3, observing and simulating the correct temperature is crucial. At the same time, the removal of gas-phase NO_Y due to PSC formation suppresses gas-phase chemistry involving NO_Y. Thus the amount of HNO_3 uptake into PSCs and the resulting SAD must be simulated sufficiently well. Total NO_Y might be increased in the lower stratosphere by strong EPP indirect effects, hence including EPP can be important even for the lower stratosphere. In order to include dynamical features like the BDC, PWs, polar vortex, and mixing across the polar vortex edge, chemical tracers are essential and are ideally supported by wind measurements. A good example for a lower stratospheric tracer is N_2O due to its lifetime exceeding the duration of dynamical processes [*Loewenstein et al.*, 1990]. In addition,

observations and simulation of these tracers and all other species investigated must be available with a spatial coverage of at least the polar cap as well as profile information from the tropopause to the mid-stratosphere and higher. Before heterogeneous chemistry followed by photodissociation of Cl_2 occurs, the chemical lifetime of O_3 exceeds its dynamical lifetime and thus O_3 is a tracer in early winter. However, the chemical lifetime of lower stratospheric O_3 is dramatically reduced in late winter. A quantification of chemical polar O_3 variability thus requires the distinction between dynamical and chemical contributions to O_3 changes as described in Chapter 2.

From ≈ 25 km - 45 km O_3 loss is determined primarily by catalytic NO_X reactions [*Brasseur and Solomon*, 2005], as described in Section 2.2.2. Since the upper stratosphere is exposed to shorter wavelength radiation than the lower stratosphere, and for a longer period of time, O_3 in the upper stratosphere is controlled by photochemistry to a greater extent than in the lower stratosphere. The chemical lifetime of O_3 in the upper stratosphere in early winter is only a few days, compared to a year in the lower stratosphere [e.g., *Brasseur and Solomon*, 2005]. Especially during solar maximum, the UV irradiance oscillates with a ≈27 day period[11] [*Dessler et al.*, 1998] with shortest wavelengths varying strongest (e.g., ≈8 % at 200 nm). This results in a variation of the O_3 abundance (see Reaction 2.4) on the order of 1 - 2 %. Another solar influence is represented by the previously introduced EPP producing HO_X and NO_X in the upper stratosphere. The O_3 equilibrium established due to existing NO_X can be disturbed due to EPP events, potentially causing substantial O_3 loss.

Fulfilling the previously explained observational requirements, is further complicated by the fact that a few species are difficult or even impossible to observe. For instance, investigating the Cl_Y partitioning ideally requires the observation of Cl, ClO, Cl_2, hypochlorite dimer (ClOOCl), chlorine dioxide (OClO), HOCl, $ClONO_2$, HCl, and BrCl. When not all necessary species of the Cl_Y family are observed, a common approach is to focus on the members of the Cl_Y family that make up the largest fraction and consider the rest as a quantifiable error. But even that approach

[11] Because UV is high around sun spots which appear in clusters preferably on one side of the sun, UV is elevated when the sunspots face the Earth. Since the sun has a rotation period of ≈27 days, the UV irradiance oscillates with that frequency as well.

creates strong demands on observations in spatial, vertical, and temporal coverage. For example, the ClO_X family comprised of Cl, ClO, and ClOOCl is subject to a strong diurnal variation. In order to investigate the complete picture of ClO_X a full temporal coverage or the simultaneous observation of all local times must be available. Intrinsically no single instrument can provide this information, but atmospheric Eulerian models provide these "atmospheric snapshots" of all Cl_Y species by default. Hence, spatially and temporally comprehensive information about complete Cl_Y partitionind can only be provided by a Eulerian model.

A model, which is evaluated to produce realistic output, can complement the observations by adding spatial and temporal coverage as well as providing estimates for species that are not observed. For this purpose not only O_3 must be positively evaluated but related species and dynamics must prove to be valid as well. This is required in order to confidently infer O_3 loss since it is not observed directly like other trace gases. The most prominent species involved in O_3 chemistry were introduced in the previous sections. Each related species is part of chemical, dynamical, and/or microphysical processes. For instance, HNO_3 is influenced by dynamics through transport of the gas-phase and sedimentation of the solid-phase, by chemistry through gas-phase reactions and EPP-NO_X supply, and by microphysics through PSC formation and evaporation. Thus HNO_3 as a single species must be sufficiently well simulated in all three process categories. Hence the positive evaluation of a model prior to its scientific use becomes a crucial part of a successful analysis.

2.4 Science Questions

The previous sections showed that the evolution of O_3 is a complex field since it is influenced by dynamics of the whole atmosphere, altitude and latitude dependent gas-phase chemistry, PSC microphysics, and solar variability in form of EPP events and UV irradiance. In return the atmosphere is influenced by the evolution of O_3 through heating the atmosphere by UV absorption which feeds back on dynamics. The recent WMO report illustrates this entangled situation using a simplified picture including feedback processes (see Figure 2.9).

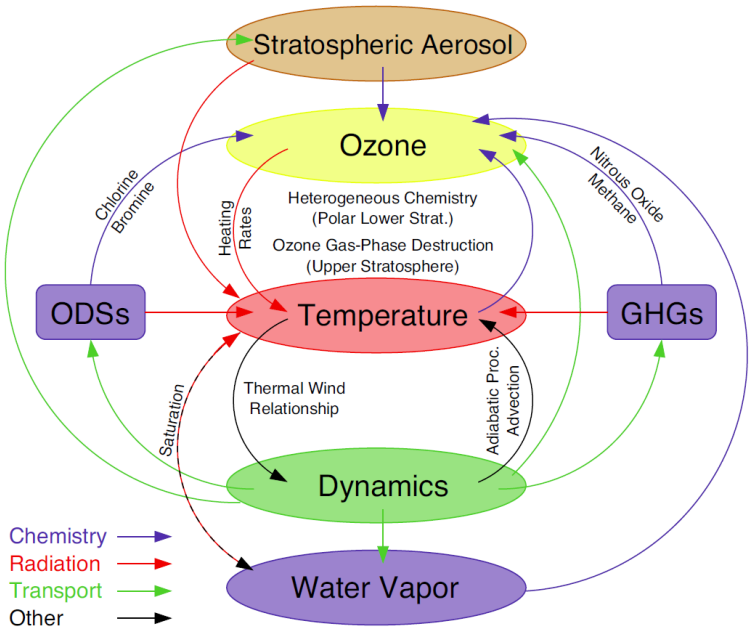

Figure 2.9: "Schematic of O_3-focused stratospheric chemistry-climate interactions. Links between elements of the chemistry-climate system are indicated with arrows representing chemistry (blue), radiation (red), transport (green), and other mechanisms (black). Simple and more complex feedback cycles can be constructed following the linking mechanisms. A simple example is O_3 depletion in the upper stratosphere leading to lower temperatures. Lower temperatures slow the gasphase destruction of O_3, thereby reducing the amount of O_3 depletion. [...]".[12]

Section 2.3 showed that not all involved processes can be sufficiently observed but a model can be used to complement the missing parts if it is positively evaluated. At the same time the model can be used to identify causes of coupled effects individually, thus allowing their quantification. One example is the separation between dynamical and chemical O_3 evolution as described in the beginning of Chapter 2. Such investigations require using a CCM [*WMO*, 2011a], which includes the whole atmosphere, has explicit or parameterized PSC microphysics, and which can be initialized with observations as well as driven by reanalysis data. The CESM from the National Center for Atmospheric Research (NCAR) with the Specified Dynamics Whole Atmosphere Community Climate Model (SD-WACCM) component set (hereafter called SD-WACCM and explained in more

[12] Reproduced with permission of WMO. WMO (World Meteorological Organization) (2011), Scientific Assessment of Ozone Depletion: 2010, Global Ozone Research and Monitoring Project - Report No. 52.

detail in [*Kinnison et al.*, 2013] and Chapter 3) fulfills these requirements. The development of an analysis to evaluate SD-WACCM regarding O_3 evolution answers the first science question:

1. Is SD-WACCM a tool sophisticated enough for quantitative O_3 evolution investigations?

An answer to this question needs to be provided for both hemispheres individually because of the differences explained in Section 2.1.3 and Section 2.2.5. This evaluation effort entails improvements to the model which are further tested and refined during subsequent analyses. Once the model is positively evaluated, O_3 evolution of past winter seasons can be attributed to individual processes described in the previous sections. Since O_3 loss is an inferred quantity, the following second question can only be answered with confidence using the evaluated model:

2. How much O_3 loss can be accurately attributed to the stratospheric O_3 loss processes induced by halogens, EPP, and NO_X individually?

The study needed to answer this question requires experimental model simulations excluding individual causes for O_3 loss compared to a comprehensive reference simulation. The confidence gained by the first two studies is not necessarily valid in uncommon conditions, thus special test cases are investigated that represent extreme perturbations of the average conditions. One test case, due to natural variability, is the unusually prolonged NH 2010/11 season. In this particular season unprecedented O_3 loss was observed [*Manney et al.*, 2011], which raises the next science question attributing the underlying processes of the extreme O_3 loss:

3. Why is the observed O_3 in the NH 2010/2011 winter exceptionally low, despite high dynamical variability, which is usually associated with less O_3 loss?

The short-term scientific gain in answering these questions is an evaluation of our understand-

ing of various atmospheric processes as well as our ability to implement our understanding in state of the art ESMs. The long-term scientific gain is the ability to model our atmosphere more accurately and thus provide more robust prognostic simulations along the lines "(...) from a phase of discovery to one of understanding, and finally to one of comprehensive modeling and prediction." [*Shepherd*, 2000].

Chapter 3

SD-WACCM simulations of the Arctic winter 2004/05

Contents

In order to answer the first science question raised in the previous section a comprehensive model evaluation is developed and performed. The Arctic winter season 2004/05 is chosen since this winter is exceptionally cold, which challenges the implementation of PSC formation in the model. Recent studies have shown that cold Arctic winters are getting even colder [*Rex et al.*, 2004, 2006; *WMO*, 2011a] and O_3 loss is getting larger [*Manney et al.*, 2011; *Sinnhuber et al.*, 2011] even though Cl loading of the stratosphere is getting smaller. Hence, accurate simulations of Arctic O_3 chemistry are important. This study evaluates SD-WACCM simulations of the 2004/05 Arctic winter, and in particular addresses the impact of small temperature variations. Due to the work on this project, the PSC parameterization in SD-WACCM was greatly improved.

The analysis concludes with the finding that SD-WACCM is an appropriate model for O_3 loss studies, but that correctly simulating temperature is crucial. The questions left open by this

study are about the model's validity in the SH and the attribution of total O_3 loss to individual causes. In the next chapter these points are investigated in depth.

3.1 Evaluation of Whole Atmosphere Community Climate Model simulations of ozone during Arctic winter 2004-2005[1]

M. Brakebusch[1], C. E. Randall[1], D. E. Kinnison[2], S. Tilmes[2], M. L. Santee[3], and G. L. Manney[3,4,5]

[1]Department of Atmospheric and Oceanic Sciences and Laboratory for Atmospheric and Space Physics, University of Colorado at Boulder, Boulder, Colorado, USA.

[2]Atmospheric Chemistry Division, National Center for Atmospheric Research, Boulder, Colorado, USA.

[3]Jet Propulsion Laboratory, California Institute of Technology, Pasadena, California, USA.

[4]also at New Mexico Institute of Mining and Technology, Socorro, New Mexico, USA.

[5]now at NorthWest Research Associates, Socorro, New Mexico, USA.

The work presented here evaluates polar stratospheric O_3 simulations from the WACCM for the Arctic winter of 2004-2005. We use the Specified Dynamics version of WACCM (SD-WACCM), in which temperatures and winds are nudged to meteorological assimilation analysis results. Model simulations of O_3 and related constituents generally compare well to observations from the Earth Observing System (EOS) Microwave Limb Sounder (MLS). At most times, modeled O_3 agrees with MLS data to within $\approx 10\,\%$. However, a systematic high bias in O_3 in the model of $\approx 18\,\%$ is found in the lowermost stratosphere in March. We attribute most of this O_3 bias to too little heterogeneous processing of halogens late in the winter. We suggest that the model under-predicts $ClONO_2$ early in the winter, which leads to less heterogeneous processing and too little activated chlorine. Model HCl could also be overestimated due to an underestimation of HCl uptake into STS particles. In late winter, the model overestimates gas-phase HNO_3, and thus NO_Y, which leads

[1] Reproduced with permission from John Wiley and Sons. Brakebusch, M., C. E. Randall, D. E. Kinnison, S. Tilmes, M. L. Santee, and G. L. Manney (2013), Evaluation of Whole Atmosphere Community Climate Model simulations of ozone during Arctic winter 2004-2005, *J. Geophys. Res.-Atmos.*, 118, 2673-2688, doi:10.1002/jgrd.50226.

to an over-prediction of $ClONO_2$ (under-prediction of activated chlorine). A sensitivity study, in which temperatures for heterogeneous chemistry reactions were reduced by 1.5 K, shows significant improvement of modeled O_3. Chemical O_3 loss is inferred from the MLS observations using the pseudo-passive subtraction approach. The inferred O_3 loss using this method is in agreement with or less than previous independent results for the Arctic winter of 2004-2005, reaching 1.0 ppmv on average and up to 1.6 ppmv locally in the polar vortex.

3.1.1 Introduction

Understanding the recovery of polar stratospheric O_3 is important because O_3 shields the Earth's surface from harmful solar radiation and is itself a radiatively active gas. It is expected that the recovery of polar stratospheric O_3 will be influenced by, and influence, global climate change [e.g., *WMO*, 2011a; *Akiyoshi et al.*, 2010]. To reliably predict future O_3 variations, it is important to understand the dynamical and chemical processes relevant to O_3 loss. Although in general the mechanisms behind polar stratospheric O_3 loss are well understood [e.g., *Solomon*, 1999; *Brasseur and Solomon*, 2005], there are still differences in the chemistry modules of state-of-the-art chemistry climate models, differences in the parameterizations and approximations applied, and differences in the dynamical description of the vortex that can lead to significant discrepancies in the representation of polar O_3 loss [*SPARC CCMVal*, 2010, chapter 6]. The overall goal of this study is to assess WACCM [*SPARC CCMVal*, 2010, chapter 2.4.16 and references therein] simulations of polar stratospheric O_3 by comparing WACCM results to observations from the EOS MLS (hereafter called MLS) onboard NASA's Aura satellite. The NH winter of 2004-2005 is chosen for the model/measurement comparisons since this winter was one of the coldest in recent years, and it has been investigated by numerous authors, as described later in this section [*Jin et al.*, 2006a; *Manney et al.*, 2006; *Rex et al.*, 2006; *von Hobe et al.*, 2006; *Feng et al.*, 2007a; *Grooß and Müller*, 2007; *Singleton et al.*, 2007; *Tsvetkova et al.*, 2007; *El Amraoui et al.*, 2008; *Jackson and Orsolini*, 2008; *Rösevall et al.*, 2008; *Santee et al.*, 2008; *Feng et al.*, 2011]. This winter thus provides a good test case for evaluating WACCM.

The meteorology of the 2004-2005 Arctic winter is described in detail by *Manney et al.* [2006] and is briefly summarized here. The Arctic winter 2004-2005 was colder than average, but the polar vortex was quite variable in shape and location. The vortex was disturbed by warmings in late December, late January, and February. These caused mixing events across the vortex edge that led to variations in trace gases. Descent was the dominant transport process until late January, when chemical O_3 loss became significant. Throughout February and persisting until the early final warming around 10 March, transport was dominated by mixing events inside the polar vortex and across the polar vortex edge. Intrusions of extra-vortex air into the vortex were evident as the vortex began to break up. More details of the meteorology will be discussed in Section 3.1.3.3.

Chemistry relevant to O_3 loss during the 2004-2005 Arctic winter is described in detail by *Santee et al.* [2008]. With large areas of the polar vortex being cold enough for PSCs for significant periods of time, substantial growth of PSC particles and subsequent denitrification occurred [*Kleinböhl et al.*, 2005; *Dibb et al.*, 2006; *Jin et al.*, 2006b]. PSCs consisting of STS particles and NAT particles were observed [*Blum et al.*, 2006], and ice particles were inferred from water vapor observations [*Jimenez et al.*, 2006]. The onset of Cl activation was found in MLS observations in late December/early January, with highest ClO enhancements at 490 K after 10 January. Reactive Cl peaked in late January and early February, with 80-90 % of total Cl activated.

Quantifying chemical O_3 loss requires identifying the separate contributions of transport and chemistry to observed O_3 changes. Chemical O_3 loss in the Arctic 2004-2005 winter has been quantified using several different techniques. *Manney et al.* [2006] estimated the loss using the polar vortex average descent technique [*Hoppel et al.*, 2002], which was also used by *El Amraoui et al.* [2008]. In the vortex average descent technique, differences between the observations and a simulated descended O_3 profile in the polar vortex represent chemical O_3 loss. A similar approach, in which diabatic descent was estimated from a radiation model, was used by *Tsvetkova et al.* [2007] to quantify O_3 loss. *Rex et al.* [2006] used a Lagrangian approach where air parcels were probed along their trajectory by O_3 sondes, and changes in the O_3 mixing ratios were attributed to chemical O_3 loss [e.g., *Rex et al.*, 1999]. Tracer correlation techniques [*Michelsen et al.*, 1998;

Proffitt et al., 1992] take advantage of the fact that O_3 chemistry will perturb the relationship between N_2O and O_3 that is established when both act as tracers [e.g., *Tilmes et al.*, 2004]. This method was also used by *von Hobe et al.* [2006] to estimate chemical O_3 loss in the Arctic 2004-2005 polar vortex. *Rösevall et al.* [2008] used a modified tracer correlation method to derive chemical O_3 loss. They also calculated O_3 loss applying the passive subtraction technique [originally developed by *Manney et al.* [1995]], which is also used here and is described in Section 3.1.4.1. *Jackson and Orsolini* [2008], *Grooß and Müller* [2007], and *Singleton et al.* [2007] also applied the passive subtraction method. *Jin et al.* [2006a] used a variety of techniques: tracer correlation, artificial tracer correlation [*Esler and Waugh*, 2002], vortex average profile descent [*Manney et al.*, 2006], and correlations between potential PSC volume and chemical O_3 loss [*Rex et al.*, 2004]. Results of these studies are listed in Section 3.1.5 along with a comparison to findings from this study.

Section 3.1.2 describes the observations from MLS and the simulations from WACCM used for this study. In Section 3.1.3, we compare WACCM simulations of temperature, polar stratospheric O_3 and related constituents to observations from MLS for the 2004-2005 winter. We quantify chemical O_3 loss using the passive subtraction method in Section 3.1.4. Also shown in Section 3.1.4 is a temperature sensitivity study for modeled heterogeneous chemistry. Section 3.1.5 summarizes the results, compares findings to previous studies, and provides conclusions.

3.1.2 Method

The CESM version 1.0.3 WACCM component set is a coupled chemistry climate model developed at the NCAR, originally based on the software framework of the Community Atmosphere Model (CAM) [*Collins et al.*, 2006]. The WACCM chemistry module is taken from the Model for OZone And Related chemical Tracers (MOZART) [*Brasseur et al.*, 1998; *Hauglustaine et al.*, 1998; *Horowitz et al.*, 2003; *Kinnison et al.*, 2007; *Emmons et al.*, 2010] but is extended to include 122 species [*Lamarque et al.*, 2012]. The upper atmosphere module is taken from the Thermosphere-Ionosphere-Mesosphere Electrodynamics General Circulation Model (TIME-GCM) [*Roble and Ridley*, 1987]. The specified dynamics version of WACCM, SD-WACCM, is a modified

version of WACCM in which the meteorology is constrained to match observations to within a user-defined tolerance [*Lamarque et al.*, 2012; *Kunz et al.*, 2011]. Thus, whereas WACCM is a free-running general circulation model, SD-WACCM is nudged every 30 min time step with horizontal winds, temperatures, and surface pressure from a meteorological assimilation analysis to prevent divergence from real dynamical conditions. Additionally, SD-WACCM is forced with surface wind stress and sensible as well as latent surface heat flux.

The simulations described below use SD-WACCM with a horizontal resolution of $1.9° \times 2.5°$ (latitude $\times$ longitude) and a vertical hybrid sigma-pressure coordinate with 88 levels that range in resolution from about 0.5 to 4 km and cover an altitude range from the surface to about 145 km. Vertical resolution in the lower stratosphere, the region of primary interest here, is $\approx$1 km. Winds, temperature, surface pressure, surface wind stress, and heat fluxes used here are from the Goddard Earth Observing System 5 (GEOS5) analysis [*Rienecker*, 2008]. This analysis product has a 6 h time resolution, which is interpolated by the model to the finer 30 min time resolution required. The nudging coefficient is 0.01, i.e., the winds, temperature, and surface pressure are defined by a linear combination of 1 % from GEOS5 and 99 % from the model. This nudging scheme is used below 50 km, while above 60 km the model is fully interactive; at altitudes from 50 to 60 km a linear transition occurs from 1 % to 0 % nudging. Although the nudging coefficient seems small in magnitude, it is compounded at each time step. Thus after an initial spin-up time period (see below), the SD-WACCM winds and temperatures are very similar to GEOS5 and require only a small amount of nudging to remain so. More specifically, the mean differences (SD-WACCM minus GEOS5 $\pm$ one standard deviation (σ) over the winter) are -0.16$\pm$0.77 K for temperature, -0.08$\pm$1.83 m/s for zonal wind, and -0.01$\pm$1.9 m/s for meridional wind. Vertical transport is derived by SD-WACCM following a transport scheme developed by *Lin and Rood* [1996] and *Lin* [2004]. GWs are parameterized [*Richter et al.*, 2010] while PWs are resolved. In the model, wind stress and heat fluxes are forced (not nudged) to exactly match GEOS5. SD-WACCM can therefore simulate the atmosphere up to about the stratopause with specific dynamics representing a particular season, enabling direct comparison to tropospheric and stratospheric observations. In

contrast, a climatological WACCM simulation will be representative of an average season, but will not replicate crucial characteristics of a specific season.

The SD-WACCM simulations employed here correspond to the time period from 1 December 2004 to 31 March 2005. For these simulations the model had a spin-up time from 1980 to the end of 2003 in fully interactive mode, i.e., free-running WACCM, without specified dynamics, was used for the initial spin-up. On 1 January 2004, the model was switched to SD-WACCM; the 11-month period from January to December 2004 was a sufficient spin-up time for the nudging, as mentioned above. In order to evaluate SD-WACCM via comparison of modeled to observed species, initial conditions in the model are set equal to the observations used for comparison (MLS in this case, as explained below). This is necessary in order to accurately interpret deviations between the model results and observations. Thus, within the accuracy and precision of the observations, these deviations can be attributed to the model. At the same time the simulations can only be compared to data from the instrument used for the initialization since biases between instruments exist. For a model simulation without this initialization (not shown), the same conclusions were drawn qualitatively but a quantification of model/instrument differences was not possible. The initialization date chosen in this study is 1 December 2004, which is before the first halogen-catalyzed lower stratospheric O_3 loss occurs. Because MLS provides near global observations, it is used for the initialization, as described in more detail below. This allows for initialization of gas-phase O_3, N_2O, HNO_3, HCl, and H_2O.

In addition to data from other instruments, well-validated limb emission data since August 2004 are available from the MLS instrument [*Livesey*, 2011], with nearly global coverage and a vertical resolution of 3-10 km, which varies with constituent and altitude. For this study we use version 3.3 Level 2 data. For the vertical range of interest for this study, 17-100 hPa, accuracy (precision) is on the order of ±0.1 ppbv to ±0.05 ppbv (±0.1 ppbv) for ClO, ±4 % to ±8 % (±6 % to ±15 %) for H_2O, 0.1 ppbv to 0.2 ppbv (0.2 ppbv to 0.3 ppbv) for HCl, ±0.5 ppbv to ±2 ppbv (±0.7 ppbv) for HNO_3, 13 ppbv to 70 ppbv (13 ppbv to 24 ppbv) for N_2O, 0.05 ppmv to 0.25 ppmv (0.04 ppmv to 0.1 ppmv) for O_3, and -2 K to +1 K (±0.6 to ±0.8 K) for T [*Livesey*, 2011]. The

low bias correction suggested by *Livesey* [2011] for MLS ClO version 3.3 was applied to all ClO observations used in this study. For the NH lower stratosphere polar vortex region, the bias correction is on the order of 7-160 pptv and strongly depends on latitude and pressure.

For model initialization, a regularly gridded form of the MLS Level 2 data is required. The grid for one day of MLS observations is created by applying to the observations, separately for each pressure level, a spatial Delaunay Triangulation [*Knuth*, 1992, and references therein]. Spatial noise is reduced by applying a distance-weighted smoothing. As an example, Figure 3.1 shows one day of NH MLS O_3 measurements on the 100 hPa pressure level (potential temperature $\approx$ 420 K, or $\approx$ 16 km), depicted as symbols that are color-coded according to the observed O_3 volume mixing ratio. The color contours show the same data after gridding to a regular 1.9° $\times$ 2.5° field. The largest interpolations occur between 30°N and 30°S, where zonal distances in the MLS sampling are $\approx$ 14°. Data gaps at latitudes poleward of 82° are filled by interpolating across the poles. Near-global coverage of MLS observations on any level is required to create the above described gridded product. Data for the lowest and highest retrieved levels of MLS observations may not fulfill this criterion; hence the altitude range for each species used for the gridded product may be reduced from the published valid range.

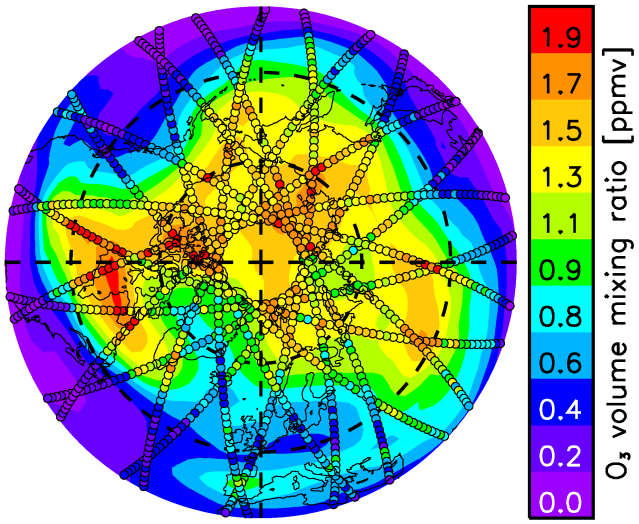

Figure 3.1: Contour map of gridded MLS O_3 data at 100 hPa on 1 December 2004. Colored dots represent MLS measurements from which the gridded data was produced (see text).

By default WACCM is initialized with all atmospheric constituents from a previously com-

pleted climatological simulation. For the initialization in this study, each profile of H_2O, HCl, HNO_3, N_2O, and O_3 from the default initialization is replaced globally with the gridded MLS data described above, within the altitude range over which both the MLS data and the gridding procedure are valid. At the upper and lower altitude limits of this range, the profiles smoothly transition back to the climatological WACCM profiles. Table 3.1 lists the altitude ranges for each constituent over which the different initializations are used. For example, the initialization profiles of O_3 are equal to MLS O_3 between 101 hPa and 2.95 hPa, and to the 1 December WACCM profiles at pressure levels greater than 164 hPa or smaller than 0.91 hPa. Between 164 hPa and 101 hPa (2.95 hPa and 0.91 hPa), a linear transition is made across two (four) pressure levels. When this technique was applied to HCl, it introduced unrealistic structure in the HCl profiles at altitudes above 0.91 hPa; thus for HCl only, WACCM mixing ratios at altitudes above 0.91 hPa are scaled to MLS mixing ratios in the transition region. For pressure levels greater than 44 hPa, the slope of the N_2O volume mixing ratio profile with respect to altitude steepens sharply, which causes the initialization of N_2O to become particularly sensitive to the number of transition levels. Thus for pressure levels greater than 44 hPa, N_2O is initialized with the climatological WACCM profiles.

	SD-WACCM	MLS	SD-WACCM
O_3	≥164 hPa (≤350 K)	101-2.95 hPa (400-1350 K)	≤0.91 hPa (≥2000 K)
N_2O	≥101 hPa (≤400 K)	43.9-2.95 hPa (550-1350 K)	≤0.91 hPa (≥2000 K)
H_2O	≥164 hPa (≤350 K)	101-0.06 hPa (400-3550 K)	≤0.015 hPa (≥5050 K)
HNO_3	≥101 hPa (≤400 K)	61.5-12.5 hPa (475-825 K)	≤4.56 hPa (≥1150 K)
HCl	≥101 hPa (≤400 K)	61.5-2.95 hPa (475-1350 K)	≤0.91 hPa (≥2000 K)

Table 3.1: SD-WACCM initialization altitudes.

In order to improve WACCM's capability to accurately simulate polar O_3 and related con-

stituents, several modifications to the representation of heterogeneous chemistry were included. In this paragraph, we describe the default WACCM without improvements first and then introduce the modifications. In its standard configuration, the WACCM heterogeneous module is based on an equilibrium approach and the observed sulfate surface area density of a volcanically clean atmosphere is used [*Kinnison et al.*, 2007]. In the equilibrium approach, the total available HNO_3 is partitioned between STS and NAT particles based on temperature and composition factors. This approach allows NAT to form at $\approx 195\,K$, several degrees warmer than the temperature at which STS becomes important in taking up HNO_3. Therefore, in early winter, NAT particles are the primary HNO_3 containing particles and subsequent denitrification rapidly occurs. Based on observational evidence, this approach was modified for the current work [Wegner, T., D. E. Kinnison, R. R. Garcia, S. Madronich, S. Solomon, and M. von Hobe (2013), Polar Stratospheric Clouds in SD-WACCM4, manuscript in preparation, hereafter called *Wegner et al.*, 2013a]. In the new approach, the partitioning of total available HNO_3 is forced to not exceed 80 % uptake into STS and 20 % into NAT. Further, the NAT particle density is reduced to $10^{-3}\,cm^{-3}$, which again is based on observational evidence [*Pitts et al.*, 2009]. These two modifications have greatly improved the absolute and temporal agreement of model gas-phase HNO_3 as observed by MLS [*Wegner et al.*, 2013a]. In terms of chlorine activation, heterogeneous chemistry reactions on STS particles have been found to be the dominant source of reactive chlorine [*Wegner et al.*, 2012; *Drdla and Müller*, 2012]. A third modification, HCl condensation into STS, has also been added. This parameterization is based on laboratory measurements and is highly dependent on temperature and H_2O vapor abundance [*Lowe and MacKenzie*, 2008]. This process allows gas-phase HCl to be absorbed into the particle. The soluble HCl will only be activated if there is enough $ClONO_2$, HOCl, or hypobromous acid (HOBr) available to heterogeneously react [Wegner, T.,D. E.Kinnison, R. R. Garcia, S. Madronich, S. Solomon, and M. von Hobe (2013), Chlorine Partitioning in the Antarctic Stratosphere: Implications of HCl uptake into STS, manuscript in preparation, hereafter called *Wegner et al.*, 2013b].

In addition, the total inorganic bromine abundance in the model was increased globally on

1 December 2004 by a factor of 1.5 (from ≈16 pptv to ≈24 pptv). This increase in total inorganic bromine was applied as a surrogate to represent very short-lived (VSL) organic bromine species not included in the WACCM chemical mechanism. See *Salawitch et al.* [2010], *WMO* [2011a], and *Tilmes et al.* [2012] for more details on VSL halogen abundances in the atmosphere. The photolysis approach used in WACCM is based on a lookup table described by *Kinnison et al.* [2007] and evaluated by *SPARC CCMVal* [2010].

3.1.3 Model/Measurement Comparisons

This section shows comparisons between SD-WACCM simulations and measurements of temperature, O_3, and chemical constituents that serve as diagnostics of transport and chemistry. The area of interest is the lower polar stratosphere, i.e., the potential temperature range from 400 K (≈18 km or ≈100 hPa) to 700 K (≈28 km or ≈17 hPa). For the comparisons, SD-WACCM is sampled at MLS observation positions and times, within the model accuracy, which is ±1.25° longitude, ±0.9° latitude, and ±15 min, i.e. the closest profile is chosen and no interpolation is done. Subsequently, all SD-WACCM profiles of any species shown in this study are modified by applying the averaging kernels from the MLS retrieval as described in detail by *Livesey* [2011]. All observations inside the polar vortex are averaged to a single, daily profile unless stated otherwise. The polar vortex is defined by scaled potential vorticity (sPV) [*Dunkerton and Delisi*, 1986] values greater than $1.4\times10^{-4}s^{-1}$. In contrast to Ertel's PV, sPV does not depend on altitude but retains all spatial variations as well as conservation properties. Thus a single threshold as a polar vortex edge criterion can be applied for the entire altitude range in this study. Because of the relatively dense MLS measurement sampling at high latitudes, the polar vortex is well sampled equatorward of 82°N. That is, the MLS measurement locations generally range from the inner vortex core out to the edge and beyond. Therefore, averaging observations or model output at MLS observation positions within the vortex is typically representative of an average full range of conditions in the polar vortex. For polar map projection figures, observations and simulations from that particular day are gridded in the same way as described for the model initialization.

Comparison results are summarized in Figure 3.2. A 7-day weighted running average is applied in each panel to cover temporal gaps in the MLS observations. The statistical significance of the model/measurement comparisons is defined by the Wilcoxon signed-rank test [*Wilcoxon*, 1945; *Wilks*, 2006] using the distributions of values within the polar vortex from SD-WACCM and MLS for each day and isentropic surface individually. Thus, the statistical significance indicates whether mean differences between the model and measurements are significant relative to variability within the vortex. The Wilcoxon signed-rank test was chosen here since the underlying distributions tested negative for normality; thus Student's t-test does not apply [*Dowdy et al.*, 2004]. Differences between SD-WACCM and MLS that are statistically insignificant with a confidence of 95 % are shaded in column 3 of Figure 3.2.

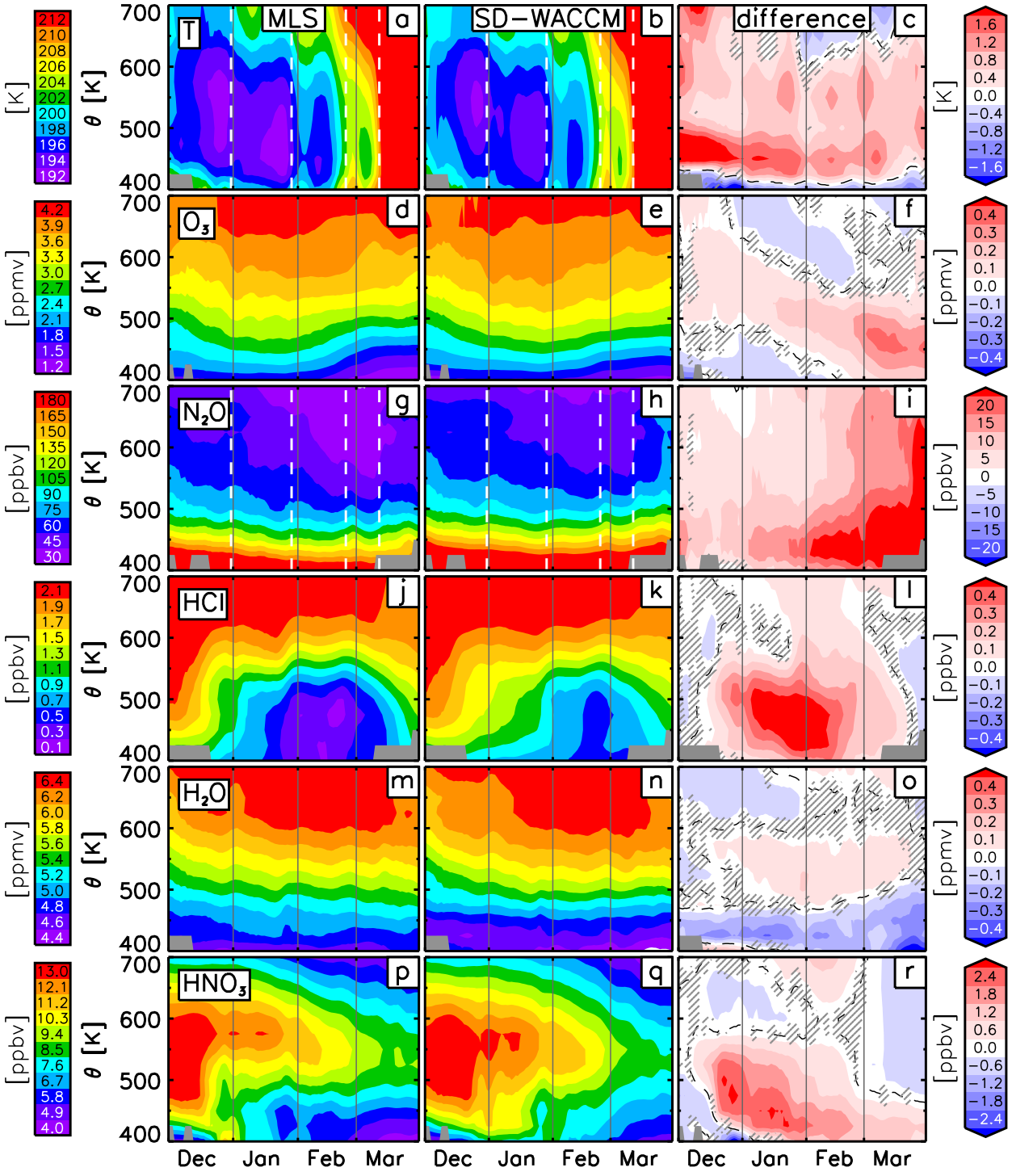

Figure 3.2: Evolution of vortex averaged MLS observations (left), SD-WACCM (center), and their difference (right) for temperature, O_3, N_2O, HCl, H_2O, and HNO_3 (top to bottom). Differences are calculated as (SD-WACCM - MLS). Gray areas denote potential temperatures where data were either missing or acquired only outside the polar vortex. White dashed lines indicate warming events mentioned in Section 3.1.3.2. Hatched areas in right column indicate differences that are not statistically significant at the 95 % confidence level. Black dashed lines denote the zero difference contour.

3.1.3.1 Temperature

SD-WACCM is nudged with GEOS5 temperatures, so lower stratospheric SD-WACCM temperatures differ from GEOS5 temperatures only insignificantly (not shown). MLS temperatures are shown in Figure 3.2a, SD-WACCM (equivalently, GEOS5) temperatures are shown in Figure 3.2b, and the differences between the two are shown in Figure 3.2c. Morphologically the temperatures are quite similar, and differences are usually less than ±2 K. At polar latitudes and between 100 hPa and 17 hPa, the validation of MLS version 3.3 temperature shows differences (GEOS5 minus MLS) of -0.5±0.3 K to +1.5±0.6 K [*Livesey*, 2011; *Schwartz et al.*, 2008]. Although small, the impact of these temperature differences on heterogeneous chemistry is significant; this is discussed in Section 3.1.4.2. Here the evolution of simulated and observed temperature is discussed in the context of dynamics only. PW activity causes deceleration of the zonal wind and thus a warming below the forcing region [*Shepherd*, 2000]. Such temperature increases are evident throughout the entire potential temperature range of 400-700 K in late December through early January, late January, in the second half of February through early March, and during the final warming around 10 March. All of these warmings are equally pronounced in the observations and SD-WACCM. The largest statistically significant temperature differences occur in December and January below the 500 K isentropic surface, with SD-WACCM overestimating temperatures by up to 3 K relative to MLS. In general GEOS5 and thus SD-WACCM temperatures are higher than MLS temperatures, a point that is further discussed in Section 3.1.4.2.

3.1.3.2 Ozone

The evolution of NH polar vortex O_3 during the winter of 2004-2005 from MLS and SD-WACCM is shown in Figure 3.2d and Figure 3.2e. The overall morphology of O_3 as simulated by SD-WACCM is in good agreement with that observed by MLS. Figure 3.2f shows that differences never exceed 0.35 ppmv; this corresponds to differences that are generally less than 15 %. Small (mostly statistically insignificant) differences on day 1 of the simulation are caused in part by an

inexact match between the actual MLS data and the gridded product used to initialize SD-WACCM. The inexact match on day 1 is due to the 7-day running average as well as the spatial smoothing explained in Section 3.1.2.

Figure 3.3 illustrates the O_3 variability within the vortex in more detail for the 475 K potential temperature level. Here the solid red (black) curve represents vortex mean SD-WACCM (MLS) O_3 mixing ratios during the 2004-2005 winter; shaded areas show the vortex mean $\pm 1\sigma$.On any given day the number of MLS profiles averaged is between ≈ 100 and ≈ 500. The standard deviation shown in Figure 3 reflects spatial variations inside the polar vortex. The model and measurements both show increasing O_3 mixing ratios until late January, followed by decreases throughout February and early March. SD-WACCM mixing ratios begin to diverge from MLS mixing ratios in late January, with differences reaching about 0.35 ppmv ($\approx 13\,\%$) by mid March. Part of this deviation is caused by the small high bias of ≈ 0.1 ppmv seen in Figure 2f above 500 K in early December, which descends throughout the season. We attribute the December high bias to a deficiency in the initialization procedure for O_3. The remainder of the difference between MLS and SD-WACCM seen in Figure 2f in March below 500 K is attributed to errors in chemistry as explained in section 3.4. The model shows considerably less variation inside the vortex than MLS, as indicated by the narrower shaded area in the model in Figure 3; but the 1s distribution in the model strongly overlaps the 1s distribution in the observations until early March. Based on the underlying distributions producing the averages, the Wilcoxon signedrank test shows that differences between vortex-averaged MLS and SD-WACCM O_3 mixing ratios are statistically significant after late January. Thus, Figures 2d-2f and 3 indicate that SD-WACCM in general overestimates O_3 during the Arctic 2004-2005 winter in the primary O_3 loss region inside the polar vortex below ≈ 525 K. To investigate the reasons behind this overestimate, diagnostics of transport and chemistry are evaluated in the following sections.

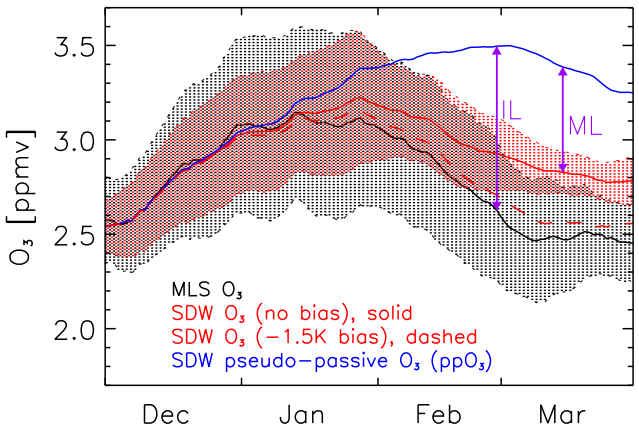

Figure 3.3: Evolution of vortex averaged MLS O_3 (black), SD-WACCM O_3 (red), and SD-WACCM ppO_3 (blue) at 475 K. Here, IL (purple) is the difference between MLS O_3 (black) and SD-WACCM ppO_3 (blue); ML (purple) is the difference between SD-WACCM O_3 (red) and SD-WACCM ppO_3 (blue). The black (red) shaded area is MLS (SD-WACCM) O_3 vortex average ± one standard deviation (σ) of the data used for the vortex average. Also shown is the evolution of vortex averaged SD-WACCM O_3 with a -1.5 K bias for heterogeneous chemistry (dashed red, see text).

3.1.3.3 Transport

Vertical transport and mixing in SD-WACCM are investigated by comparing modeled N_2O to MLS measurements. N_2O has a very long lifetime in the lower stratosphere, and is thus a good tracer of transport [*Loewenstein et al.*, 1990]. Figure 3.2g and Figure 3.2h show the observed and modeled evolution of vortex average N_2O. As for O_3, the overall morphology of SD-WACCM N_2O is similar to that observed by MLS. Contours at altitudes below about 600 K generally slope downward throughout most of December and January, indicative of diabatic descent inside the vortex. In February the model and measurement contours in this altitude range flatten; they rise toward the end of February, although not as much in the observations as in the model. This is consistent with descent being the dominant transport mechanism in December and January, with mixing becoming more important in February, as discussed by *Manney et al.* [2006]. As also noted by *Manney et al.* [2006], rapid increases in the N_2O mixing ratios after early March indicate the beginning of the vortex breakup.

There are, however, significant differences in the details of the MLS and SD-WACCM comparisons. In particular, SD-WACCM mixing ratios vary more smoothly than observed; for instance, there are smaller deviations during apparent mixing and warming events (indicated by the white dashed lines in Figure 3.2). At the time of the final warming around 10 March [*Manney et al.*, 2006], MLS N_2O mixing ratios indicate substantial mixing. SD-WACCM mixing ratios of N_2O show less

pronounced changes associated with the warming events. Throughout March modeled N_2O mixing ratios increase gradually and relatively smoothly. The final warming is captured appropriately in the simulation, as expected since the meteorology is nudged to GEOS5 data.

Differences between MLS and SD-WACCM N_2O are quantified in Figure 3.2i. On 1 December differences are below about +10 % (SD-WACCM>MLS). Differences on this date reflect deficiencies in the initialization. As shown in Table 3.1, SD-WACCM is not initialized with MLS data below 550 K, which explains the overestimate below 500 K. The overestimate at higher altitudes likely results from discrepancies that arise from the initialization procedure. Because of these initial disagreements, differences between MLS and SD-WACCM N_2O mixing ratios are interpreted here in a relative sense, focusing on their temporal evolution, not absolute values.

Figure 3.2i shows increasingly positive N_2O differences (SD-WACCM>MLS) in late February and early March in particular. Over the course of the season descent is gradually replaced by isentropic mixing as the dominant transport process [*Manney et al.*, 2006] and thus becomes less important for controlling constituent distributions. The most likely explanation for these positive differences, therefore, is errors in the SD-WACCM specification of isentropic mixing. At the altitudes shown here, N_2O mixing ratios are lower inside the vortex than outside. Thus an overestimate of N_2O mixing ratios inside the vortex would be consistent with too much SD-WACCM mixing across the vortex edge.

That SD-WACCM overestimates mixing across the vortex edge is supported by Figure 3.4, which shows N_2O profiles versus equivalent latitude in the descent-dominated early season (5 December, first column), in the mixingdominated late season (10 March, third column), and in between (20 January, second column). Equivalent analyses are shown for MLS (top row) and SD-WACCM (bottom row). Changes in N_2O that occurred in the first half of the season are shown by the differences plotted in Figure 3.4d (Figure 3.4i) for MLS (SD-WACCM). These differences indicate strong descent, as shown by a decrease in volume mixing ratio inside the polar vortex. The increase outside the polar vortex is caused by extra-vortex advection or mixing (see below). The N_2O plots for MLS and SD-WACCM on 5 December and 20 January are very similar in character,

so we conclude that descent is fairly well simulated by the model in the first half of the season. Changes in N_2O that occurred in the second half of the season, shown in Figure 3.4e (Figure 3.4j) for MLS (SD-WACCM), are more complex with respect to different zones inside the polar vortex [*Manney et al.*, 2006]: At the vortex edge, cross-edge mixing is dominant above 550 K, as indicated by the N_2O increase over time; below 550 K descent is the dominant transport, as in the first half of winter. Inside the vortex above ≈ 450 K, mixing becomes more dominant towards the core region of the polar vortex, as indicated by an increase in N_2O. SD-WACCM captures the overall behavior throughout the vortex, but shows a high bias in the N_2O change near the vortex edge (see Figure 3.4j). This indicates an overestimate in mixing across the vortex edge in SD-WACCM. To support this finding, Figure 3.5 shows the same panels as Figure 3.4 but for O_3. Below 500 K in late winter in particular, the O_3 gradient across the vortex edge is small compared to N_2O, i.e., effects of mixing across the vortex edge will be smaller than effects of descent, in contrast to N_2O. In fact, in the latter half of the winter the O_3 difference in Figure 3.5e and Figure 3.5j agree well with each other, emphasizing that descent is correctly simulated. Throughout the winter, a small cross-edge gradient exists above 500 K that is captured well by SD-WACCM. Thus, isentropic mixing results in a weak isentropic dipole structure, with declining O_3 just outside the vortex edge, and increasing O_3 just inside the edge. Such a weak dipole structure is evident above 600 K in Figure 3.5j, but not in Figure 3.5e. From both Figure 3.4 and Figure 3.5, we thus conclude that SD-WACCM is overestimating mixing across the polar vortex edge and within the polar vortex at all isentropic levels between 400 and 700 K. With regard to Figure 3.2g-h, we confirm the overestimate in isentropic cross-edge mixing in the latter half of the season; at the same time there is no clear indication for significant errors in descent.

The O_3 mixing ratios near the edge of the vortex are higher than those inside at altitudes between 400 and 700 K (not shown); thus too much mixing of air across the vortex edge and from the vortex edge into the vortex core in SD-WACCM would lead to a high bias in O_3, consistent with Figure 3.2f. In conclusion, SD-WACCM captures the general morphology of N_2O, but shows stronger mixing across the vortex edge and throughout the vortex in February and early March in

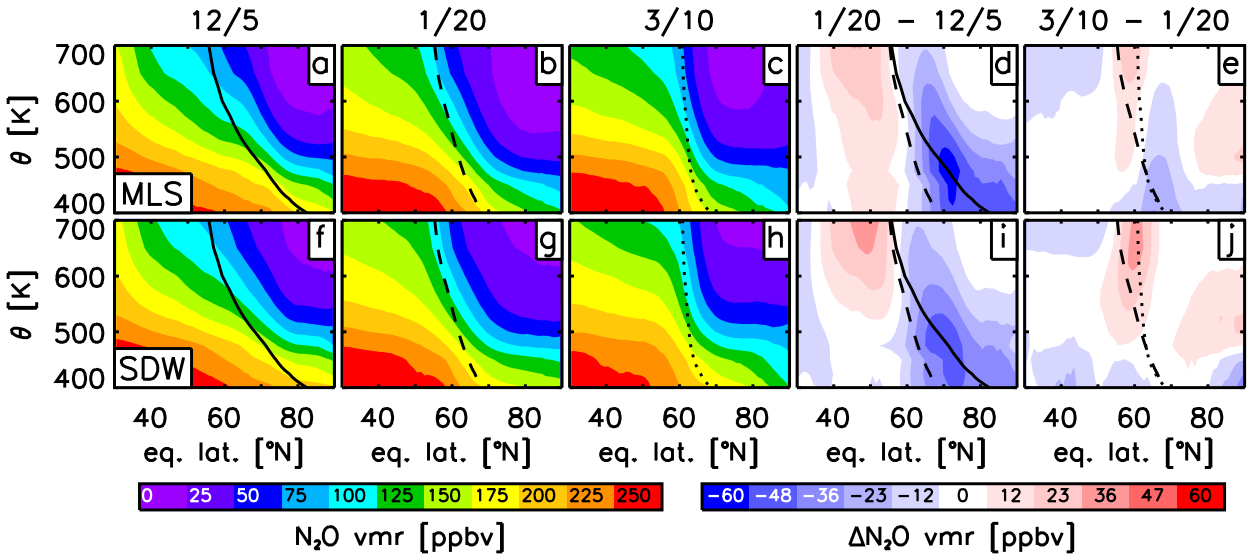

Figure 3.4: Distribution of N_2O from MLS (top) and SD-WACCM (bottom) versus equivalent latitude and potential temperature for the dates shown above each column. Superimposed in black is the polar vortex edge as a $1.4 \times 10^{-4} s^{-1}$ sPV line contour (line style coded by date). Panel d (i) shows the 20 January minus 5 December differences for MLS (SD-WACCM). Panel e (j) shows the analogous differences for 10 March minus 20 January.

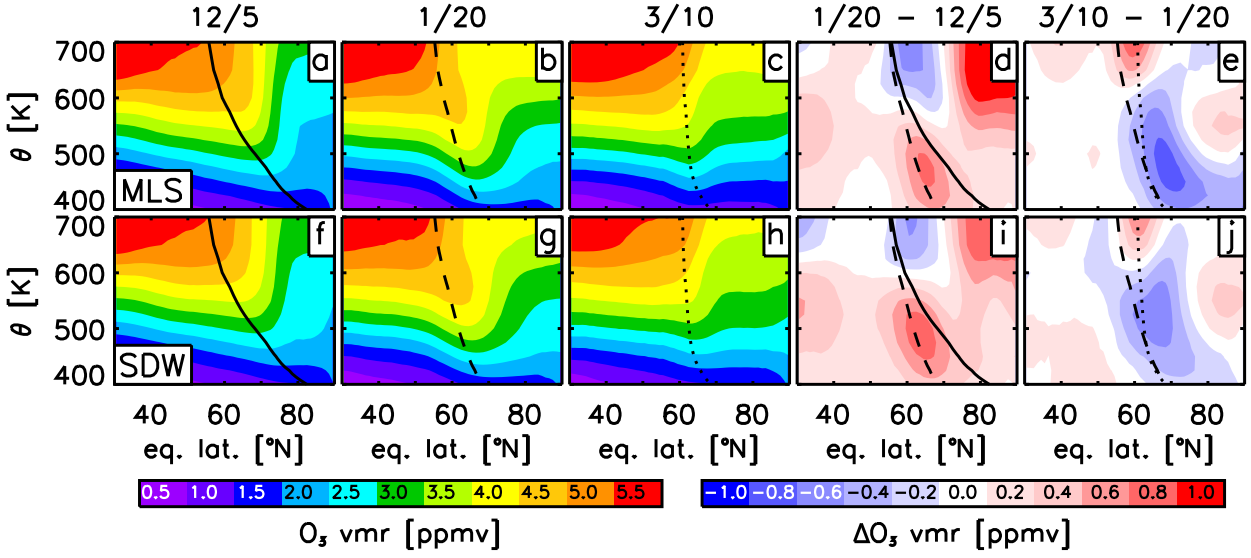

Figure 3.5: Same as Figure 3.4, but for O_3.

particular. This contributes to an overestimate in the simulated O_3 mixing ratios inside the vortex.

3.1.3.4 Halogen Chemistry

In the Arctic winter/spring lower stratosphere, Cl is important for catalytic O_3 destruction [e.g., *Brasseur and Solomon*, 2005]. Chlorine is present in the atmosphere either in the form of inactive, reservoir species HCl and $ClONO_2$, or in the form of reactive species ClO, Cl, hypochlorite dimer (ClOOCl), and HOCl. Of these constituents, the MLS instrument measures HOCl, HCl and ClO.

Figure 3.6 shows that during daytime SD-WACCM ClO is biased low relative to MLS by $\approx 34\,\%$ on average. If indicative of an underestimate in total reactive chlorine, this would be consistent with an overestimate of O_3 (underestimate of O_3 loss). Fully assessing the SD-WACCM treatment of reactive chlorine partitioning requires observations of Cl and ClOOCl in the vortex throughout the winter, but such observations are not available. We thus cannot infer from Figure 3.6 errors in total reactive chlorine.

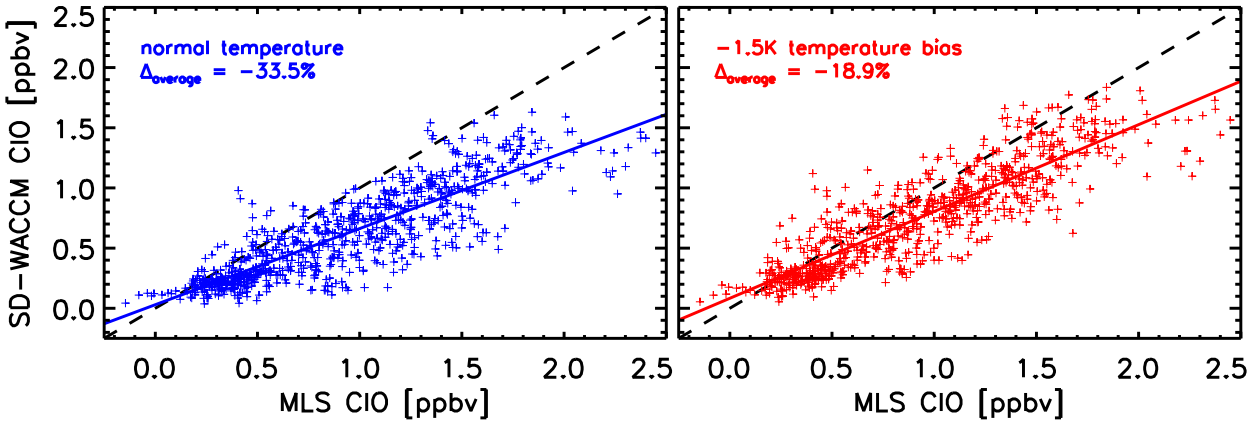

Figure 3.6: Scatter plot of SD-WACCM ClO versus MLS ClO (blue crosses) on 2 February 2005 between 400 K and 500 K inside the polar vortex. Only daytime values are shown here, identified by a solar zenith angle of less than 90°. The dashed black line shows the ideal 1:1 relation. Also shown is the scatter plot of ClO for the SD-WACCM simulation with a -1.5 K temperature bias for heterogeneous chemistry vs. MLS (red crosses). Linear regressions are shown as solid lines of the same color as the data on which they are based. These regressions only serve as a guide to the eye and were not used for any quantification.

Figure 3.2j and Figure 3.2k show that qualitatively, SD-WACCM and MLS HCl compare reasonably well. Both MLS and SD-WACCM show mixing ratios below 550 K that decline from

December into February, and then increase throughout March. The decline is steeper in MLS than in SD-WACCM, however, resulting in the high bias in SD-WACCM mixing ratios evident in Figure 3.2l in December-February below about 550 K. As an example, at 450 K MLS shows a decline in HCl of ≈94 %, whereas SD-WACCM shows a decline of ≈69 %. By late February, therefore, HCl mixing ratios at 450 K in SD-WACCM are higher than those measured by MLS by more than 50 %. We attribute the overestimate below 550 K to errors in chemistry, as described in the next two paragraphs.

The overall decline that is observed in HCl from January to February is caused primarily by heterogeneous processing of HCl. Based on observations from both MLS and the Atmospheric Chemistry Experiment Fourier Transform Spectrometer (ACE-FTS), [*Santee et al.*, 2008] found that before the onset of Cl activation, HCl at 490 K in the 2004-2005 Arctic winter vortex represented ≈75 % of Cl_Y. Heterogeneous processing led to a decline in HCl so that by late January it represented only ≈10 % of Cl_Y. That HCl in SD-WACCM declines less than in the observations is thus consistent with too little heterogeneous processing in SD-WACCM, which would lead to an underestimate of Cl activation. This might explain part of the overestimate in O_3 that is evident in Figure 3.2f, since an underestimate of Cl activation would lead to less chemical loss.

A possible factor contributing to the overestimate of HCl by SD-WACCM is an error in Cl reservoir partitioning. Studies have shown that the $ClONO_2$ abundance entering winter is rapidly converted to active chlorine by heterogeneous reactions on STS (and to a lesser extent NAT) by the reactions of $ClONO_2$ with HCl and H_2O [*Portmann et al.*, 1996]. Once the pre-winter $ClONO_2$ is depleted, additional HCl will not be significantly depleted until later in the winter, when photolytic processes reform $ClONO_2$. In this work, prewinter $ClONO_2$ is not initialized with observations due to scarcity of data on 1 December 2004. There is some indication that the model $ClONO_2$ is biased low (≈0.2-0.4 ppbv) in early winter, below 500 K, relative to ACE-FTS observations (not shown). However, the scarcity of $ClONO_2$ data limits this conclusion. The possible low bias in model $ClONO_2$ is not yet understood, but is most likely related to the uncertainty in the $ClONO_2$ gas-phase reaction kinetics, along with possible errors in transport that may lead to an underestimate

of prewinter abundances of inorganic chlorine and inorganic nitrogen. All other things being equal, such an underestimate will lead to too little chlorine activation, and thus too much O_3 (too little O_3 loss), consistent with the results in Figure 3.2.

As mentioned previously, this version of SD-WACCM includes a parameterization of HCl solubility in STS [*Lowe and MacKenzie* [2008]; *Wegner et al.*, 2013b]. This parameterization is highly dependent on the local water vapor abundance and temperature. *Wegner et al.* [2013b] have shown that a temperature sensitivity of ±1 K centered at 188 K, with a H_2O abundance of 4.5 ppmv, will change the fraction of HCl in the solution phase to the gas-phase from 25 % (-1 K) to 0 % (+1 K). In addition, assuming the atmospheric temperature is 188 K, the sensitivity of a ±0.5 ppmv H_2O abundance centered at 4.5 ppmv will change this same fraction from 20 % (+0.5 ppmv) to 0 % (-0.5 ppmv). Therefore, a high bias in temperature or a low bias in H_2O vapor will shift the HCl equilibrium from the solution to the gas-phase, thus contributing to the overestimate of modeled HCl. Modeled HCl condensation in this winter does not exceed a polar vortex average of 6 pptv in late January below 500 K (not shown), which corresponds to a maximum of ≈0.5 % of total HCl in the condensed phase.

3.1.3.5 PSC Formation

The ratio between inactive and reactive Cl is determined in part by the PSC surface area, since heterogeneous chemistry on the surfaces of primarily STS particles converts inactive Cl to the photoreactive intermediate Cl_2; per convention, we refer to this process as heterogeneous chlorine activation. Subsequent photolysis of Cl_2 then provides Cl for the catalytic O_3 destruction cycles [*Solomon*, 1999]. PSC particles in general are formed by uptake of H_2O and HNO_3, which can lead to permanent dehydration and denitrification if the PSC particles freeze and grow large enough to sediment. Errors in simulating H_2O or HNO_3 can thus indicate errors in simulating the PSC SAD, which would then lead to errors in Cl activation and O_3 loss if SAD was the rate limiting property. Thus, comparisons of MLS and SD-WACCM H_2O and HNO_3 can be useful for probing errors in the simulated partitioning between reservoir and active Cl.

Gas-phase H_2O from MLS and SD-WACCM, shown in Figure 3.2m-o, compare well; but there is a small (<7 %) low bias in the model below 475 K and a small (<3 %) high bias above 475 K in December through February. It is possible that the low bias indicates that SD-WACCM slightly overestimates the uptake of H_2O by PSCs. A transient decrease in gas-phase H_2O in late January below 550 K indicates the very brief period with water ice formation described by [*Jimenez et al.*, 2006], as well as the intrusion of extra-vortex air described by *Schoeberl et al.* [2006]. The overall morphology of SD-WACCM gas-phase HNO_3 is qualitatively similar to that of MLS, as shown in Figure 3.2p-r. Quantitatively, however, these comparisons are less favorable than the H_2O comparisons. Below 550 K, SD-WACCM exhibits a high bias in December through February, with short-term differences up to +30 %. In late January and mid February below ≈500 K, both SD-WACCM and MLS show transient decreases in HNO_3 separated by a brief increase, but the variations are less pronounced in SD-WACCM. The low HNO_3 mixing ratios at these times and altitudes likely represent pulses of increased heterogeneous processing in which gas-phase HNO_3 is taken up by PSCs. These pulses coincide with low temperatures shown in Figure 3.2a-b.

Figure 3.7 shows MLS and SD-WACCM partial columns of gas-phase HNO_3 from 400 K to 700 K. Also shown is the partial column of SD-WACCM condensedphase HNO_3 and the MLS temperature at 550 K. In contrast to Figure 3.2, Figure 3.7 shows column densities, which are vertically integrated quantities. The lower isentropic levels of Figure 3.2 are weighted more heavily than higher levels because the atmospheric density decreases with altitude. Therefore some of the SD-WACCM minus MLS differences that are apparent in Figure 3.2 are not evident in Figure 3.7. Partial columns of HNO_3 are discussed here as opposed to volume mixing ratios in order to show the total transient exchange between the gas phase and the condensed phase in the lower stratosphere. This exchange is largely controlled by temperature inside the vortex, but the resulting profiles of gas- and condensed-phase HNO_3 inside the vortex are also determined by the amount of descent. Therefore, comparisons of mixing ratios and temperatures on individual isentropic levels do not necessarily provide a self-consistent explanation of physical and chemical processes. For instance, after PSCs are formed by gas-phase HNO_3 uptake, they will descend. This means that atmospheric

temperatures at a lower isentropic level are not necessarily well correlated with condensed-phase HNO_3 that originated at higher altitudes. A similar argument can be made for gas-phase HNO_3 because of evaporation of PSCs due to higher temperature at lower levels. Thus, Figure 3.7 adds to the information that can in part be inferred from Figure 3.2 by showing partial columns rather than individual isentropic levels. The time series of gas-phase HNO_3 partial columns (Figure 3.7) for SD-WACCM and MLS show very similar relative variations. However, the absolute difference is consistent with the model's overestimate of gas-phase HNO_3 after mid December that is shown in Figure 3.2r. The late January and mid February episodic decreases in the partial column of gas-phase HNO_3 are accompanied by increases in condensed phase HNO_3 in SD-WACCM and decreases in temperature, suggesting that those transient declines in gas-phase HNO_3 were indeed caused by PSC uptake. Similarly, the strong anti-correlation from mid December through late February between SD-WACCM condensed- phase HNO_3 and gas-phase HNO_3 from both SD-WACCM and MLS suggests that many of the observed, short-term fluctuations in HNO_3 were caused by ongoing exchanges between the gas and condensed phases.

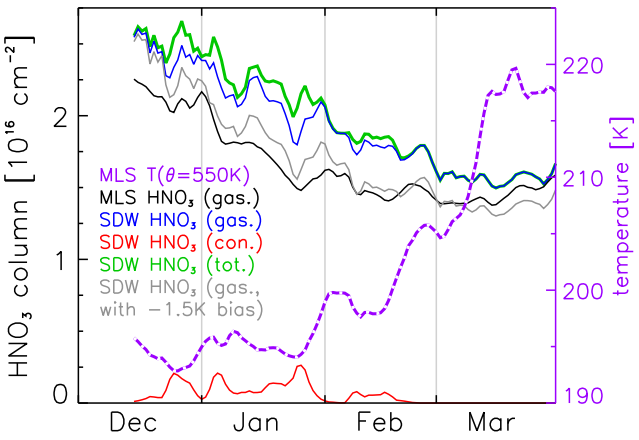

Figure 3.7: Partial columns (400-700 K) of polar vortex averaged gas-phase HNO_3 from MLS (black) and SD-WACCM (blue). Also shown is modeled condensed-phase HNO_3 (red) and total HNO_3 (green). Note that the sum of the condensed phase HNO_3 and the gas phase HNO_3 is exactly the total HNO_3. MLS temperature at 550 K is superimposed (dashed purple) following the right ordinate. Also shown is SD-WACCM gas-phase HNO_3 with a -1.5 K temperature bias for heterogeneous chemistry (gray). A 7-day running average is applied to all data shown.

Also shown in Figure 3.7 is the total (sum of gas-phase and condensed-phase) HNO_3 simulated by SD-WACCM. The simulated total HNO_3 declines gradually by $\approx 40\,\%$ throughout January and February, leveling off in March. This apparent loss of HNO_3 is due to diabatic descent and sedimentation of NAT particles to isentropic levels below 400 K, which is evident from Figure 3.2q

especially in late December through January. Transport from higher altitudes will also decrease the HNO_3 partial column, but not enough to account for the apparent loss shown in Figure 3.7. Also, isentropic mixing across the vortex edge reduces gas-phase HNO_3 inside the vortex because mixing ratios outside are generally lower between 400 K and 700 K (not shown). There is very little signature in the total HNO_3 of the transient pulse discussed above, while it is noticeable in the individual condensed-phase and gas-phase time series. This is further confirmation that the observed, short-term HNO_3 variations are simply indicative of an exchange of material between the gas and condensed phases. By the end of February, SD-WACCM indicates that no more condensed-phase HNO_3 is present; it is likewise reasonable to assume that at this time the MLS observations of gas-phase HNO_3 are about equal to total HNO_3 especially since the polar vortex average temperature is warm enough for most of the condensed-phase HNO_3 to evaporate. The model was initialized with MLS HNO_3, yet the total HNO_3 is higher in SD-WACCM than in MLS in March. This reflects a small (<10 %) underestimate by SD-WACCM of HNO_3 removal from the 400 K to 700 K vortex region. With the observations shown, however, it is not possible to quantify errors in the simulated uptake of HNO_3 by PSCs, in the estimation of PSC sedimentation, or in transport/mixing.

3.1.4 Discussion

The differences between SD-WACCM and MLS described in the previous section clearly have implications for quantifying chemical O_3 loss, as mentioned above. This section shows O_3 loss calculations based on the pseudo-passive subtraction technique [*Singleton et al.*, 2005]. For the temperature regime observed in the 2004-2005 Arctic vortex, reaction rates for the reaction of $ClONO_2$ and HCl on aerosol surfaces are especially sensitive to small temperature variations [e.g., *Lowe and MacKenzie*, 2008]. Hence, this section also discusses the temperature sensitivity of the O_3 loss simulations.

3.1.4.1 Ozone Loss

To calculate O_3 loss using the pseudo-passive subtraction technique, two simulations are run [*Singleton et al.*, 2005]. In the first, O_3 is fully active; it is allowed to participate in all relevant reactions, and active halogen species are produced via standard heterogeneous chemistry. This is the run to which MLS measurements have been compared in the previous section. In the second simulation, O_3 is treated as a pseudo-passive tracer. In this case O_3 is allowed to participate in all relevant reactions, but no halogen-containing heterogeneous chemistry is allowed, so halogens are not activated. The heterogeneous reaction of N_2O_5 with H_2O is allowed, in order to maintain the correct NO_Y partitioning. In many of the previous passive subtraction studies [e.g., *Manney et al.*, 1995; *Deniel et al.*, 1998; *Manney et al.*, 2003; *Grooß and Müller*, 2007; *Singleton et al.*, 2007; *Jackson and Orsolini*, 2008], O_3 has been treated as a fully passive tracer that is not allowed to participate in any chemical reactions. Because the lack of chemistry outside the vortex can lead to large errors in the amount of O_3 transported into the vortex, a fully passive tracer simulation was not employed in the work described here. In the pseudo-passive subtraction approach, the O_3 loss inferred from the observations (IL) is defined as the observed O_3 minus the simulated, pseudo-passive O_3. This difference quantifies the O_3 loss catalyzed by halogens activated by heterogeneous chemistry. In the potential temperature regime of 400 to 600 K, halogens are the dominant O_3 loss catalyst. Since NO_X is the dominant O_3 loss catalyst above 600 K, the O_3 loss presented here is representative of the total chemical O_3 loss in the lower stratosphere. Analogous to the IL, the modeled O_3 loss (ML) is defined as the simulated, fully active O_3 minus the simulated, pseudopassive O_3. Thus, the differences between the red (black) and solid blue curves in Figure 3.3 represent the ML (IL) using MLS and SD-WACCM results at 450 K.

Figure 3.8 shows contour plots of the vortex average inferred and modeled O_3 loss from 400-700 K throughout the winter. Note that since the IL is simply the measured O_3 minus the pseudo-passive O_3, and the ML is the simulated (active) O_3 minus the pseudo-passive O_3, the difference between the two panels in Figure 3.8 (not shown) is equal to the difference between MLS

O_3 and SD-WACCM O_3 in Figure 3.7f. As expected, both the inferred and modeled loss maximize in early March before the final warming. The altitude of the peak loss, both inferred from the observations and in the model, is at about 475 K. The O_3 loss inferred from the observations is larger throughout January-March, however, with a maximum inferred loss of about 1.0 ppmv and maximum modeled loss of only $\approx$0.6 ppmv. A more conservative choice of the polar vortex edge definition leads to slightly higher O_3 loss; e.g., an sPV threshold of 1.6×10^{-4}s^{-1} corresponds to a maximum of 1.1 ppmv for vortex-averaged O_3 loss.

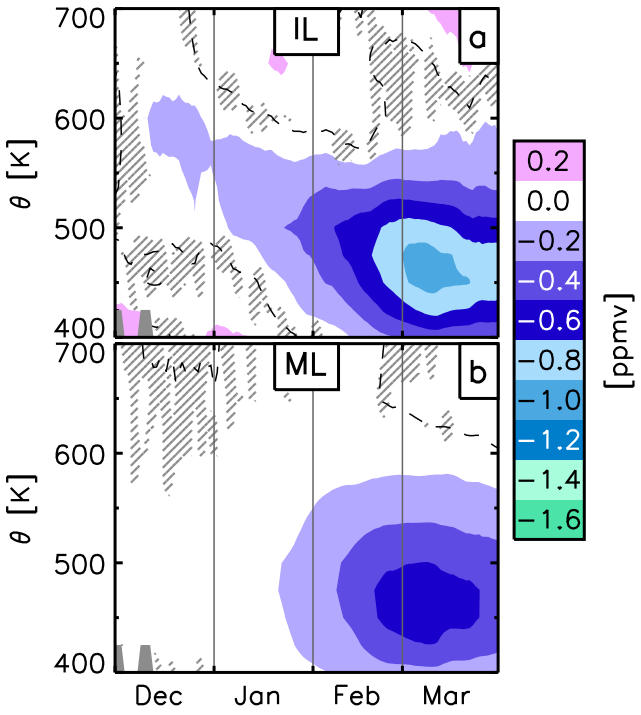

Figure 3.8: Evolution of the O_3 loss profile using the pseudo-passive subtraction technique for the inferred loss (MLS O_3 - SD-WACCM ppO_3;a) and for the modeled loss (SD-WACCM O_3 - SD-WACCM ppO_3;b). Both panels show O_3 loss due to heterogeneously activated halogens only. Hatched areas denote insignificant O_3 loss (95 % confidence level). Black dashed lines denote the zero O_3 loss contour.

Since polar vortex averages cannot be used to quantify local peaks in O_3 loss, Figure 3.9 shows the spatial distribution of inferred O_3 loss on the 475 K isentropic surface for 7 March 2005. This date and altitude were chosen to coincide with the greatest O_3 loss found in Figure 3.8. Note that for Figure 3.9 the whole day of MLS observations and sampled SD-WACCM output were gridded as described in Section 3.1.2. The superimposed polar vortex edge is from 12 UTC. The distribution of O_3 loss inside the polar vortex is not homogeneous: local inferred loss due to heterogeneous chemistry ranges from 0.4 to 1.6 ppmv. This is consistent with findings of local O_3 loss maxima by *Manney et al.* [2006]. Figure 3.9 also shows O_3 loss outside the polar vortex, which

likely arises from mixing across the polar vortex edge: an air parcel can experience O_3 loss inside the polar vortex and then be transported outside the polar vortex. Another possibility, in which an air parcel containing Cl_2 or activated Cl is transported outside the polar vortex, where O_3 loss then occurs, is rather unlikely due to efficient Cl deactivation outside the polar vortex [*Douglass et al.*, 1991; *Lee et al.*, 2002].

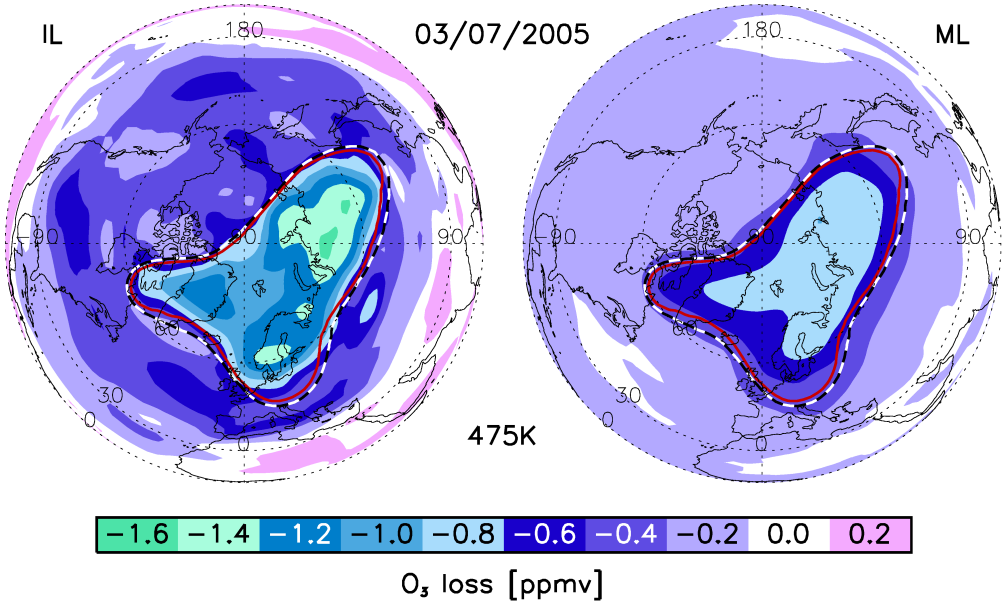

Figure 3.9: Spatial distribution of inferred O_3 loss (MLS O_3 - SD-WACCM ppO_3; left) and modeled O_3 loss (SD-WACCM O_3 - SD-WACCM ppO_3; right) at 475 K on 7 March 2005. The white/black dashed contour denotes the polar vortex edge as defined by an sPV threshold of $1.4 \times 10^{-4} s^{-1}$. The red contour line denotes the polar vortex edge using a $1.6 \times 10^{-4} s^{-1}$ sPV threshold.

As explained above, the most likely factors contributing to the differences between the inferred and modeled O_3 loss are too much mixing across the vortex edge and from the edge into the vortex core later in the winter, as well as too little halogen activation. In the absence of chemical O_3 loss, lower stratospheric O_3 mixing ratios outside the vortex would be lower than inside in late winter because of more descent inside the vortex. Too much mixing will therefore cause the simulated pseudo-passive O_3 in the lower stratospheric vortex to be underestimated; thus subtracting it from the observations will result in too little IL. Even though our mixing errors contribute a negative bias to the simulated O_3 in the lower stratosphere late in the winter, the simulated, fully active

O_3 mixing ratios are clearly too high (e.g., Figure 3.2f). Thus we conclude that even if mixing were simulated accurately, the HCl comparisons in late February suggest that SD-WACCM would underestimate chemical loss because of too little halogen activation. Indeed, the mixing errors are masking some of the halogen activation error that leads to too little simulated chemical loss.

3.1.4.2 Temperature Sensitivity

Temperatures inside the polar vortex drop sufficiently low for STS and NAT particle formation in the second half of December and January [*Lowe and MacKenzie*, 2008]. In addition, localized temperatures are sometimes sufficiently low for small scale water ice particle formation [*Jimenez et al.*, 2006; *Lowe and MacKenzie*, 2008]. The temperature differences between MLS and SD-WACCM that are shown in Figure 3.2c are significant in the context of PSC formation probabilities and heterogeneous reaction rates. Thus in order to quantify the sensitivity of the O_3 loss calculations to temperature variability and possible temperature errors, we repeated the full chemistry O_3 simulation with a temperature bias of -1.5 K for the uptake reaction coefficients for all STS reactions [*Lowe and MacKenzie*, 2008; *Shi et al.*, 2001]. Also affected by the temperature bias is the parameterization of SAD formed by STS and NAT particles, as well as the HCl solubility. The choice of -1.5 K as a temperature modification for the heterogeneous chemistry in WACCM is justified by the discrepancies between MLS and SD-WACCM/GEOS5 temperature as discussed in Section 3.1.3.1 and shown in Figure 3.2c at $\approx$450 K. The temperature modification also falls in the range of known biases in MLS temperature of -2 to +1 K for isentropic levels between 400 and 700 K with a precision of $\pm$0.6 to $\pm$0.8 K [*Livesey*, 2011]. In order to keep modeled dynamics consistent, the temperature bias is not applied in general but only to reaction coefficients and parameterizations in the heterogeneous chemistry module, as well as the HCl solubility in SD-WACCM.

Figure 3.10 shows the same comparison as done in Figure 3.2 but applying a -1.5 K temperature bias to heterogeneous processing only. Figure 3.10b-c show this modified temperature. Observed and modeled O_3 agree to within 0.2 ppmv. In addition, the initial high O_3 bias that descends throughout the season, as explained in Section 3.1.3.2, remains at a nearly constant value

of ≈0.1 ppmv. Figure 3.4 shows that an overestimate in mixing across the vortex edge does not significantly increase O_3 inside the polar vortex below 500 K, since the cross-edge O_3 gradient in late winter is small. As a tracer N_2O is not significantly changed by the temperature bias. In general, more HCl is heterogeneously processed with the -1.5 K bias, as can be seen from the fact that the SD-WACCM minus MLS differences are smaller (less positive) with the -1.5 K bias. This is also supported by an increase in ClO (Figure 3.6, right), improving the averaged underestimate by SD-WACCM from ≈34 % without the temperature bias to ≈19 % with the temperature bias. Modeled HCl condensation with the temperature bias does not exceed a polar vortex average of 32 pptv in late January below 500 K (not shown), which corresponds to a maximum of ≈3.5 % of total HCl in the condensed phase. But the late onset of heterogeneous processing, likely due to the $ClONO_2$ discrepancy and/or too little condensation of HCl as suggested in Section 3.1.3.4, is still evident. Note that below 500 K, applying the -1.5 K bias brought the simulated and observed HCl into better agreement. There is a ≤0.35 ppmv low bias in SD-WACCM H_2O relative to MLS (Figure 3.10o) in the region where there is a remaining high bias in HCl (Figure 3.2 and Figure 3.10), i.e., H_2O mixing ratios are independent of the temperature bias. This coupled with the uncertainty in the laboratory data [*Wegner et al.*, 2013b] used in the parameterization of HCl condensation could help explain the model high bias in HCl below 500 K. Above 500 K, however, the simulated HCl is now significantly too low. This makes sense since the temperature bias was chosen based on the 450 K level as described previously. Figure 3.10 and Figure 3.7 show improvement of modeled gas-phase HNO_3, especially from mid January to the end of the season. From the improvement of the above-described related diagnostics, we conclude that with the temperature bias the heterogeneous processing is represented more realistically in the model.

Figure 3.3 shows the effect of a 1.5 K temperature decrease on O_3 (dashed, red curve). The 1.5 K negative bias improves the agreement with observations from MLS (black curve) in February and March. When the temperature bias is applied, the maximum of the polar vortex averaged ML changes from 0.6 ppmv (shown in Figure 3.8b) to 1.0 ppmv (can be inferred from Figure 3.3, 7 March), which matches the IL. We conclude, therefore, that the parameterization of PSC mi-

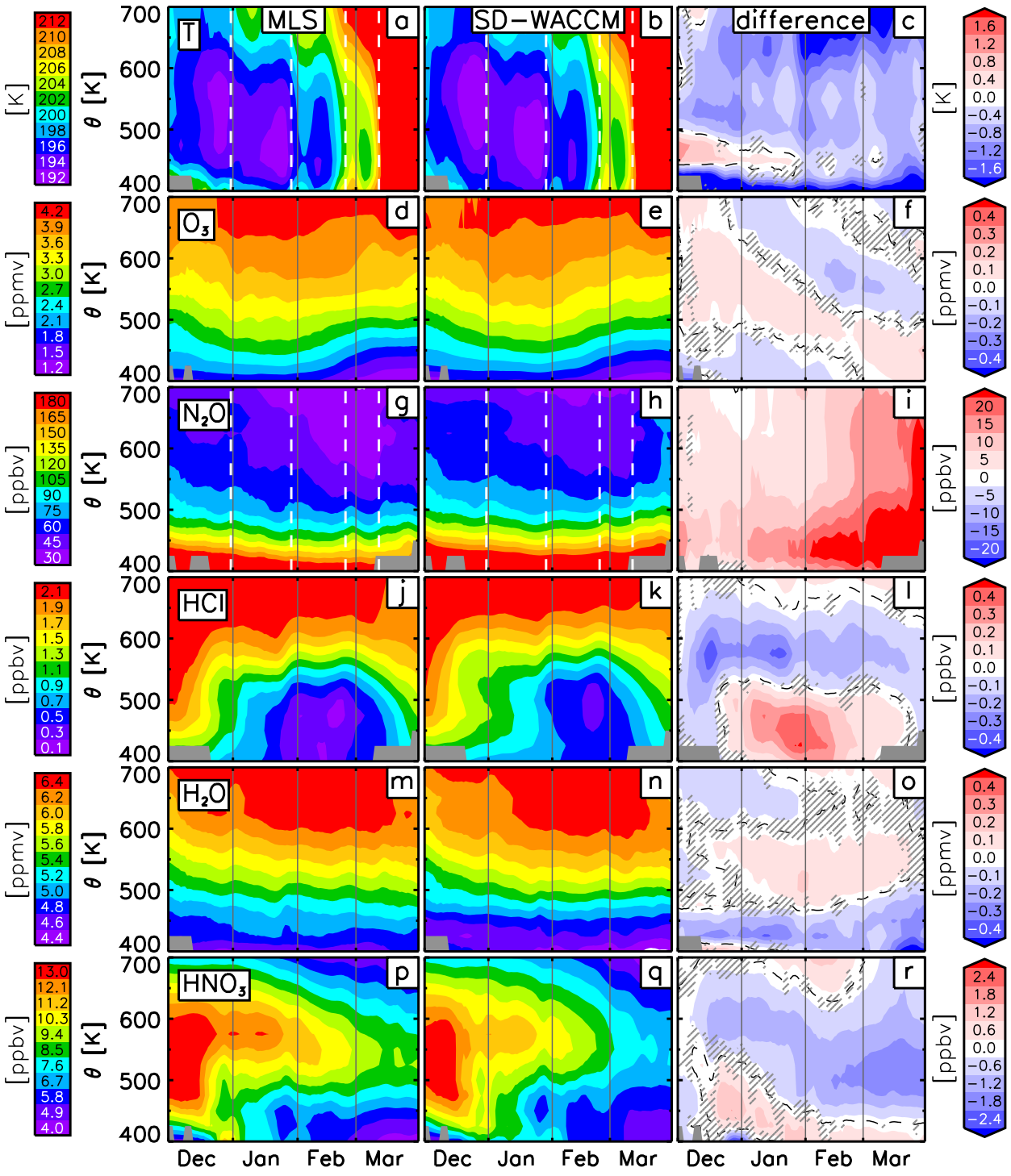

Figure 3.10: Same as Figure 3.2, but for SD-WACCM simulation using a -1.5 K temperature bias for heterogeneous chemistry reactions (see text).

crophysics in WACCM and the partitioning between NAT and STS in particular is improved as described by *Wegner et al.* [2013a]. *Lowe and MacKenzie* [2008] concluded that a sufficiently efficient and accurate parameterization of PSC microphysics and chemistry was not yet available for global chemistry climate models such as WACCM at that time. *Feng et al.* [2011] used the SLIMCAT 3-D CTM (SLIMCAT) coupled to a detailed microphysical model to study the 2004-2005 Arctic winter. Their simulations of denitrification and O_3 compared well with MLS observations, leading them to conclude, in agreement with *Lowe and MacKenzie* [2008], that robust simulations of Arctic O_3 loss in chemistry climate models might require a full microphysical treatment. Our results show that simulations using the improved WACCM PSC parameterization are sufficiently accurate to warrant its use in order to conserve computational resources.

3.1.5 Summary and Conclusions

The SD-WACCM simulations of O_3 inside the polar vortex in the Arctic winter of 2004-2005 generally compare well with O_3 observed by MLS. Agreement is within $\approx 10\,\%$, indicating that SD-WACCM is a useful tool for investigating polar O_3 loss. However, there is a persistent high bias in SD-WACCM O_3 in the O_3 loss region below 550 K that is likely caused by deficiencies in the initialization procedure for O_3 (+0.1 ppmv) and too little heterogeneous processing (+0.3 ppmv). SD-WACCM simulations are most likely deficient in $ClONO_2$ in early winter, so that even in the presence of significant aerosol surface area, the reaction of HCl with $ClONO_2$ is too slow. The reason for the underestimate of $ClONO_2$ is not yet understood. Also the condensation of gas-phase HCl is likely underestimated due to an underestimate in ambient water vapor and an overestimate in temperature. SD-WACCM slightly overestimates isentropic mixing across the polar vortex edge and between the outer and inner regions of the vortex; descent inside the vortex is well simulated.

Polar vortex average chemical O_3 loss was estimated to be 1.0 ppmv for the 2004-2005 Arctic winter using the pseudo-passive subtraction technique, with peak localized losses as high as 1.6 ppmv. Figure 3.11 compares absolute values of our vortex average results with previous findings based on various techniques that were briefly explained in Section 3.1.1. O_3 loss estimates

presented here are on the low end of the range of previous results. Vortex edge definitions used in the studies shown in Figure 3.11, however, were more conservative and thus emphasize O_3 loss in the vortex core more than in this study. A more conservative vortex edge definition is shown in Figure 3.9 as the red line and corresponding vortex averaged O_3 loss results are depicted by the red profile in Figure 3.11.

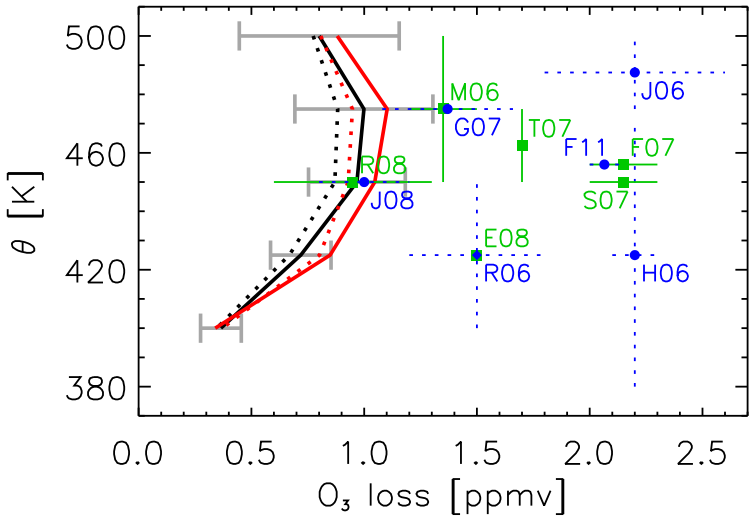

Figure 3.11: Comparison of our inferred (modeled) O_3 loss results (absolute values) shown as solid (dotted) line, using sPV thresholds of $1.4 \times 10^{-4}s^{-1}$ (black) and $1.6 \times 10^{-4}s^{-1}$ (red) as the vortex edge definition, with previous research listed in Section 3.1.1: *Manney et al.* [2006] (M06); *Jin et al.* [2006a] (J06); *Rex et al.* [2006] (R06); *von Hobe et al.* [2006] (H06); *Feng et al.* [2007a] (F07); *Grooß and Müller* [2007] (G07); *Singleton et al.* [2007] (S07); *Tsvetkova et al.* [2007] (T07); *El Amraoui et al.* [2008] (E08); *Jackson and Orsolini* [2008] (J08); *Rösevall et al.* [2008] (R08); and *Feng et al.* [2011] (F11). Horizontal and vertical lines show the O_3 loss range and the altitude range over which it was quantified. Blue and green colors as well as linestyles and symbols were chosen for better legibility and do not have any further meaning. Also shown are standard deviations of inferred O_3 loss results using an sPV threshold of $1.4 \times 10^{-4}s^{-1}$ (gray).

The temperature sensitivity study in Section 3.1.4.2 shows that the modeled evolution of O_3 agrees better with observations when a temperature bias of -1.5 K is imposed on heterogeneous chemistry reactions and SAD formation. In this case, only the high bias in SD-WACCM O_3 of ≈ 0.1 ppmv that is attributed to the initialization procedure remains. Imposing such a temperature bias, however, does not resolve the late onset of HCl depletion, which is likely due to a $ClONO_2$ deficiency and/or an underestimate of HCl condensation. In order to investigate the $ClONO_2$

deficiency, an in-depth analysis as presented here is planned for several winter seasons in which a better temporal coverage of $ClONO_2$ observations is available. Such an analysis also evaluates the interannual variability simulated by WACCM that could not be investigated in this study. Further work is required to more accurately simulate both isentropic mixing across the vortex edge as well as heterogeneous chemistry in WACCM.

In conclusion, we have shown through comprehensive model-measurement comparisons that SD-WACCM reliably simulates most O_3 related processes in the Arctic winter of 2004-2005, but questions remain regarding processes involving chlorine chemistry. Since models differ in, e.g., their parameterizations of various processes, the results of this study cannot be extrapolated in order to draw general conclusions about other CCMs and chemical transport models (CTMs). Thus similar in-depth analyses and model/measurement comparisons or model inter-comparisons, e.g., the SPARCs CCMVals Report [*SPARC CCMVal*, 2010], are necessary to assess other individual CCMs and CTMs.

Acknowledgments We thank C.S. Singleton for helpful discussions. M.B. and C.E.R. were funded by JPL/NASA grant 1350080 and NSF award AGS 1135432. The SD-WACCM simulations were carried out at NCAR. NCAR is sponsored by the National Science Foundation. Work at the Jet Propulsion Laboratory, California Institute of Technology, was done under contract with the National Aeronautics and Space Administration.

Chapter 4

SD-WACCM simulations of the Antarctic winter 2005

Contents

One of the goals of this study is to attribute separately O_3 loss caused by halogens and O_3 loss caused by NO_X. The main source of stratospheric NO_X is oxidation of N_2O transported from the troposphere. But in the middle and upper stratosphere in the polar winter, EPP can also contribute significantly to NO_X [*Randall et al.*, 1998, 2001, 2007]. The largest observed influx of NO_X from EPP to the SH stratosphere occurred in 2000 after the 14 July "Bastille Day" solar

proton event (SPE) [*Randall et al.*, 2001, 2007]. Thus for this investigation we quantify not only total O_3 loss caused by NO_X, but also separately quantify O_3 loss caused by NO_X created by solar proton (SP) during the SH winter of 2005. Only SPEs that occur during the winter (May-Aug) are expected to have large effects; since only small or moderate SPEs occurred during these months in 2005, one would not expect NO_X from SPEs to contribute substantially to O_3 loss during the SH 2005 season. It is possible that NO_X from precipitating electrons, during the SPEs and/or at other times during the winter, contributed to the O_3 loss observed that winter/spring, but this is not quantified in this investigation.

A secondary goal of this study is to quantify dynamical feedbacks from O_3 experienced by the experiment simulations: all experiment simulations are done with reduced chemistry, i.e., O_3 is expected to be higher in the experiment simulations compared to the reference simulation resulting in potential feedback on O_3 loss reactions.

4.1 Introduction

Chemical loss of polar stratospheric O_3 during the winter seasons is caused by several different processes. The two most dominant processes are catalytic destruction by halogens and NO_X. Accurately quantifying contributions to O_3 loss from these different processes is necessary in order to understand how stratospheric O_3 will evolve under changing atmospheric conditions. For instance, decreases in stratospheric halogen loading are expected to lead to decreases in halogen-induced O_3 loss [*WMO*, 2011a]. At the same time, increases in anthropogenic CO_2 emissions will cool the stratosphere [*Clough and Iacono*, 1995; *WMO*, 2011a]. This will lead to changes in reaction rates and circulation that might either increase or decrease O_3 loss rates, depending on the particular process involved.

This chapter describes an investigation of the SH winter of 2005 in which the contributions to observed changes in stratospheric O_3 from individual processes are quantified. The SH 2005 winter is an interesting one in that there were several moderately strong SPEs. Total O_3 loss and halogen-induced O_3 loss due to heterogeneous chemistry are quantified, the O_3 loss due to all

NO_X is inferred, and the O_3 loss due to NO_X created by the SPEs in this winter is quantified. This study also provides an analysis of dynamical feedback in experiment simulations that have changed chemistry. The investigation uses CESM/WACCM for a reference simulation matching observations and two experiment simulations with modified chemistry: the reference simulation includes full chemistry, in the first experiment simulation heterogeneous chemistry is switched off as done in Chapter 3 [*Brakebusch et al.*, 2013], and in the second experiment simulation no SPEs are included. As explained in Section 2.3, O_3 loss in the lower stratosphere is dominated by loss due to halogens, and O_3 loss in the upper stratosphere is dominated by catalytic reactions with NO_X. Contributions to the total column O_3 loss above the stratosphere are small in an absolute sense. Hereafter O_3 loss quantified as the difference between total O_3 loss and halogen-induced O_3 loss is thus assumed to be O_3 loss due to total NO_X. While this is a reasonable assumption, other O_3 loss processes, e.g., HO_X-induced O_3 loss, are part of what is here called total NO_X induced O_3 loss and are not explicitly quantified.

The SH polar vortex generally forms in March and April, and is well established by May. It often shrinks in September, and is well defined only in the lower half of the stratosphere (i.e., below $\approx 1000\,\mathrm{K}$) in October. In the SH 2005 season, robust conclusions about the upper stratosphere in October become difficult due to shrinking of the polar vortex and in November robust conclusions are possible only in the lower stratosphere.

During the SH 2005 winter several SPEs with medium to strong ionization impact occurred (see Figure 4.1). The strongest SPE occurred in September, and increased NO production all the way down to the stratopause. However, this NO_X was not observed to descend into the middle stratosphere where it might have contributed significantly to O_3 loss [*Randall et al.*, 2007]. EPP earlier in the winter from other SPEs and other geomagnetic activity produced upper atmospheric NO_X that subsequently descended and reached the stratosphere in June through August. The total amount of EPP-NO_X that descended into the stratosphere in the SH winter of 2005 was about average for the years 1992-2005 [*Randall et al.*, 2007].

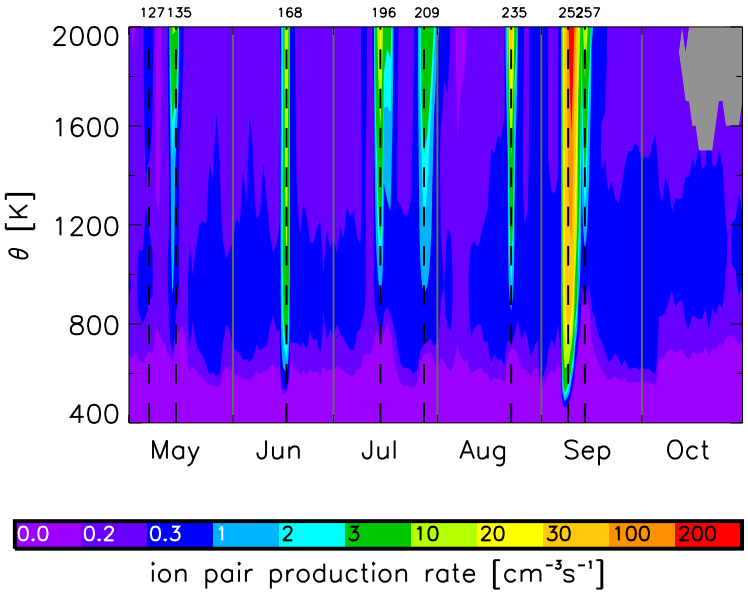

Figure 4.1: Evolution of the SP ion pair production rate in the stratosphere and lower mesosphere that is used to parameterize SPs in SD-WACCM.

In comparison with other winters, the SH 2005 season did not exhibit extraordinary total O_3 loss [*WMO*, 2011a].

4.2 Method

The model setup used in this work is the same as described in Chapter 3 [*Brakebusch et al.*, 2013], thus the description here is limited to a brief summary - the interested reader is referred to that study for more details. Model simulations for this study are all carried out with CESM 1.0.4 using the SD-WACCM compset. Specified dynamics (SD) for the model nudging of 5% come from the Modern-Era Retrospective analysis for Research and Applications (MERRA) [*Rienecker et al.*, 2011]. This 5% nudging is done between the Earth's surface and ≈ 50 km and is phased out between ≈ 50 km and ≈ 60 km. Above ≈ 60 km the model is essentially free running, i.e., as in WACCM without specified dynamics. MERRA assimilates several instruments [*Rienecker et al.*, 2011] which do not include MLS. Hence, differences between the two are not controversial. The evaluation of MERRA [*Rienecker et al.*, 2011] shows that errors in the Arctic stratospheric temperature does not exceed ± 0.1 K with an uncertainty of ± 1 K in the lower-most stratosphere and ± 2 K in the upper stratosphere. The climatological model initialization state on May 1 is updated with O_3,

N_2O, HCl, H_2O, and HNO_3 from the EOS MLS (hereafter called MLS) instrument as well as $ClONO_2$ from the Michelson Interferometer for Passive Atmospheric Sounding (MIPAS) in order to exactly represent the SH 2005 season. A temperature bias of -1.5 K for heterogeneous chemistry, SAD calculation, and HCl condensation on STS particles is incorporated in the model to balance overestimates in MERRA temperature (see Chapter 3 [*Brakebusch et al.*, 2013] and discussion of Figure 4.2 in Section 4.3 for details). All model output shown in this study is sampled in space and time to geolocations observed by MLS, unless otherwise noted.

In addition to a reference simulation with full chemistry, two experiment simulations are carried out. In the first experiment all heterogeneous chemistry is switched off[1] . Thus ClO_X is not created and all Cl stays in its reservoir species HCl and $ClONO_2$ (the same is true for Br). The O_3 species in the first experiment simulation is called ppO_3. Comparing ppO_3 to O_3 from the reference simulation yields a quantification of chemical O_3 loss due to halogens that were activated via heterogeneous chemistry. In the second experiment the ion pair production rate of SPEs is set to zero. For this simulation low energy (auroral) electrons are not modified; note also that no medium- or higher energy electrons (i.e., characteristic energy greater than $\approx$30keV) were included in any of the simulations. The comparison of O_3 from this experiment to O_3 from the reference simulation yields a quantification of O_3 loss due to additional NO_X created by SPs.

In each of the three simulations an ozone tracer (O_3TRAC) is included. On the first day (May 1) the O_3TRAC is set equal to O_3. After May 1 the O_3 species and O_3TRAC coexist, but O_3TRAC is not involved in any chemistry. It is necessary to have the O_3TRAC in addition to the fully active O_3 since the latter provides realistic feedback to the atmosphere (mostly heating by O_3 photolysis) that affects transport of O_3TRAC. In order to check whether there is any feedback from the reduced O_3 destruction seen in the pseudo-passive simulation, the O_3TRAC species from both the reference and the experiment are compared. If the differences between O_3 tracers are negligible, this indicates that differences between O_3 species from the reference and experimental simulations are truly due to chemistry only. Using SD-WACCM suppresses unrealistic feedback since temperature changes due

[1] Except the reaction $N_2O_5 + H_2O \longrightarrow 2HNO_3$ in order to maintain the NO_Y partitioning

to more O_3 in the pseudo-passive simulation are compensated by the temperature nudging. Thus dynamical feedback is reduced in a SD-WACCM experiment simulation. A similar explanation holds for the second experiment simulation regarding NO_X related chemistry.

In this study the subtraction method [*Manney et al.*, 1995] is used to isolate specific aspects of atmospheric chemistry. The basic concept is to compare a species from a reference model or observation to an experiment or "test" simulation in which the parameter of interest is perturbed. For instance, if chemistry is disabled in the test simulation, the subtraction method allows one to distinguish between effects of transport (i.e., advection) and chemistry (i.e., chemical creation and destruction of a species). This technique is then called the passive subtraction method [*Manney et al.*, 1995]. There are, however, three sources of uncertainties for this method: 1) dynamics in the model have to be accurate so that differences between the simulated tracer and the reference can be attributed to chemistry only [e.g., *Singleton*, 2006]; 2) both the reference species and the modeled species must start with the same "atmosphere"; i.e., the model needs to be initialized properly [e.g., *Singleton et al.*, 2005]; 3) feedbacks in an experiment simulation influence the species of interest in an unrealistic way since the experiment involves, e.g., omission of parts of chemistry, and is thus unrealistic itself; here dynamical as well as chemical feedbacks are possible. All three disadvantages are addressed in this study: the simulations are nudged with reanalysis data, the model is initialized with species from the observed atmosphere, and the O_3TRAC comparison provides a solution for dynamical feedbacks. The third concern about passive subtraction methods is not relevant for total O_3 loss since it is calculated as "O_3 minus O_3TRAC", both from the same simulation.

4.3 Evaluation Results

In this Section the evolution of polar vortex averages in the lower stratosphere from MLS and from the SD-WACCM reference simulation are compared using Figure 4.2.

4.3.1 Temperature

From late May through September, the polar vortex average temperature is sufficiently low ($\approx$ 195K) for PSC type I formation at most altitudes. The polar vortex is coldest in late July with temperatures below the nominal PSC type II formation threshold of 187 K. Since SD-WACCM temperature is nudged with MERRA temperature, essentially MERRA temperature is seen in Figure 4.2b. The nudging covers the entire vertical range shown here. The nudging temperature is higher than MLS observations.

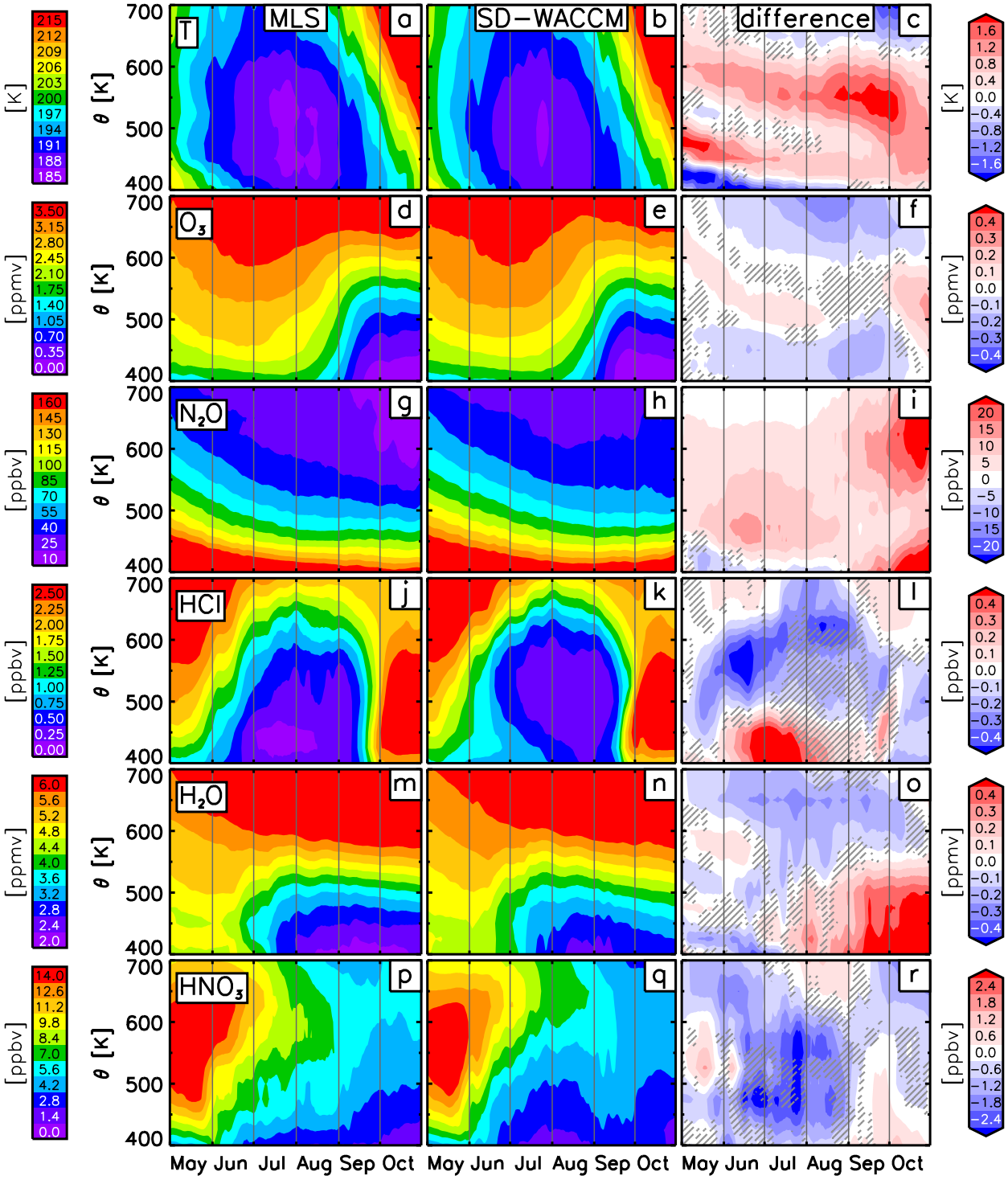

Figure 4.2: Evolution of vortex averaged MLS observations (left), SD-WACCM (center), and their difference (right) for temperature, O_3, N_2O, HCl, H_2O, and HNO_3 (top to bottom). Differences are calculated as (SD-WACCM - MLS). Gray areas denote potential temperatures where data were either missing or acquired only outside the polar vortex. Hatched areas in right column indicate differences that are not statistically significant at the 95% confidence level.

Thus a temperature bias of -1.5 K for heterogeneous chemistry, SAD formation, and HCl condensation on STS is applied for all simulations in this study as done in Chapter 3 [*Brakebusch et al.*, 2013] (in Figure 4.2b and Figure 4.2c the temperature before the temperature bias correction is shown). This temperature modification is still mostly within the MLS temperature observation accuracy (precision) interval of -2 K to +1 K (0.6 to 0.8 K) [*Livesey*, 2011].

4.3.2 Ozone

O_3 is in good agreement between MLS and SD-WACCM in the lower stratosphere with differences not exceeding ±0.3 ppmv. We can thus conclude that the heterogeneous chemistry improvements made for NH 04/05 (see Chapter 3 [*Brakebusch et al.*, 2013]) are also valid here. The onset of O_3 loss in the lowest stratosphere occurs in August and O_3 loss peaks in late September and October. Accuracy (precision) of O_3 measured by MLS is 0.05 ppmv to 0.25 ppmv (0.04 ppmv to 0.1 ppmv) [*Livesey*, 2011]. Thus differences between model and instrument shown here are within measurement uncertainties.

4.3.3 Transport

Due to its long chemical lifetime, N_2O is used as a tracer in the lower stratosphere in order to indicate discrepancies in descent and mixing across the polar vortex edge. An overestimate of mixing by the model across the vortex edge appears as an overestimate in Figure 4.2i since the volume mixing ratio of N_2O is higher outside the polar vortex than inside on the same isentropic surface. Likewise, an underestimate in descent by the model will lead to an overestimate of N_2O. A distinction between the two can be made by an analysis similarly to the one shown in Section 3.1.3.3. The strongest overestimate, of ≈25%, occurs in October when the vortex breaks up. The overestimate from May through September is usually below ≈15%. Given that the mid-winter discrepancy is very small, it is not further investigated. Overall the N_2O comparison looks better than in NH 04/05 (see Chapter 3 [*Brakebusch et al.*, 2013]); this can be attributed to a more stable vortex leading to less mixing across the vortex edge, which caused uncertainty in the NH. We con-

clude that the lower stratospheric O_3 loss maximum in late September is not affected by the small discrepancies found when comparing N_2O.

4.3.4 Halogen Chemistry

The onset of gas-phase HCl depletion occurs in May, and gas-phase HCl is depleted in the entire lower stratosphere until the rapid reformation of HCl in September. Although this model simulation was initialized with $ClONO_2$, the difference in gas-phase HCl between model and observations (Figure 4.2l) exhibits a similar morphology as found in Chapter 3 [*Brakebusch et al.*, 2013] for NH 04/05 where the simulation was not initialized with $ClONO_2$. The biggest difference occurs below ≈450K in June/July (Figure 4.2l) and coincides with too little HCl removal from the gas-phase in the simulation. This suggests that a particular process depleting gas-phase HCl is missing or is not properly implemented. We suspect that this process is the condensation of HCl on STS particles since that process is very sensitive to small temperature and H_2O changes [*Carslaw et al.*, 1995; *Wegner et al.*, 2012]. Looking at H_2O for this purpose, differences between MLS and SD-WACCM shown in Figure 4.2o are insignificant or small (<6%) for most altitudes and times when HCl is overestimated by the model in June/July below ≈500 K. The temperature bias described in Section 4.3.1 affects the HCl condensation on STS particles and reduces temperature differences in the region in question to zero. Hence, if the cause of the overestimate in gas-phase HCl is indeed due to an underestimate of HCl condensation, the implementation in the model might have to be revised. The impact of this discrepancy for lower stratospheric O_3 loss, however, is expected to be low since by the time O_3 loss commences in August, the same minimum of HCl is reached by the observations and the simulation, i.e., presumably the same amount of Cl is activated.

4.3.5 PSC Formation

In addition to increasing with altitude, gas-phase H_2O (Figure 4.2m) gets depleted when temperatures decrease below the PSC type II formation threshold of ≈187 K and H_2O condenses. The minimum in vortex-averaged H_2O is reached in late July (Figure 4.2m). Even after temper-

atures increase to levels high enough for PSC evaporation, H_2O remains depleted. SD-WACCM captures the gas-phase H_2O evolution well until September below 500 K (Figure 4.2n); differences are mostly <10%. After September, H_2O below ≈500 K is overestimated in the model simulation by at least 1 ppmv (>25%). This could indicate that too little dehydration via sedimentation of ice particles occurred during July/August in SD-WACCM, or that there is an error in transport that masks the sedimentation. The latter is currently investigated at NCAR [personal communication with Doug Kinnison].

HNO_3 is removed from the gas-phase by formation of type I PSCs. When the polar vortex breaks down, the increasing temperatures evaporate the PSCs if they were not removed from the stratosphere earlier via sedimentation. The latter is common in the SH due to prolonged cold temperatures below the type I PSC formation threshold of ≈195 K. The observations (Figure 4.2p) show a substantial decrease of about 10 ppbv during the season and no immediate recovery of the gas-phase after the polar vortex gets sufficiently warm for evaporation of PSCs in October (see Figure 4.2a). We can thus assume substantial denitrification due to sedimentation of PSC particles. Although the simulation was initialized with HNO_3 observations from MLS, significant model/instrument differences are found in early May. By June, these differences become insignificant below 550 K and are not exceeding -14% above 550 K. Thus, for the purpose of PSC formation, these differences are not considered important. Aside from this initial discrepancy, the simulation (Figure 4.2q) agrees well with the observations throughout the season, but shows a pulse of HNO_3 depletion in July and August that is not present in the observations. Since in the simulation HNO_3 is restored to the gas-phase in late August below 500 K (Figure 4.2q), even though temperatures are likely too cold for PSC evaporation, we doubt that the underlying reason for this discrepancy is related to denitrification. The apparent denitrification in July/August is investigated using Figure 4.3.

Figure 4.3 shows how the spatial distribution across the polar vortex edge evolves over the course of the season. In the vortex core, i.e., poleward of the $-2.0 \times 10^{-4} s^{-1}$ sPV contour (dashed line in Figure 4.3), gas-phase HNO_3 is completely taken up into PSCs during June. In the outermost

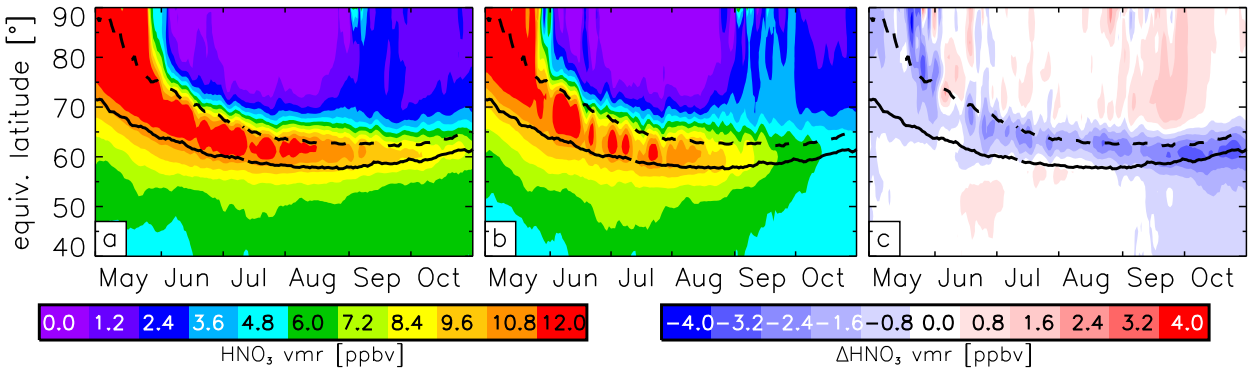

Figure 4.3: Evolution of gas-phase HNO_3 at 475 K between 40° and 90° equivalent latitude. The top edges of the panels represent the center of the polar vortex. Black lines denote sPV values $-2.0 \times 10^{-4}s^{-1}$ (dashed) and $-1.4 \times 10^{-4}s^{-1}$ (solid). The difference contour plot (right) is the difference between the SD-WACCM (center) and MLS (left) plot.

part of the polar vortex, i.e., between $-2.0 \times 10^{-4}s^{-1}$ and $-1.4 \times 10^{-4}s^{-1}$ sPV, gas-phase HNO_3 remains as high as before the onset of the denitrification in the polar vortex core as can be seen by the volume mixing ratio (VMR)s throughout the polar vortex area in May.

Looking back at Figure 4.2p and Figure 4.2q, the vertical structure of gas-phase HNO_3 seems to have descended less in June through August in the model than in the observations as indicated by the instrument/model difference in the maximum of the HNO_3 profile in late July and August. This is also confirmed by the model slightly overestimating N_2O. Given the rather negligible differences between simulation and observation of gas-phase HNO_3 in the polar vortex core (see right panel of Figure 4.3), we infer that condensed-phase HNO_3 is simulated well in the vortex core. We can thus conclude that condensed-phase HNO_3 is not overestimated in the simulation and that the subsequent denitrification is simulated properly. The latter is confirmed by the small gas-phase HNO_3 differences between model and instrument in September and October (Figure 4.2r). We thus conclude that despite the low polar vortex average of gas-phase HNO_3 the correct amount of HNO_3 is taken up to form PSCs.

4.3.6 Upper Atmosphere

In the upper atmosphere, i.e., above ≈2500 K (≈55 km), NO_2 volume mixing ratios become very small (not shown). While the morphology of observed NO_X is resembled in the simulations, absolute differences between model and instrument are large above ≈4200 K (see difference panel of Figure 4.4).

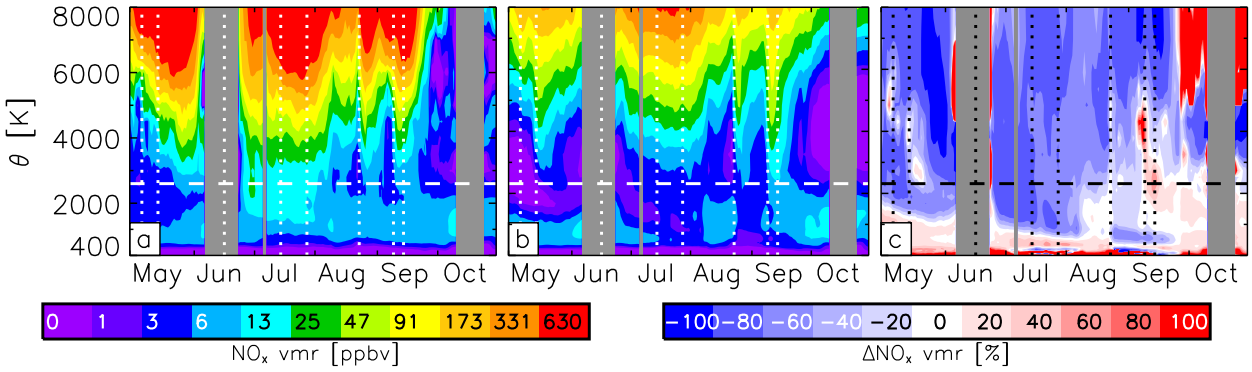

Figure 4.4: Evolution of observed (left) and modeled (center) middle and upper atmospheric NO_X in the polar region (latitude < -50°). The right panel shows the relative difference between observed and simulated NO_X. Also shown is the SD-WACCM nudging boundary as a horizontal dashed line as explained in Section 4.2). The vertical dashed lines indicate the strongest SPEs of this season (see text for details).

Observed NO_X increases in June/July and September/October between ≈2000 K and ≈4000 K are of particular importance for O_3 related processes since these enhancements of NO_X reach the stratosphere. Without using further diagnostics, it remains unclear whether the underestimate in June/July is due to insufficient production of NO_X or insufficient descent of NO_X. As for the strong SPE in September, the additional NO_X in the stratospheric region is overestimated by about 4 ppbv or ≈30% (difference panel in Figure 4.4). We can thus expect an overestimate of upper stratospheric O_3 loss in September/October (see O_3 loss discussion later) but no effect on chlorine deactivation, i.e., formation of $ClONO_2$, since the descending air mass with high NO_X does not reach the lower stratosphere.

Since carbon monoxide (CO) is a good tracer for upper atmospheric transport, it is used here

(Figure 4.5) to evaluate the upper atmosphere dynamics in order to distinguish between too little descent and too little production of NO_X which mimic each other. Because the CO abundance increases with altitude, an overestimate of CO likely indicates too strong descent. The CO difference panel shows that this is indeed the case, while vertical transport in the upper stratosphere and lower mesosphere in June/July looks reasonable. We can thus conclude that production of NO_X rather than descent causes the underestimate of NO_X in the upper stratosphere during June/July. Causes for too low production of NO_X might be an error in (1) the oxidation of N_2O (Reaction 2.24), (2) the implementation of low-energy (auroral) electron precipitation, and/or (3) the lack of medium energy electrons (MEEs) in SD-WACCM. From the diagnostics shown we can conclude that insufficient descent is not an issue here.

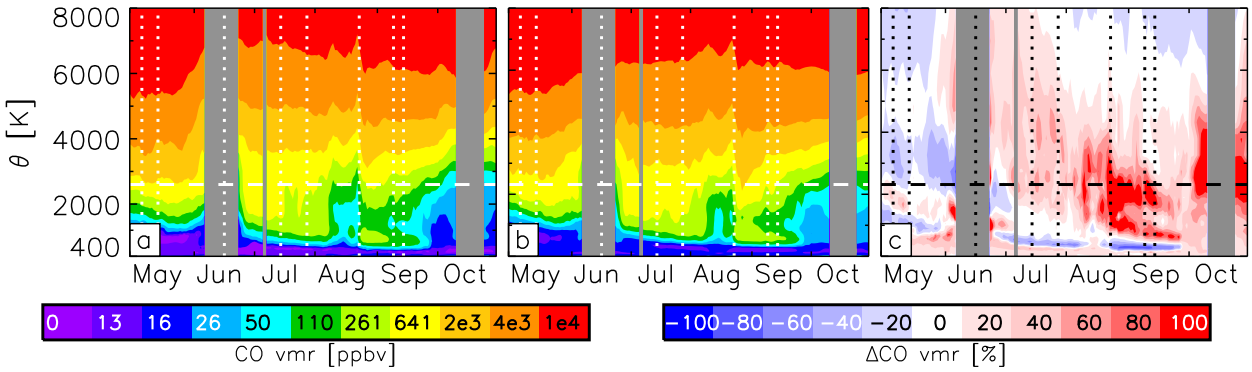

Figure 4.5: Same as Figure 4.4 but for CO.

4.4 Ozone Loss Attribution Results

In this Section the dynamical feedback of using the passive subtraction method is quantified before the O_3 loss attribution is presented. This allows quantification of the uncertainty in the results of the passive subtraction method.

4.4.1 Dynamical Feedback

As mentioned in Section 4.2, experimental simulations with reduced chemistry can alter dynamics via feedbacks from a changed O_3 abundance. In Figure 4.6, O_3 tracers (O_3TRAC) are compared.

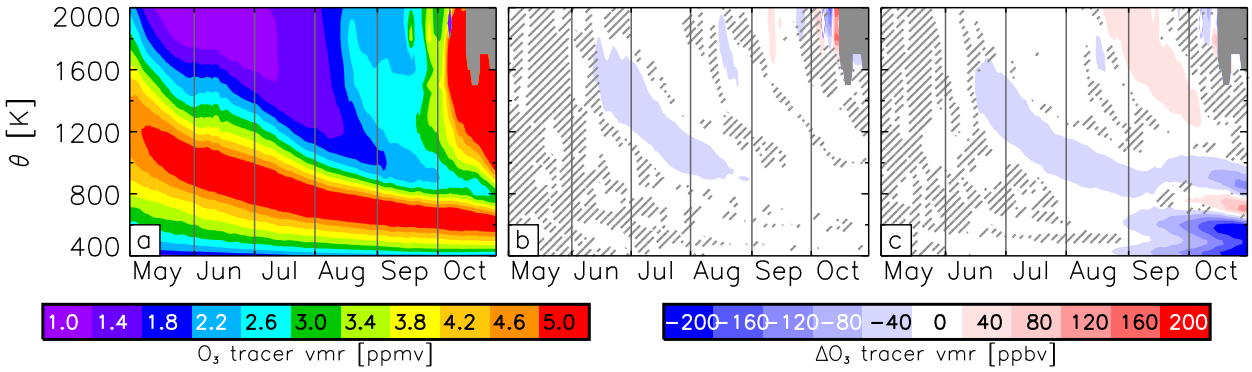

Figure 4.6: Evolution of O_3 tracers from the no SPE experiment (top-left), the full chemistry simulation (top-middle), and the no-heterogeneous-chemistry experiment (top-right) in the stratosphere. Differences between the experiments and the reference simulation are shown for the no SPE simulation (bottom-left) and for the no-heterogeneous-chemistry simulation (bottom-right).

For the no SPE experiment, absolute differences (bottom-left panel of Figure 4.6) are smaller than 0.04 ppmv almost everywhere and thus negligible compared to differences in O_3 shown in Figure 4.2f. We thus conclude that using the no-SPE O_3 tracer species in subtraction techniques produces realistic results.

For the no-heterogeneous-chemistry experiment, absolute differences (bottom-right panel of Figure 4.6) are largest in the stratosphere below $\approx$900 K in September through November. By the time observed O_3 reaches its minimum in late September (see Figure 4.2d), the difference between the tracers is $\approx$0.12 ppmv. Relative to the O_3 tracer, this difference barely exceeds 3% but compared to the O_3 abundance seen in Figure 4.2d and Figure 4.2e a difference of 0.12 ppmv corresponds to a 30% relative difference.

If the O_3 tracer from the experiment simulation is lower than the O_3 tracer from the reference simulation, then the O_3 species from the experiment simulation can be inferred as too low as well.

Since the difference between the O_3 species from the experiment and the O_3 species from the reference simulation is used for the O_3 loss calculation, the O_3 loss is underestimated by the same amount. In the case shown here the O_3 loss due to heterogeneous chemistry is thus inferred to be 0.12 ppmv larger than calculated by the subtraction technique alone.

4.4.2 Ozone Loss Attribution

As already known, the largest contributor to O_3 loss in the springtime Antarctic lower stratosphere, i.e., below $\approx$600 K, is O_3 loss due to activation of halogens via heterogeneous chemistry [*Brasseur and Solomon*, 2005]. This O_3 loss contribution is calculated as the difference between the fully active O_3 from the reference simulation and the O_3 species from the no-heterogeneous-chemistry experiment simulation (Figure 4.7a).

The largest O_3 loss of 3.1 ppmv due to this process is reached in late September at $\approx$450 K (Figure 4.7a). When the O_3 tracer comparison (Figure 4.6) is used as a correction, this increases to 3.22 ppmv. Statistically significant O_3 loss above $\approx$700 K likely reflects an uncertainty in the subtraction method since PSC formation, and thus halogen activation via heterogeneous chemistry, takes place below $\approx$650 K in the simulation of this season (not shown). The comparison between the O_3 tracers from the reference simulation and the no-heterogeneous-chemistry experiment simulation gives no indication of a discrepancy due to a dynamical feedback process in the mid-winter upper stratosphere. The contribution of O_3 loss due to NO_X generated by SPEs is calculated as the difference between the fully active O_3 from the reference simulation and the O_3 species from the no SPE experiment simulation (Figure 4.7b). The O_3 loss is very small and does not exceed 0.4 ppmv anywhere in the stratosphere. No impact from the SPE in mid-September is evident, as expected from [*Randall et al.*, 2007].

O_3 loss due to all NO_X (Figure 4.7c) is calculated as the difference between total O_3 loss and ppO_3 loss: (O_3 - O_3TRAC) - (O_3 - ppO_3). Mathematically this can be summarized as O_3 from the no-heterogeneous-chemistry experiment simulation minus the O_3 tracer from the reference simulation. The assumption that all O_3 loss that is not due to heterogeneously activated halogens

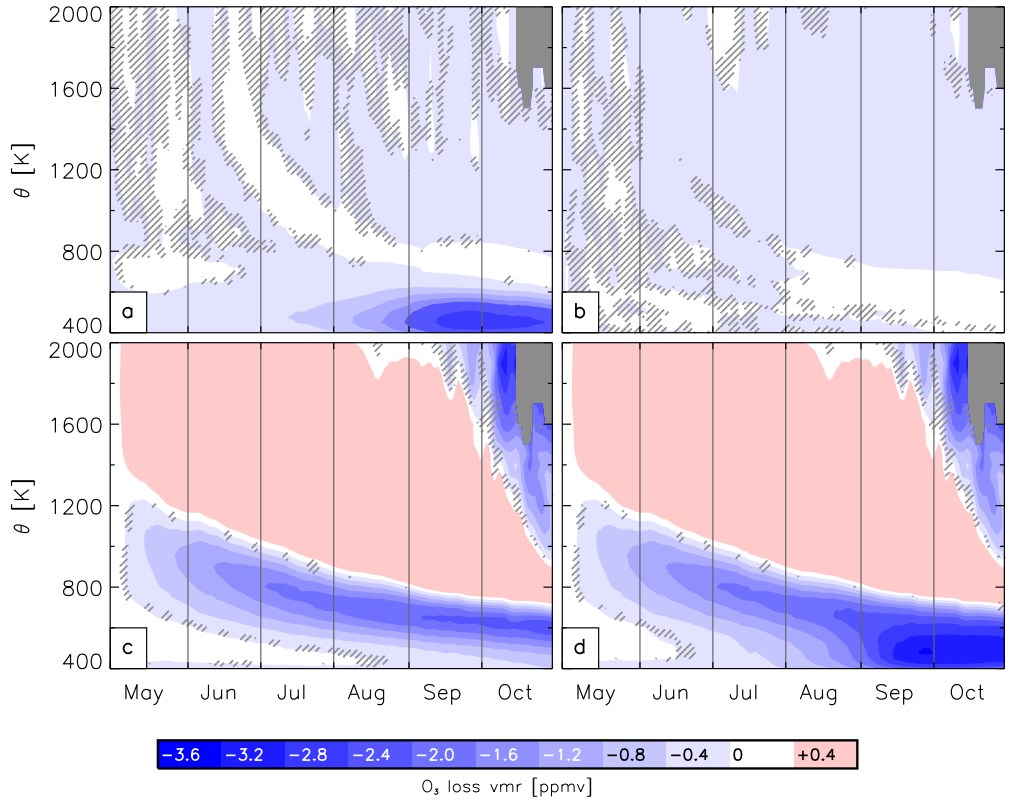

Figure 4.7: Evolution of modeled O_3 loss in the stratosphere due to halogen activation (a), NO_X created by SPs (b), and total NO_X (c). Also shown is the total O_3 loss due to all processes (d). For details see text.

can be attributed to O_3 loss due to NO_X, however, disregards O_3 loss that is due to gas-phase chemistry that was not preceded by heterogeneous chemistry. In particular that includes HO_X induced O_3 loss and part of ClO_X induced O_3 loss. This assumption is based on the fact that HO_X chemistry is not important below the mesosphere while ClO_X that is not coming from heterogeneous activation and NO_X are more important in the upper stratosphere [e.g., *Brasseur and Solomon*, 2005]. In summary, the described O_3 loss can also be named purely gas-phase O_3 loss.

The O_3 loss occurring in the mid stratosphere due to NO_X from N_2O oxidation can be identified as the descending O_3 loss throughout the season in Figure 4.7c; in the lower stratosphere O_3 loss of 2.7 ppmv is reached early November at $\approx$650 K. The O_3 loss in September and October between 900 K and 2000 K (Figure 4.7b) coincides with the timing of the NO_X increase subsequent

to the strong SPE event in September (see Figure 4.1 and Figure 4.4), but this O_3 loss cannot be identified in the SPE induced O_3 loss (Figure 4.7b). Thus non-SPE NO_X is likely the reason for the increased O_3 loss seen here. O_3 loss due to NO_X from EPPs other than SP is not quantified.

Figure 4.7d combines all O_3 loss processes described above and is calculated as the difference between O_3 and O_3 tracer, both from the reference simulation. Total O_3 loss in the lower stratosphere reaches 3.6 ppmv in late September at ≈480 K. For the UV absorption by O_3, the total number of O_3 molecules along the path of the radiation through the atmosphere is important rather than the volume mixing ratio at any given altitude. Thus the attribution of chemical O_3 loss to individual processes is investigated from a column density point of view in values of DU shown in Figure 4.8. The inferred total O_3 loss (MLS O_3 minus reference O_3TRAC) in the Antarctic 2005 season reaches a maximum of 158.4 DU in late September.

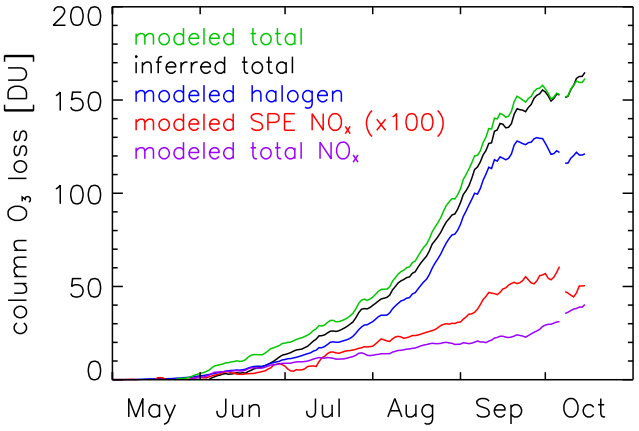

Figure 4.8: Evolution of inferred (black) and modeled (green) total chemical O_3 column loss between 400 K and 3000 K. Also shown are the O_3 column losses due to heterogeneous chemistry (blue), NO_X generated by SPEs (red), and total NO_X (purple).

Inferred total O_3 loss agrees well with modeled total O_3 loss of ≈157 DU; the timing of the simulated O_3 loss onset agrees with the observations. In June through August, total O_3 loss shown here is underestimated in the simulations by -5.0 DU ± 2.3 DU which corresponds to the small underestimate of simulated O_3 below ≈500 K seen in Figure 4.2f. The O_3 loss due to halogens activated by heterogeneous chemistry is as high as 119.5 DU; and the O_3 loss due to total NO_X reaches 37.8 DU. As expected from Figure 4.7, O_3 loss due to SPE-induced NO_X is very low and only reaches a maximum of 0.47 DU. All maxima occur in late September. After early October the upper stratospheric vortex breaks up, i.e., the upper part of the column is undefined, which

makes the calculation of the vortex O_3 column impossible. In summary, $\approx 76\%$ of the total O_3 loss is due to activated halogens, while the remaining $\approx 24\%$ is caused by NO_X from all sources. For this winter, NO_X from SPEs contributed only 0.3% of the total O_3 loss (or 1.2% of the total NO_X induced O_3 loss).

4.5 Conclusions

Investigating O_3 and related species for the SH in this study complements the evaluation of the NH carried out inChapter 3 [*Brakebusch et al.*, 2013].

Agreement with MLS is in general similar to the results from Chapter 3 [*Brakebusch et al.*, 2013]: differences in O_3 do not exceed ± 0.3 ppmv, which is within the uncertainty of MLS observations; the indicator of descent and mixing, N_2O, shows differences smaller than 15%; HCl shows substantial differences of 0.75 ppbv but reaches the same minimum by the time of the O_3 loss onset; H_2O shows agreement within 6% except a late winter model issue; modeled HNO_3 underestimates the observations, but is found to not interfere with the PSC formation; NO_X shows too little production in the upper atmosphere. We conclude that none of the differences between SD-WACCM and MLS found in the evaluation have a significant impact for O_3 loss investigations. The only exception is the underestimate of NO_X production by EPPs in the upper atmosphere since, via subsequent descent into the stratosphere, O_3 loss by NO_X could be increased significantly. We suggest that the incorporation of MEEs may fix this deficit.

The dynamical feedback from the modified chemistry in the experiment simulations is investigated: no significant dynamical feedback is found in the no-SPE simulation, but feedback in the no-heterogeneous-chemistry simulation cannot be neglected. For the latter experiment, a correction value of 0.12 ppmv is proposed in this winter. The model evaluation shown in Section 4.3 justifies the O_3 loss quantifications since they cannot be evaluated directly. The three O_3 loss processes are quantified: O_3 loss due to halogen activation via heterogeneous chemistry is 76%, O_3 loss due to total NO_X is 24%, and O_3 loss due to NO_X created by SPEs during this winter is 0.3%. It is expected that model improvement, e.g., implementation of MEEs, will increase the total NO_X

contribution relative to the halogen contribution. Hence the partitioning given here is valid for a quiescent winter regarding EPP. Overall we conclude that even if the anthropogenic halogen loading of the atmosphere reaches zero, at least 24% of the current chemical O_3 loss will still occur.

Next to the attribution of glso3 loss processes in the particular SH 2005 winter, this study contributes the experimental design for attribution studies. In addition an effective way to quantify errors in dynamical feedback in experiment simulations is developed which addresses the question raised in Section 2.4 about how to reliably investigate feedback processes.

Chapter 5

SD-WACCM simulations of the Arctic winter 2010/11

Contents

In this Chapter the unusual Arctic winter of 2010/11 is investigated. Methods for a full study are described in detail, and preliminary results are shown.

5.1 Introduction

In the Arctic winter season 2010/11 the largest NH O_3 loss occurred since the observational record began [*Manney et al.*, 2011]. In addition to cold temperatures and a prolonged season, unusual Cl partitioning was observed by, e.g., MLS and MIPAS: while $ClONO_2$ is usually depleted quickly due to heterogeneous chemistry shortly after the season onset, during the NH 2010/11 season

$ClONO_2$ was reformed, which commonly occurs only at the end of the season. Since $ClONO_2$ is usually the rate limiting factor for the reaction with HCl to form Cl_2, it determines the amount of Cl activation. In this winter, however, more than usual Cl activation was observed, possibly indicating greater availability of $ClONO_2$. The abundance of reactants, however, is not the only factor influencing Cl activation; in particular temperature and the formation/evaporation of PSCs play a huge role.

In this study we first evaluate SD-WACCM with MLS and MIPAS for the NH 2010/11 season using the same approach shown in Chapter 3 [*Brakebusch et al.*, 2013] and Chapter 4. Once the model/instrument differences are quantified, we investigate the Cl_Y and NO_Y partitioning using SD-WACCM. The model complements the observations since the above mentioned instruments can only provide an incomplete picture regarding species and sampling. This approach is explained in more detail in Section 2.3. The main question we address in this study is why the observed O_3 loss is high, despite numerous minor warmings that are usually associated with strong isentropic mixing events across the polar vortex edge, reducing O_3 loss. This questions the general assumption that more stable winter conditions, e.g., as observed in the SH, will lead to more chemical O_3 loss.

5.2 Hypothesis

In this study we investigate the chemical interplay during the NH 2010/11 season. We hypothesize that the large amount of O_3 loss was fundamentally caused by transient displacements of the polar vortex to lower, more sunlit latitudes. Through a complex mechanism, this resulted in increased Cl activation due to the reformation of $ClONO_2$ (see Section 2.4). The proposed mechanism is listed below.

(1) The polar vortex is formed by Dec 1, and the temperature inside the polar vortex gets cold enough to form PSCs in the second half of Dec. This coincides with a decrease in HCl, indicating formation of Cl_2 via Reaction 2.50; a decrease in $ClONO_2$ is expected at the same time. We can confirm this step by inferring PSC observations by interpreting HNO_3

and H_2O observations from MLS, and by investigating the evolution of HCl observations from MLS as well as $ClONO_2$ observations from MIPAS.

(2) PW activity causes temperature increases in the region of the polar vortex and displaces the polar vortex (see Section 2.1.2). These displacements to lower latitudes expose the polar vortex to sunlight several times throughout the season. This step can be confirmed by investigating the polar vortex temperature and polar vortex position, shape, and size. All of these can be analyzed using MERRA temperature and derived PV.

(3) The temperature increases described in step 2 cause evaporation of previously formed PSCs; thus gas-phase HNO_3 is increased. Therefore the reaction rate of gas-phase HNO_3 photolysis forming OH and NO_2 ($\lambda \leq 310\,\text{nm}$) is increased when the polar vortex is exposed to sunlight during a displacement from the pole. Observations of NO_2 from MIPAS may confirm this step; observations of OH from MLS are not available during the time range investigated here.

(4) NO_2 then reacts with previously activated ClO (see Reaction 2.32) and creates $ClONO_2$. While $ClONO_2$ is reformed, HCl does not increase, which changes the relative partitioning between the two. This step can be confirmed with ClO observations from MLS and MIPAS, $ClONO_2$ observations from MIPAS, and HCl observations from MLS.

(5) PSCs reform once the temperature becomes sufficiently low again. Thus gas-phase HNO_3 condenses and SAD for heterogeneous chemistry is increased (see Equation 2.57). The uptake of HNO_3 observed by MLS serves as a proxy for PSC formation here.

(6) Subsequently $ClONO_2$ created in step 4 reacts with the remaining HCl on newly formed PSCs, which increases Cl_2 (via Reaction 2.50). The decrease in $ClONO_2$ and HCl can be confirmed with observations from MIPAS and MLS.

(7) Exposure of the vortex to sunlight photolyzes Cl_2 ($\lambda \leq 350\,\text{nm}$) formed in step 6, and the O_3 loss rate is increased due to Cl-induced catalytic O_3 loss. Note that the "recycled" Cl

atom that was first taken up into $ClONO_2$ (step 4) is reproduced and an additional Cl atom was released from the HCl reservoir in step 6. Thus, the net result is double the amount of activated Cl relative to the amount that was removed from the process in step 4. This step can be confirmed by ClO observations from both MLS and MIPAS.

The net balance of the above described chain is the depletion of twice as many HCl molecules as $ClONO_2$ molecules. Since there are several minor warmings during this season, this chain of key processes is expected to repeat several times. In this process the partitioning of Cl_Y shifts from reservoir Cl towards ClO_X, which would not have been possible to the same extent without the intermediate PSC evaporation/formation and the exposure to sunlight. Thus, if this hypothesis is confirmed, the increased O_3 loss can be partly attributed to the polar vortex variability. The prolonged season, however, also contributed to the increased total O_3 loss that was observed [*Manney et al.*, 2011].

Although it is possible to confirm most steps with observations and reanalysis data, a model is needed to create a representative polar vortex average and to fill in missing species, in particular Cl_2. The work described here uses the WACCM model run in specified dynamics mode (SD-WACCM). Due to their sun-synchronous, polar orbits, MLS and MIPAS do not sample the polar NH region at all local times. MLS samples local times from 3 am through 1 pm; MIPAS samples local times from 10 am through 10 pm. To consistently explain processes in the polar vortex at any given point in space and time, simultaneous values for all polar vortex constituents are required. This requirement is fulfilled by using instantaneous or daily averaged output from SD-WACCM. The simulation used here is first evaluated based on its sampled output (i.e., similar to the evaluation described in Chapter 3).

5.3 Method

The model is set up in a manner similar to the study in Chapter 3 [*Brakebusch et al.*, 2013]. The simulation is initialized with O_3, N_2O, H_2O, HCl, and HNO_3 observations from MLS, nudged

with horizontal winds and temperature from MERRA data, and sampled to geolocations from MLS. Differences are the additional initialization of $ClONO_2$ using MIPAS data (see Chapter 4) and, in addition to using output sampled to instrument measurement locations, daily averaged model output are used for the partitioning results.

In the first part, MLS and MIPAS are used to evaluate SD-WACCM with all improvements made in Chapter 3 [*Brakebusch et al.*, 2013] and Chapter 4. SD-WACCM is compared to MLS temperature, O_3, HCl, and HNO_3 as well as to MIPAS $ClONO_2$.

In the second part, the model is used to investigate each step in the hypothesized chain of processes (see Section 5.2), since the model is independent of instrument sampling and data availability.

5.4 Evaluation Results

In this Section the evolution of polar vortex averages in the lower stratosphere in MLS observations is compared to the SD-WACCM reference simulation using Figure 5.1.

5.4.1 Temperature

Observations of polar vortex average temperature (Figure 5.1a) in the NH 2010/11 season reach minimum values of 192 K. Over the course of the season, however, the low temperature period is interrupted four times by minor warmings. The onsets (maxima) of the warmings are early January (Jan 8), end of January (Feb 3), late February (Mar 4), and mid-March (Mar 23).

Figure 5.1b shows SD-WACCM temperature, which is very close to MERRA temperature due to the nudging (see Chapter 3 [*Brakebusch et al.*, 2013]). However, as described in Chapter 3 [*Brakebusch et al.*, 2013] a temperature bias for heterogeneous chemistry, SAD formation, and HCl condensation on STS particles is used in this simulation. This modified temperature is shown in Figure 5.1b. Note that the temperature bias is only applied to part of the chemistry and not to the entire simulation in order to preserve consistency between nudging temperature and nudging wind fields.

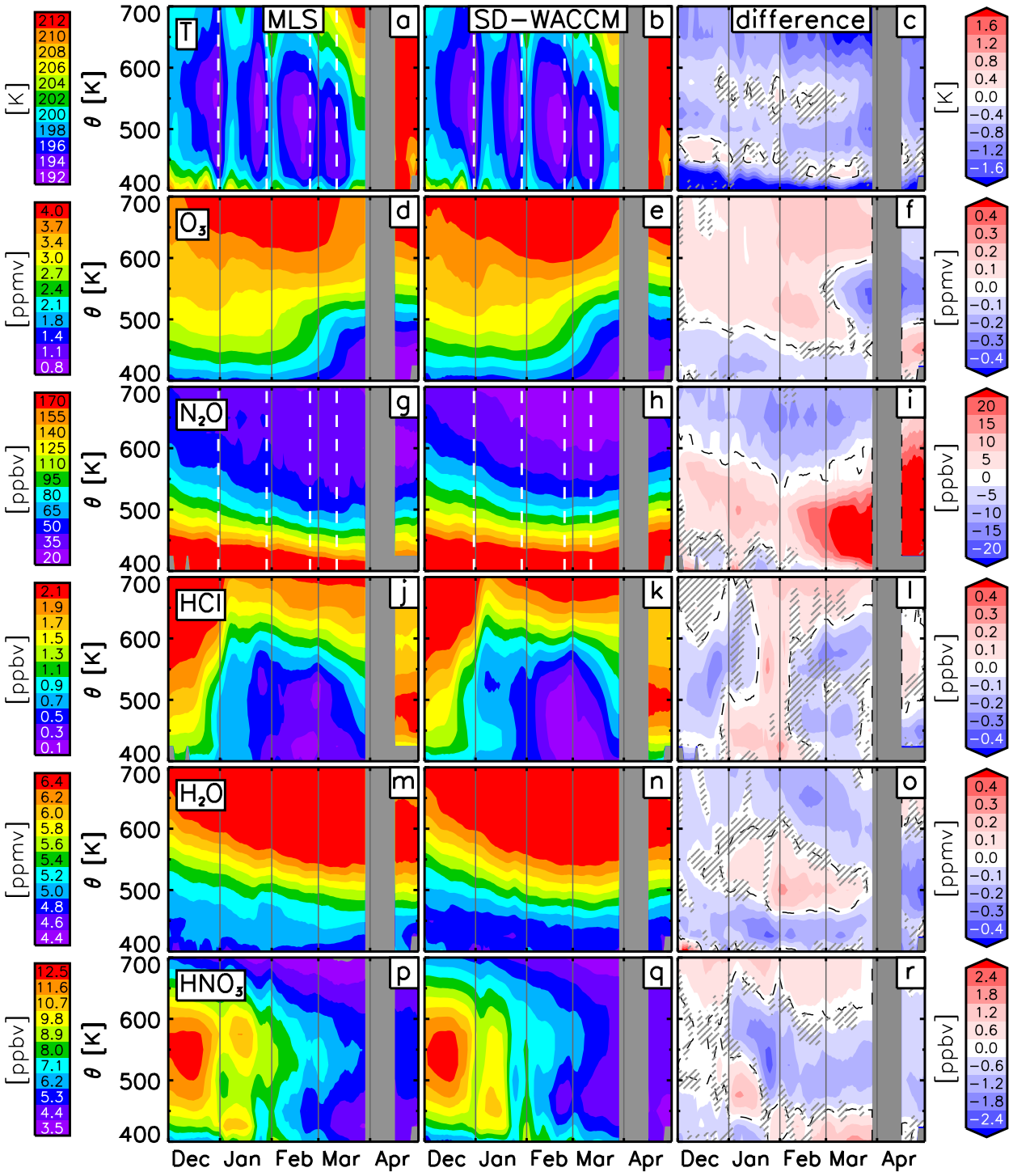

Figure 5.1: Evolution of vortex averaged MLS observations (left), SD-WACCM (center), and their difference (right) for temperature, O_3, N_2O, HCl, H_2O, and HNO_3 (top to bottom). Differences are calculated as (SD-WACCM - MLS). Gray areas denote potential temperatures where data were either missing or acquired only outside the polar vortex. Hatched areas in right column indicate differences that are not statistically significant at the 95% confidence level.

Differences between observed and adjusted MERRA temperatures are smallest at the 450 K level since the temperature bias was chosen so that instrument/model differences at this isentropic level are zero on seasonal average. The temperature on other isentropic levels is slightly underestimated in general due to the temperature bias, but the differences do not exceed -1.2 K where heterogeneous chemistry is important (425 K - 650 K).

5.4.2 Ozone

The onset of polar vortex average O_3 loss takes place in early February; largest O_3 loss in the lower stratosphere is reached by the end of March or early April. The entire period is not covered by MLS observations due to a temporal data gap between Mar 26 and Apr 19. Assuming that the largest O_3 loss is reached right before the final warming, we can estimate the largest O_3 loss to occur on April 3 (not shown).

The model simulates O_3 very well; differences between observations and model are smaller than ± 0.2 ppmv at all isentropic levels in the lower stratosphere until late March. It seems like O_3 is increasingly underestimated between 500 K and 600 K after mid-March, but an exact quantification is not possible due to the data gap. Extrapolating the morphology of O_3 discrepancies for the data gap in the lowermost stratosphere below 475 K hints at near-zero differences between model and instrument. Thus we assume that the O_3 minimum is correctly simulated.

5.4.3 Transport

In the lower stratosphere, the chemical lifetime of N_2O exceeds the timescale of dynamical processes, so N_2O can be used as an indicator of transport [e.g., *Brakebusch et al.*, 2013]. Decreasing VMRs along all isentropic surfaces until March indicate diabatic descent inside the vortex. Compared to Figure 3.2 in Chapter 3 and Figure 4.2 in Chapter 4, the diabatic descent in the NH 2010/11 season appears to be more similar to the SH 2005 season than to the NH 2004/05 season. This confirms the statement by [*Manney et al.*, 2011] that polar dynamics in the NH 2010/11 season are more typical for an SH winter. Increasing VMRs in March and April are an

indication of isentropic mixing across the polar vortex edge, since N_2O VMRs outside the polar vortex are higher than inside (not shown). Small changes in the slope of the described contours coincide with the minor warmings listed in Section 5.4.1. Compared to N_2O in the NH 04/05 winter (see Figure 3.2g-i in Chapter 3), the transient increases in N_2O are small, i.e., we can assume that only minor isentropic mixing with extra-vortex air masses due to the intermediate minor warmings occurred in the NH 2010/11 season.

The simulation reproduces the morphology of the observations, with differences not exceeding +16% below 600 K and 33% above 600 K in Dec and Jan. Starting in February, simulated N_2O VMRs gradually increase on isentropic levels below 600 K, overestimating the observations by up to 40%. A similar behavior was found for the NH 2004/05 season (see Figure 3.2h in Chapter 3) and the SH 2005 season (see Figure 4.2h in Chapter 4). There, the conclusion was drawn that SD-WACCM might overestimate isentropic mixing across the polar vortex edge. Since all other species in Figure 5.1 do not show systematic model/instrument differences beginning in late February and throughout March, no severe impact on the investigation shown in Section 5.5 is expected. Chemistry involving the Cl_Y (and NO_Y) family converts one family member to another and thus the total abundance of the family is not changed. Therefore Cl_Y and NO_Y are susceptible to changes in dynamics rather than chemistry and can thus be interpreted as tracers. Changes in the Cl_Y and NO_Y VMRs in late February and March may thus be interpreted regarding the discrepancy in mixing diagnosed here.

5.4.4 Halogen Chemistry

Lower stratospheric HCl is rapidly depleted in the second half of December and then reaches its minimum in late February more gradually. Below 550 K, 92% to 96% of HCl is removed from the gas-phase and is either activated, transformed into $ClONO_2$, and/or condensed on STS particles. Again, the highest isentropic level experiencing removal of HCl (≈700 K) is more typical for an Antarctic season (e.g., Figure 4.2j in Chapter 4) than for an Arctic season (e.g., Figure 3.2j in Chapter 3) as suggested by *Manney et al.* [2011]. Around the time of the final warming HCl

increases and gas-phase VMRs return to pre-winter conditions by mid-April.

The simulation agrees well with the observations, with differences usually not exceeding ±0.2 ppmv. In comparison to the NH 2004/05 study shown in Chapter 3, the model/instrument discrepancy in the HCl abundance below 500 K in January and February is significantly smaller. This is attributed to the initialization with $ClONO_2$, which is included for the NH 2010/11 season but could not be done for the NH 2004/05 season due to availability of observations.

5.4.5 PSC Formation

The comparison of H_2O and HNO_3 between MLS and SD-WACCM shows differences very similar to the findings in Chapter 3 [*Brakebusch et al.*, 2013]. Thus the conclusion that SD-WACCM compares well to MLS is considered to be valid here as well. The model/instrument agreement in bulk uptake of H_2O and HNO_3 suggests that a reasonable amount of PSC formation is simulated. Inferred from transient decreases of gas-phase HNO_3, PSCs are assumed to be present in late December / early January, in the second half of January, and throughout February. The fact that the gas-phase HNO_3 abundance does not return to early winter conditions after the final warming indicates substantial denitrification. However, Figure 5.1p is inconclusive regarding the timing of the denitrification that must occur during March until the final warming, i.e., no robust statement can be made from Figure 5.1p about availability of SAD in March and early April.

5.5 Partitioning results

In this section the evolution of the partitioning of Cl_Y and NO_Y is investigated in order to confirm the individual steps of the hypothesis described in Section 5.2. For this purpose Figure 5.2 shows output from the SD-WACCM simulations at 475 K.

According to the simulation of condensed phase HNO_3 (light green and cyan lines in middle panel of Figure 5.2), PSCs are formed in the NH 2010/11 season for the first time in the second half of December. This coincides with a rapid decrease in HCl and $ClONO_2$ (orange and purple lines in top panel of Figure 5.2) due to heterogeneous chemistry; only part of this uptake, however,

is reflected by an increase of ClO. The latter is inconclusive in that ClO only shows part of ClO_X. This paragraph, however, confirms the first step of the hypothesis.

During the first half of January, PSCs evaporate due to a temperature increase from the first minor warming. At the same time $ClONO_2$ increases gradually via Reaction 2.41, with NO_2 originating from HNO_3 photolysis. The expected decrease in ClO, however, cannot be confirmed from Figure 5.2. It is possible that the photolysis of remaining Cl_2 from the previous paragraph is balancing the ClO uptake here. This suggests that steps 2 through 4 of the hypothesis are correct.

When temperatures become sufficiently low again for PSC formation in the second half of January, HCl decreases further, which indicates an increase in the heterogeneous chemistry reaction rate of Reaction 2.50. Controversely, $ClONO_2$ increases during that time period which cannot be explained with Figure 5.2; a more comprehensive representation of Cl_Y is suggested (Section 6.3).

The minor warming in late-January / early-February coincides with a transient but steep increase in $ClONO_2$ and HCl. Right after this warming both HCl and $ClONO_2$ drop rapidly again indicating heterogeneous processing. By this time $ClONO_2$ abundances are higher than HCl abundances which is an atypical situation for polar winter seasons [e.g., *Santee et al.*, 2008].

Throughout February PSCs exist and HCl is further depleted while $ClONO_2$ remains about constant. Reactive Cl increases to its maximum in late February as inferred from ClO. At the same time the O_3 decrease (bottom panel) gets steeper.

During the first half of March both Cl reservoir species are reformed while ClO remains about constant. This behavior cannot be explained with the Cl_Y species shown so far. O_3 loss continues and about half of the O_3 loss seen in Figure 5.2 occurs during March, confirming that the prolonged season contributes to the total amount of O_3 loss [*Manney et al.*, 2011]. In conclusion we find no contradictions to the hypothesis posed in Section 5.2. A more detailed analysis especially including more ClO_X species would add to these preliminary results (see Section 6.3). A time series of solar insulation inside the polar vortex is beneficial but not possible with the sampled model output used in Figure 5.2. The model/instrument agreement shown in Section 5.4 and the brief investigation described in this section suggest that it is worth pursuing this analysis further.

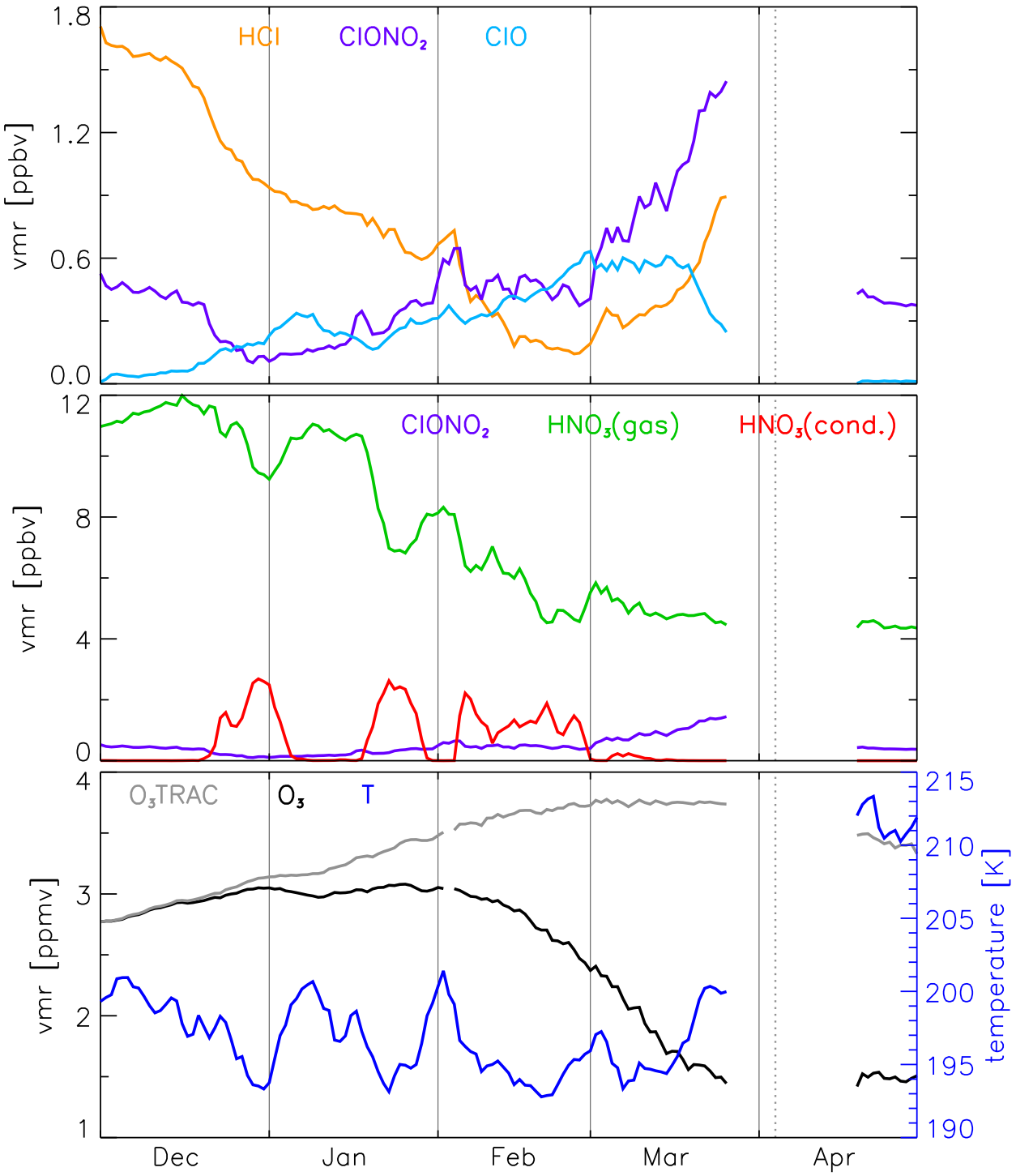

Figure 5.2: Evolution of polar vortex averaged Cl_Y partitioning (top), NO_Y partitioning (middle), and O_3, O_3TRAC, as well as temperature (bottom) at 475 K. In the middle panel, the sum of all species appearing in the legend is approximately the same as NO_Y before the vortex breaks up. In the bottom panel, the difference between O_3TRAC (gray) and O_3 (black) is the total O_3 loss at 475 K.

Chapter 6

Conclusions and Outlook

Contents

In this chapter the science questions posed in Section 2.4 are answered in the first section; contributions to the scientific community are listed in the second section. The chapter concludes with a third section about an outlook on future plans.

6.1 Conclusions

The studies shown in Chapters 3, 4, and 5 answer the science questions posed in Section 2.4. This section provides these answers as well as embeds them in a greater scientific context.

(1) *Is SD-WACCM a tool sophisticated enough for quantitative O_3 evolution investigations?*

In Chapter 3 [*Brakebusch et al.*, 2013], SD-WACCM is thoroughly evaluated with regard to the evolution of winter polar stratospheric O_3. By means of a NH 2004/05 case

study, SD-WACCM is found to be a useful tool to quantify the O_3 evolution; remaining model/instrument discrepancies are identified and explained. The absolute comparison between observations and SD-WACCM output is mandatory to identify processes that need improvement in the model. As a further conclusion, accurate temperature is found to be a key requirement for simulating the effects of heterogeneous chemistry on PSC surfaces. Answering the above science question entailed several improvements in SD-WACCM which are explained in detail in Chapter 3 [*Brakebusch et al.*, 2013] and Section 6.2.2. SD-WACCM is then used for the SH 2005 season (Chapter 4) and the NH 2010/11 season (Chapter 5) with results of similar quality. Thus the conclusion that SD-WACCM is a useful tool to quantify O_3 evolution is confirmed. For the scientific community, improving SD-WACCM results in a well evaluated CCM available for polar stratospheric O_3 studies - now SD-WACCM output of polar stratospheric O_3 and related species can be used with confidence.

(2) *What are the individual contributions of halogens, NO_X from EPP, and NO_X from N_2O to O_3 loss in the polar vortex?*

The SH 2005 season is used in Chapter 4 as a case study because of moderately strong SPE activity. Separation of the individual processes contributing to O_3 loss shows a partitioning of $\approx 74\,\%$ column O_3 loss due to halogen chemistry and $\approx 26\,\%$ O_3 loss due to NO_X, of which $< 1\,\%$ is due to SPEs. NO_X enhancements in the observations that are not simulated are likely due to the missing MEE implementation in SD-WACCM. For the scientific community this study enables a quantification of future O_3 loss in the mid to late 21st century when the halogen burden of the stratosphere relaxes back to natural abundances. The method applied in Chapter 4 can be extended to a quantification of NO_X induced O_3 loss in simulations investigating climate change.

(3) *Why is the observed O_3 loss in the NH 2010/2011 winter so high, despite high dynamical variability, which is usually associated with less O_3 loss?*

From the preliminary results shown in Chapter 5 it is inferred that the hypothesized chain

of processes (see Section 5.2) is valid: it is suggested that severe O_3 loss in the NH 2010/11 can in part be attributed to the atypical intermediate formation of $ClONO_2$ and is not due to the prolonged season alone. In Section 6.3 improvements to the analysis are described.

6.2 Contributions

Substantial contributions of both a technical and scientific nature are made by the presented work . This section illustrates these two sets of contributions.

6.2.1 Technical contributions

In order to develop a sophisticated analysis, several technical improvements were necessary first to streamline the analysis procedure.

As explained in [*Brakebusch et al.*, 2013], a model initialization with data from the instrument used for the model evaluation is necessary. The technical requirement for this initialization is to create a gridded data product from the observations to match the model resolution. This procedure is explained in Appendix A and the implementation is described in [*Brakebusch et al.*, 2013].

In order to evaluate the model with any instrument, the model output must be sampled at the geolocations, i.e., space and time, observed by the instrument. This is done by means of a prescribed list of these geolocations, which is called a "satellite history" file and was developed as part of this work. This file may contain observed geolocations from several instruments to enable multiple evaluations. The "satellite history" file was constantly updated; the current version of the file, including 37 instruments for the time range of 1970 through present day, contains more than 67 million observations and is also used for the SPARC Earth System Model Validation (ESMVal) effort. More details about the creation of the satellite history file can be found in Appendix D.

Artificial model tracers were created for NO_X, NO_Y, and O_3. Without the latter the attribution of O_3 loss (Chapter 4) is not possible. The key characteristic of these tracers is that they do not replace their chemical equivalent but instead coexist. Thus the simulated atmosphere may still change the "active" species and get feedback from the "active" species; hence the atmosphere

remains realistic. This also enables the quantification of feedback errors in experiment simulations with, e.g., modified chemistry as done in Chapter 4.

Intermediate data products are created during the analysis introduced by [*Brakebusch et al.*, 2013]. For instance, one of these intermediates contains derived meteorological products, e.g., relative vorticity, PV, sPV, equivalent latitude, stream function, and velocity potential. These quantities are prerequisites for polar vortex definitions and spatial polar coordinates. Use of these derived meteorological products is not limited to the work shown here, but is applied for other analyses, e.g., the Concordiasi campaign.

6.2.2 Contributions to science

The scientific interest in polar stratospheric O_3 and related processes increased with the discovery of the Antarctic O_3 hole. Subsequent WMO reports about O_3 depletion summarize advances in our understanding since 1985. By now most of the processes related to polar stratospheric O_3 are understood, thus advances in science became smaller over time. Although atmospheric models improved greatly over time, the implementation of some processes remains challenging. To date, state-of-the-art CCMs have not yet achieved the capability to robustly and consistently predict temperature and O_3 loss in the, especially Arctic, polar region for the whole century [e.g., *Charlton-Perez et al.*, 2010]. Investigations of diagnostic simulations are thus used to contribute to the identification, quantification, and improvements of missing details, which lead to the overarching goal to achieve prediction capability.

This work contributes a sophisticated analysis for CCM simulations of polar stratospheric O_3 and related processes [*Brakebusch et al.*, 2013] to the scientific community. Because of the interlinked dynamics and chemistry shown in Chapter 2, a comprehensive analysis includes several key species and in particular discusses temperature accuracy, which was found to be crucial by [*Brakebusch et al.*, 2013]. This is the first published model/instrument comparison to involve such a comprehensive evaluation of CCM simulation capabilities of polar stratospheric O_3 loss (see Table 6.1).

study	T	O_3	N_2O	HCl	H_2O	HNO_3	$ClONO_2$	ClO	CH_4	NO_X	ClO_X	NO_Y
B13	x	x	x	x	x	x		x				
Chapter 4	x	x	x	x	x	x				(x)		
Chapter 5	x	x	x	x	x	x	x					
F07	(x)	x										
F11		x	x	x		x		x			(x)	(x)
G07		x										
S07		x							x			
S11	x	x	x		x	x	x	x				
H06		x	x						x		(x)	(x)

Table 6.1: Recent model studies regarding polar stratospheric O_3: *Brakebusch et al.* [2013] (B13), *Feng et al.* [2007b] (F07), *Feng et al.* [2011] (F11), *Grooß and Müller* [2007] (G07), *Singleton et al.* [2007] (S07), *Sinnhuber et al.* [2011] (S11), *von Hobe et al.* [2006] (H06). Species with check marks are included in the studies; species with check marks in parenthesis are included in the analysis but not compared to observations. The only similarly comprehensive study is by *Sinnhuber et al.* [2011] and the "model used in this study is an isentropic 3-D CTM" [*Sinnhuber et al.*, 2011].

Subsequent model improvements were identified and implemented. This had not been possible before the above mentioned analysis was developed. Improvements include but are not limited to:

- PSC parameterization

  CESM/WACCM was known to over-denitrify the winter polar stratosphere due to the formation of primarily NAT rather than STS. This indicated a limitation of the so-far purely thermodynamical equilibrium approach for a PSC parameterization. Detailed examination of the HNO_3 simulation performance provided the comprehensive picture needed to develop the improvement (collaboration with Doug Kinnison).

- Bromine budget correction

  Although Br is less abundant in the lower stratosphere, it is nevertheless important for O_3 loss since it is more efficient in destroying O_3 than Cl. Currently, CESM/WACCM chemistry does not include VSL Br species. Since implementing VSL halogens in CCMs is an ongoing effort, an artificial increase of Br-carrying species quantified by *Salawitch et al.* [2010] is used as a temporary solution.

The effect of these improvements are summarized in Figure 6.1, showing the model performance at the beginning of this work and now.

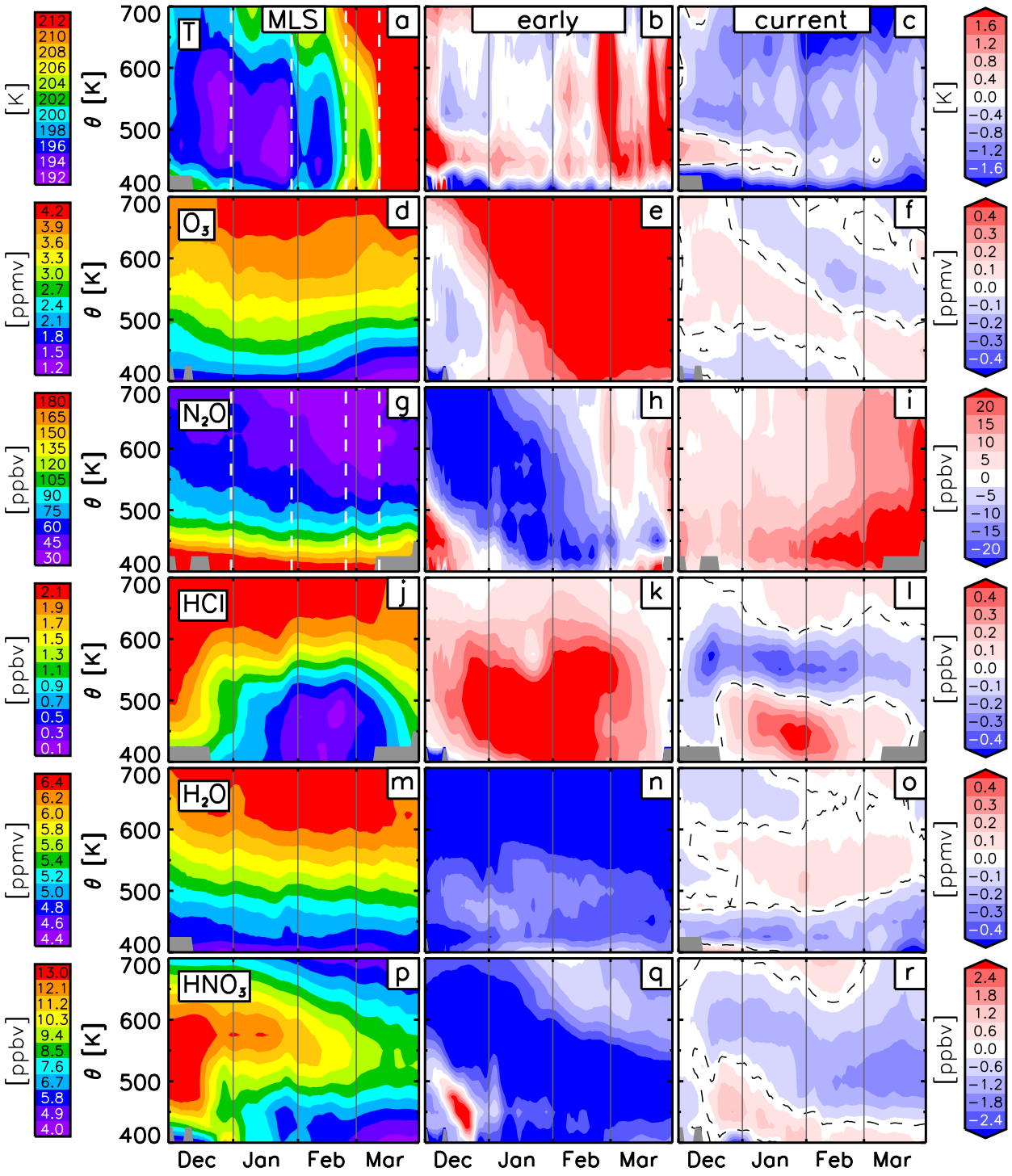

Figure 6.1: Evolution of polar vortex average differences between SD-WACCM and MLS in the NH 04/05 season in the lower stratosphere. The left column shows observations from MLS, the center column shows model/instrument differences of the first model simulation done for this work; the right column shows the model/instrument differences of a current simulation. The left and right columns are reproductions of the same columns in Figure 3.10 from [*Brakebusch et al.*, 2013].

The study presented by [*Brakebusch et al.*, 2013] was necessary to evaluate the previously described improvements and thus built the foundation for the subsequent studies described in Chapter 4 and Chapter 5.

The attribution of O_3 loss to various processes (Chapter 4) requires simulations with modified chemistry and the inclusion of O_3 tracer species. As examples, simulations without heterogeneous chemistry and without SPEs were run in order to quantify the individual impact on O_3 loss. This principle is widely used for other chemical questions already. In addition the O_3 tracers can be used to investigate dynamical feedback (Chapter 4) from the chemistry modifications. With the confidence gained by the first study, both the modified chemistry and the O_3 tracer can be trusted. Thus, the subsequent study (Chapter 4) contributes useful tools needed to investigate attribution and feedback questions.

As explained by [*Brakebusch et al.*, 2013], the agreement between simulated and observed gas-phase H_2O and HNO_3 is a first indication of whether PSC formation is simulated correctly. The correct amount of uptake (release) from (to) gas-phase bulk material, however, is a necessary but insufficient requirement for the simulation of PSCs. For instance, particle radii are important for denitrification, and particle densities as well as size distribution determine the SAD. In Chapter 5 the investigation of microphysical parameters used by the parameterization is pursued via comparison to observations (Cloud-Aerosol Lidar and Infrared Pathfinder Satellite Observation (CALIPSO)) and explicit microphysics (WACCM/Community Aerosol and Radiation Model for Atmospheres (CARMA)). The PSC parameterization was evaluated and found to work well regarding uptake of H_2O and HNO_3 [see *Brakebusch et al.* [2013] and Chapter 4]. The performance of the PSC parameterization regarding the microphysical parameters listed above is not yet quantified. Contributing both the evaluation of species uptake and microphysical parameters is expected to support the development of explicit PSC microphysics.

6.3 Future Plans

In this section some of the still unresolved but necessary model improvements are briefly described and plans for an experiment showing the theoretically largest possible impact of an extreme SPE event are outlined.

6.3.1 Additional analysis for the NH 2010/11 study

In Chapter 5 the quality of the PSC parameterization in SD-WACCM is inferred by evaluation of HNO_3 and H_2O. But from the quantification of HNO_3 and H_2O uptake alone the formation of SAD cannot be calculated. The correct amount of SAD is important because it affects Cl activation (see Reaction 2.57). In order to simulate SAD in SD-WACCM, a prescribed particle number density for STS and NAT particles and a constant width of the particle size distribution is used in addition to the uptake of HNO_3 and H_2O. The analysis in Chapter 5 will be improved when an evaluation of the PSC parameterization is included because it supports the discussion of Cl activation.

Considering CALIPSO backscatter observations of PSCs enables an evaluation of the PSC parameterization used by SD-WACCM. Backscatter from PSC particles can be calculated from the simulation using the above mentioned parameters. Since the bulk uptake of HNO_3 and H_2O was evaluated before (see Section 5.4), differences between simulated and observed backscatter can be attributed to the calculation of particle size distribution and the number density assumed.

The scientific benefit of this additional analysis is that it provides the basis for further improvements of the PSC parameterization while still conserving computational resources compared to explicit microphysics.

6.3.2 Identified but unresolved model deficiencies

One finding of Chapter 4 is that upper atmospheric NO_X is not well simulated in WACCM. The conclusion in this chapter was insufficient production of NO_X by EPP. One reason for this is that MEE are not represented in SD-WACCM. Another reason is insufficient descent. That is,

NO_X created by EPP in the upper atmosphere must descend for stratospheric O_3 loss to occur. This requires a robust simulation of upper atmospheric descent. *Smith et al.* [2011] concludes that simulated NO_X descent in SD-WACCM might underestimate observations. Some studies suggest that resolving GWs is a crucial part of improving simulated upper atmospheric circulation and thus descent, but at the same time resolving this issue is expected to be difficult [e.g., *Hamilton et al.*, 1999; *Shepherd*, 2000].

One conclusion of [*Brakebusch et al.*, 2013] was that O_3 loss is very sensitive to small temperature changes and that the exact temperature is one of the most crucial requirements for polar stratospheric O_3 simulations of high quality. For the temperature bias on heterogeneous chemistry, SAD formation, and HCl condensation in CESM/WACCM, a constant value was used in [*Brakebusch et al.*, 2013], Chapter 4, and Chapter 5. This value represents a polar vortex average fit for the whole season at one isentropic level only. A change of that bias over the course of the season or a distinction between vortex core and the outermost vortex area was not made. In order to reproduce observations better, the temperature bias needs to vary spatially and temporally. This, however, requires temperature observations with higher accuracy.

6.3.3 Experiment about hypothetical extreme SPEs

In late October 2003, some of the strongest SPE events on record were observed. The ion pair production rate exceeded the values shown in Chapter 4 by one order of magnitude. Solar protons penetrated the Earth's atmosphere down to the stratosphere, and a substantial increase in NO_X and decrease in O_3 was observed [*Seppälä et al.*, 2004]. This event happened prior to the onset of the NH polar winter period; increased levels of stratospheric NO_X were not observed anymore by the time the polar vortex formed in December [*Funke et al.*, 2011; *Friederich et al.*, 2013]. SPEs are unpredictable and sporadic, i.e., this event could have occurred at a later time as well. Three alternative times of this event are expected to result in completely different impacts on O_3 loss in the stratosphere. First, if the event happened early in the season, e.g., in December, catalytic O_3 loss via the NO_X cycle (see Reaction 2.25) is expected in the upper stratosphere

since sunlight is not available for lower stratospheric NO_X-induced O_3 loss. Also, the formation of HNO_3 via the intermediate N_2O_5 could increase the HNO_3 abundance and thus provide additional "material" for PSC formation effectively increasing SAD. Secondly, if the event happened during mid-season when Cl is already activated, the additional NO_X may act to deactivate ClO_X by the formation of $ClONO_2$. This then results in an increase of the heterogeneous chemistry reaction rate of Reaction 2.50 if SAD is still available. Thus a net increase in Cl is expected followed by increased O_3 loss. Thirdly, if the event happened late in the season when SAD is not available anymore, the formation of $ClONO_2$ would result in the final deactivation of Cl, which greatly reduces O_3 loss. [*Brakebusch et al.*, 2013] and Chapter 5 have shown that CESM/WACCM reproduces the Arctic atmosphere realistically; and thus it can be expected to simulate the three potential situations described above with the same quality.

Bibliography

Abarca, J. F., and C. Casiccia (2002), Skin cancer and ultraviolet-B radiation under the Antarctic ozone hole: southern Chile, 1987-2000, *Photodermatol Photo*, *18*, 294–302. *[cited on page 2.]*

Akiyoshi, H., Y. Yamashita, K. Sakamoto, L. B. Zhou, and T. Imamura (2010), Recovery of stratospheric ozone in calculations by the Center for Climate System Research/National Institute for Environmental Studies chemistry-climate model under the CCMVal-REF2 scenario and a no-climate-change run, *J. Geophys. Res.*, *115*, D19301, doi:10.1029/2009JD012683. *[cited on page 38.]*

Andrews, D. G., J. R. Holton, and C. B. Leovy (1987), *Middle Atmosphere Dynamics*, *International Geophysics Series*, vol. 40, 489 pp., Academic Press, 525 B Street, Suite 1900, San Diego, California 92101-4495. *[cited on page 12.]*

Bates, D. R., and M. Nicolet (1950), Atmospheric Hydrogen, *Publ. Astron. Soc. Pacific*, *62*, 106. *[cited on page 17.]*

Bates, T. S., B. K. Lamb, A. Guenther, J. Dignon, and R. E. Stoiber (1992), Sulfur emissions to the atmosphere from natural sources, *J. Atmos. Chem.*, *14*(1-4), 315–337, doi:10.1007/BF00115242. *[cited on page 23.]*

Blum, U., F. Khosrawi, G. Baumgarten, K. Stebel, R. Müller, and K. H. Fricke (2006), Simultaneous lidar observations of a polar stratospheric cloud on the east and west sides of the Scandinavian mountains and microphysical box model simulations, *Ann. Geophys.*, *24*, 3267–3277, doi:10.5194/angeo-24-3267-2006. *[cited on page 39.]*

Brakebusch, M., C. E. Randall, D. E. Kinnison, S. Tilmes, M. L. Santee, and G. L. Manney (2013), Evaluation of Whole Atmosphere Community Climate Model simulations of ozone during Arctic winter 2004-2005, *J. Geophys. Res.-Atmos.*, *118*(6), 2673–2688, doi:10.1002/jgrd.50226. *[cited on pages 8, 72, 73, 74, 78, 79, 88, 91, 93, 94, 96, 98, 101, 102, 103, 104, 105, 106, 107, 109, 110, 125 and 126.]*

Brasseur, G., and S. Solomon (2005), *Aeronomy of the Middle Atmosphere - Chemistry and Physics of the Stratosphere and Mesosphere*, *Atmospheric and Oceanographic Sciences Library*, vol. 32, 3rd ed., 644 pp., Springer, P.O. Box 17, 3300 AA Dodrecht, The Netherlands, iSBN-10 1-4020-3284-6 (HB) ISBN-13 978-1-4020-3284-4 (HB) ISBN-10 1-4020-3824-0 (e-book) ISBN-13 978-1-4020-3824-1 (e-book). *[cited on pages 11, 18, 23, 25, 29, 31, 38, 55, 85 and 86.]*

Brasseur, G. P., D. A. Hauglustaine, S. Walters, P. J. Rasch, J. F. Muller, C. Granier, and X. X. Tie (1998), MOZART, a global chemical transport model for ozone and related chemical tracers 1. Model description, *J. Geophys. Res.-Atmos.*, *103*(D21), 28,265–28,289. *[cited on page 40.]*

Brewer, A. W. (1949), Evidence for a world circulation provided by the measurements of helium and water vapour distribution in the stratosphere, *Quart. J. Roy.*, *75*(326), 351–363, doi:10.1002/qj.49707532603. *[cited on page 10.]*

Carslaw, K. S., S. L. Clegg, and P. Brimblecombe (1995), A Thermodynamic Model of the System HCl-HNO3-H2SO4-H2O, Including Solubilities of HBr, from 200 to 328 K, *J. Phys. Chem.*, *99*(29), 11,557–11,574, doi:10.1021/j100029a039. *[cited on pages 24 and 79.]*

Carslaw, K. S., T. Peter, and S. L. Clegg (1997), Modeling the composition of liquid stratospheric aerosols, *Rev. Geophys.*, *35*(2), 125–154, doi:10.1029/97RG00078. *[cited on page 26.]*

Carslaw, K. S., et al. (1998a), Particle microphysics and chemistry in remotely observed mountain polar stratospheric clouds, *J. Geophys. Res.-Atmos.*, *103*(D5), 5785–5796, doi:10.1029/97JD03626. *[cited on page 25.]*

Carslaw, K. S., et al. (1998b), Increased stratospheric ozone depletion due to mountain-induced atmospheric waves, *Nature*, *391*(6668), 675–678, doi:10.1038/35589. *[cited on page 25.]*

Chapman, S. (1930), On ozone and atomic oxygen in the upper atmosphere, *Philos. Mag.*, *10*(64), 369–383, doi:10.1080/14786443009461588. *[cited on page 15.]*

Charlton-Perez, A. J., et al. (2010), The potential to narrow uncertainty in projections of stratospheric ozone over the 21st century, *Atmos. Chem. Phys.*, *10*(19), 9473–9486, doi:10.5194/acp-10-9473-2010. *[cited on pages 1, 5 and 104.]*

Charney, J. G., and P. G. Drazin (1961), Propagation of Planetary-Scale Disturbances from Lower into Upper Atmosphere, *J. Geophys. Res.*, *66*(1), 83. *[cited on page 10.]*

Clough, S. A., and M. J. Iacono (1995), Line-By-Line Calculation Of Atmospheric Fluxes And Cooling Rates .2. Application To Carbon-Dioxide, Ozone, Methane, Nitrous-Oxide And The Halocarbons, *J. Geophys. Res.-Atmos.*, *100*(D8), 16,519–16,535, doi:10.1029/95JD01386. *[cited on pages 4 and 71.]*

Collins, W. D., et al. (2006), The Formulation and Atmospheric Simulation of the Community Atmosphere Model Version 3 (CAM3), *J. Climate*, *19*, 2144–2161, doi:10.1175/JCLI3760.1. *[cited on page 40.]*

Cox, R. A., W. J. Bloss, R. L. Jones, and D. M. Rowley (1999), OIO and the atmospheric cycle of iodine, *Geophys. Res. Lett.*, *26*(13), 1857–1860, doi:10.1029/1999GL900439. *[cited on page 20.]*

Crutzen, P. J. (1970), The influence of nitrogen oxides on the atmospheric ozone content, *Quarterly Journal of the Royal Meteorological Society*, *96*(408), 320–325, doi:10.1002/qj.49709640815. *[cited on page 19.]*

Crutzen, P. J. (1976), Possible Importance of CSO for Sulfate Layer of Stratosphere, *Geophys. Res. Lett.*, *3*(2), 73–76, doi:10.1029/GL003i002p00073. *[cited on page 23.]*

Crutzen, P. J., and F. Arnold (1986), Nitric acid cloud formation in the cold Antarctic stratosphere: a major cause for the springtime 'ozone hole', *Nature*, *324*(6098), 651–655. *[cited on page 22.]*

Crutzen, P. J., I. S. A. Isaksen, and G. C. Reid (1975), Solar Proton Events - Stratospheric Sources of Nitric-Oxide, *Science*, *189*(4201), 457–459, doi:10.1126/science.189.4201.457. *[cited on page 27.]*

Deniel, C., R. M. Bevilacqua, J. P. Pommereau, and F. Lefèvre (1998), Arctic chemical ozone depletion during the 1994-1995 winter deduced from POAMII satellite observations and the REPROBUS three-dimensional model, *J. Geophys. Res.*, *103*(D15), 19,231–19,244, doi:10.1029/98JD01446. *[cited on page 61.]*

Dessler, A. E., M. D. Burrage, J. U. Grooss, J. R. Holton, J. L. Lean, S. T. Massie, M. R. Schoeberl, A. R. Douglass, and C. H. Jackman (1998), Selected science highlights from the first 5 years of the Upper Atmosphere Research Satellite (UARS) Program, *Rev. Geophys.*, *36*(2), 183–210, doi:10.1029/97RG03549. *[cited on page 31.]*

Dibb, J. E., E. Scheuer, M. Avery, J. Plant, and G. Sachse (2006), In situ evidence for renitrification in the Arctic lower stratosphere during the polar aura validation experiment (PAVE), *Geophys. Res. Lett.*, *33*, L12815, doi:10.1029/2006GL026243. *[cited on page 39.]*

Dobson, G. M. B. (1956), Origin and Distribution of the Polyatomic Molecules in the Atmosphere, *Proc. Roy. Soc. London*, *236*(1205), 187–193. *[cited on page 10.]*

Douglass, A. R., R. B. Rood, J. A. Kaye, R. S. Stolarski, D. J. Allen, and E. M. Larson (1991), The influlence of polar heterogeneous processes on reactive chlorine at middle latitudes: Three dimensional model implications, *Geophys. Res. Lett.*, *18(1)*, 25–28, doi:10.1029/90GL02601. *[cited on page 63.]*

Dowdy, S., S. Wearden, and D. Chilko (2004), *Statistics for Research*, 3 ed., Wiley, Hoboken, New Jersey, USA, iSBN: 978-0-471-26735-5. *[cited on page 47.]*

Drdla, K., and R. Müller (2012), Temperature thresholds for chlorine activation and ozone loss in the polar stratosphere, *Ann. Geophys.*, *30*(7), 1055–1073, doi:10.5194/angeo-30-1055-2012. *[cited on page 45.]*

Dunkerton, T. J., and D. P. Delisi (1986), Evolution of Potential Vorticity in the Winter Stratosphere of January-February 1979, *J. Geophys. Res.-Atmos.*, *91*(D1), 1199–1208. *[cited on page 46.]*

Dye, J. E., B. W. Gandrud, D. Baumgardner, K. R. Chan, G. V. Ferry, M. Loewenstein, K. K. Kelly, and J. C. Wilson (1990), Observed particle evolution in the polar stratospheric cloud of January 24, 1989, *Geophys. Res. Lett.*, *17*(4), 413–416, doi:10.1029/GL017i004p00413. *[cited on page 25.]*

Dye, J. E., D. Baumgardner, B. W. Gandrud, S. R. Kawa, K. K. Kelly, M. Loewenstein, G. V. Ferry, K. R. Chan, and B. L. Gary (1992), Particle size distributions in Arctic polar stratospheric clouds, growth and freezing of sulfuric acid droplets, and implications for cloud formation, *J. Geophys. Res.-Atmos.*, *97*(D8), 8015–8034, doi:10.1029/91JD02740. *[cited on page 25.]*

El Amraoui, L., N. Semane, V.-H. Peuch, and M. L. Santee (2008), Investigation of dynamical processes in the polar stratospheric vortex during the unusually cold winter 2004/2005, *Geophys. Res. Lett.*, *35*(3), L03803, doi:10.1029/2007GL031251. *[cited on pages 38, 39 and 68.]*

Emmons, L. K., et al. (2010), Description and evaluation of the Model for Ozone and Related chemical Tracers, version 4 (MOZART-4), *Geosci. Model Dev.*, *3*(1), 43–67. *[cited on page 40.]*

Esler, J. G., and D. W. Waugh (2002), A method for estimating the extent of denitrification of Arctic polar vortex air from tracer-tracer scatter plots, *J. Geophys. Res.-Atmos.*, *107*(D13), doi:10.1029/2001JD001071. *[cited on page 40.]*

Fahey, D. W., K. K. Kelly, G. V. Ferry, L. R. Poole, J. C. Wilson, D. M. Murphy, M. Loewenstein, and K. R. Chan (1989), In situ measurements of total reactive nitrogen, total water, and aerosol in a polar stratospheric cloud in the Antarctic, *J. Geophys. Res.-Atmos.*, *94*(D9), 11,299–11,315, doi:10.1029/JD094iD09p11299. *[cited on pages 23 and 25.]*

Fahey, D. W., K. K. Kelly, S. R. Kawa, A. F. Tuck, M. Loewenstein, K. R. Chan, and L. E. Heidt (1990), Observations of denitrification and dehydration in the winter polar stratospheres, *Nature*, *344*(6264), 321–324, doi:10.1038/344321a0. *[cited on page 25.]*

Fahey, D. W., et al. (2001), The Detection of Large HNO3-Containing Particles in the Winter Arctic Stratosphere, *Science*, *291*(5506), 1026–1031, doi:10.1126/science.1057265. *[cited on page 25.]*

Farman, J. C., B. G. Gardiner, and J. D. Shanklin (1985), Large Losses of Total Ozone in Antarctica Reveal Seasonal ClOx/NOx Interaction, *Nature*, *315*(6016), 207–210. *[cited on page 21.]*

Feng, W., M. P. Chipperfield, M. Dorf, K. Pfeilsticker, and P. Ricaud (2007a), Mid-latitude ozone changes: studies with a 3-D CTM forced by ERA-40 analyses, *Atmos. Chem. Phys.*, *7*(9), 2357–2369, doi:10.5194/acp-7-2357-2007. *[cited on pages 38 and 68.]*

Feng, W., M. P. Chipperfield, S. Davies, P. von der Gathen, E. Kyroe, C. M. Volk, A. Ulanovsky, and G. Belyaev (2007b), Large chemical ozone loss in 2004/2005 Arctic winter/spring, *Geophys. Res. Lett.*, *34*(9), L09803, doi:10.1029/2006GL029098. *[cited on page 105.]*

Feng, W., M. P. Chipperfield, S. Davies, G. W. Mann, K. S. Carslaw, S. Dhomse, V. L. Harvey, C. E. Randall, and M. L. Santee (2011), Modelling the effect of denitrification on polar ozone depletion for the Arctic winter 2004/2005, *Atmos. Chem. Phys.*, *11*, 6559–6573, doi:10.5194/acp-11-6559-2011. *[cited on pages 38, 67, 68 and 105.]*

Friederich, F., T. von Clarmann, B. Funke, H. Nieder, J. Orphal, M. Sinnhuber, G. P. Stiller, and J. M. Wissing (2013), Lifetime and production rate of NOx in the upper stratosphere and lower mesosphere in the polar spring/summer after the solar proton event in October-November 2003, *Atmos. Chem. Phys.*, *13*(5), 2531–2539, doi:10.5194/acp-13-2531-2013. *[cited on page 109.]*

Fritts, D. C., and M. J. Alexander (2003), Gravity wave dynamics and effects in the middle atmosphere, *Rev. Geophys.*, *41*(1), doi:10.1029/2001RG000106. *[cited on pages 12 and 13.]*

Funke, B., et al. (2011), Composition changes after the "Halloween" solar proton event: the High Energy Particle Precipitation in the Atmosphere (HEPPA) model versus MIPAS data intercomparison study, *Atmos. Chem. Phys.*, *11*(17), 9089–9139, doi:10.5194/acp-11-9089-2011. *[cited on page 109.]*

Grooß, J.-U., and R. Müller (2007), Simulation of ozone loss in Arctic winter 2004/2005, *Geophys. Res. Lett.*, *34*(5), L05804, doi:10.1029/2006GL028901. *[cited on pages 38, 40, 61, 68 and 105.]*

Hamilton, K., R. J. Wilson, and R. S. Hemler (1999), Middle atmosphere simulated with high vertical and horizontal resolution versions of a GCM: Improvements in the cold pole bias and generation of a QBO-like oscillation in the tropics, *J. Atmos. Sci.*, *56*(22), 3829–3846. *[cited on page 109.]*

Hanson, D., and K. Mauersberger (1988), Laboratory Studies of the Nitric-Acid Trihydrate - Implications for the South Polar Stratosphere, *Geophys. Res. Lett.*, *15*(8), 855–858. *[cited on page 25.]*

Hauglustaine, D. A., G. P. Brasseur, S. Walters, P. J. Rasch, J.-F. Müller, L. K. Emmons, and C. A. Carroll (1998), MOZART, a global chemical transport model for ozone and related chemical tracers 2. Model results and evaluation, *J. Geophys. Res.-Atmos.*, *103*(D21), 28,291–28,335, doi:10.1029/98JD02398. *[cited on page 40.]*

Holton, J. R. (2004), *An Introduction to Dynamic Meteorology*, vol. 88, 4th ed., 535 pp., Academic Press, San Diego. *[cited on pages 10 and 11.]*

Hoppel, K., et al. (2002), POAM III observations of arctic ozone loss for the 1999/2000 winter, *J. Geophys. Res.-Atmos.*, *107*(D20), doi:10.1029/2001JD000476. *[cited on page 39.]*

Horowitz, L. W., et al. (2003), A global simulation of tropospheric ozone and related tracers: Description and evaluation of MOZART, version 2, *J. Geophys. Res.-Oc. Atm.*, *108*(D24), doi:10.1029/2002JD002853. *[cited on page 40.]*

IPCC (2007), *Climate Change 2007: The Physical Science Basis, Working Group I Report*, Cambridge University Press. *[cited on page 23.]*

Jackman, C. H. (1991), Effects of Energetic Particles on Minor Constituents of the Middle Atmosphere, *J. Geomagn. Geoelectr.*, *43 (Suppl.)*(2, S), 637–646, 7th Quadrennial Solar Terrestrial Symp / 27th Cospar Meeting, The Hague, Netherlands, Jul 25-30, 1990. *[cited on page 28.]*

Jackson, D. R., and Y. J. Orsolini (2008), Estimation of Arctic ozone loss in winter 2004/05 based on assimilation of EOS MLS and SBUV/2 observations, *Quart. J. Roy.*, *134*(636, Part A), 1833–1841, doi:10.1002/qj.316. *[cited on pages 38, 40, 61 and 68.]*

Jackson, D. R., S. J. Driscoll, E. J. Highwood, J. E. Harries, and J. M. Russell (1998), Troposphere to stratosphere transport at low latitudes as studies using HALOE observations of water vapour 1992-1997, *Quart. J. Roy.*, *124*(545), 169–192, doi:10.1002/qj.49712454508. *[cited on page 18.]*

Jimenez, C., H. C. Pumphrey, I. A. MacKenzie, G. L. Manney, M. L. Santee, M. J. Schwartz, R. S. Harwood, and J. W. Waters (2006), EOS MLS observations of dehydration in the 2004-2005 polar winters, *Geophys. Res. Lett.*, *33*(16), L16806, doi:10.1029/2006GL025926. *[cited on pages 39, 58 and 64.]*

Jin, J. J., et al. (2006a), Severe Arctic ozone loss in the winter 2004/2005: observations from ACE-FTS, *Geophys. Res. Lett.*, *33*(15), L15801, doi:10.1029/2006GL026752. *[cited on pages 38, 40 and 68.]*

Jin, J. J., et al. (2006b), Denitrification in the Arctic winter 2004/2005: Observations from ACE-FTS, *Geophys. Res. Lett.*, *33*(19), doi:10.1029/2006GL027687. *[cited on page 39.]*

Junge, C. E., and J. E. Manson (1961), Stratospheric aerosol studies, *J. Geophys. Res.*, *66*(7), 2163–2182, doi:10.1029/JZ066i007p02163. *[cited on page 24.]*

Junge, C. E., C. W. Chagnon, and J. E. Manson (1961), Stratospheric Aerosols, *J. Meteorol.*, *18*, 81–108. *[cited on page 24.]*

Kelly, K. K., et al. (1989), Dehydration in the lower Antarctic stratosphere during late winter and early spring, 1987, *J. Geophys. Res.-Atmos.*, *94*(D9), 11,317–11,357, doi:10.1029/JD094iD09p11317. *[cited on page 25.]*

Kinnison, D. E., et al. (2007), Sensitivity of chemical tracers to meteorological parameters in the MOZART-3 chemical transport model, *J. Geophys. Res.-Atmos.*, *112*(D20), doi:10.1029/2006JD007879. *[cited on pages 40, 45 and 46.]*

Kinnison, D. E., et al. (2013), Description and Evaluation of the Specified Dynamics version of the Whole Atmosphere Community Climate Model (SD-WACCM), *Geosci. Model Dev.*, *in preparation*. *[cited on page 34.]*

Kleinböhl, A., H. Bremer, H. Küllmann, J. Kuttippurath, E. V. Browell, T. Canty, R. J. Salawitch, G. C. Toon, and J. Notholt (2005), Denitrification in the Arctic mid-winter 2004/2005 observed by airborne submillimeter radiometry, *Geophys. Res. Lett.*, *32*(19), L19811, doi:10.1029/2005GL023408. *[cited on page 39.]*

Kley, D., A. L. Schmeltekopf, K. Kelly, R. H. Winkler, T. L. Thompson, and M. McFarland (1982), Transport of water through the tropical tropopause, *Geophys. Res. Lett.*, *9*(6), 617–620, doi:10.1029/GL009i006p00617. *[cited on page 17.]*

Knuth, D. E. (1992), *Axioms and Hulls*, Springer-Verlag, Berlin/Heidelberg, Germany. *[cited on pages 43 and 123.]*

Kunz, A., L. L. Pan, P. Konopka, D. E. Kinnison, and S. Tilmes (2011), Chemical and dynamical discontinuity at the extratropical tropopause based on START08 and WACCM analyses, *J. Geophys. Res.-Atmos.*, *116*, D24302, doi:10.1029/2011JD016686. *[cited on page 41.]*

Lamarque, J.-F., et al. (2012), CAM-chem: description and evaluation of interactive atmospheric chemistry in the Community Earth System Model, *Geosci. Model Dev.*, *5*(2), 369–411, doi:10.5194/gmd-5-369-2012. *[cited on pages 40 and 41.]*

Leaf, A. (1993), *Loss of Stratospheric Ozone and Health Effects of Increased Ultraviolet Radiation*, Cambridge, MA: The MIT Press. *[cited on page 2.]*

Lee, A. M., R. L. Jones, I. Kilbane-Dawe, and J. A. Pyle (2002), Diagnosing ozone loss in the extratropical lower stratosphere, *J. Geophys. Res.-Atmos.*, *107*(D11), doi:10.1029/2001JD000538. *[cited on page 63.]*

Lin, S. J. (2004), A "vertically Lagrangian" finite-volume dynamical core for global models, *Mon. Weather Rev.*, *132*(10), 2293–2307, doi:10.1175/1520-0493(2004)132⟨2293:AVLFDC⟩2.0.CO;2. *[cited on page 41.]*

Lin, S. J., and R. B. Rood (1996), Multidimensional flux-form semi-Lagrangian transport schemes, *Mon. Weather Rev.*, *124*(9), 2046–2070, doi:10.1175/1520-0493(1996)124⟨2046:MFFSLT⟩2.0.CO;2. *[cited on page 41.]*

Livesey, e. a., N. J. (2011), Earth Observing System (EOS) Aura Microwave Limb Sounder (MLS) Version 3.3 Level 2 data quality and description document, *Tech. rep.*, Jet Propulsion Laboratory, California Institute of Technology, Pasadena, California. *[cited on pages 42, 43, 46, 49, 64, 78 and 123.]*

Loewenstein, M., J. R. Podolske, K. R. Chan, and S. E. Strahan (1990), N2O as a dynamical tracer in the Arctic vortex, *Geophys. Res. Lett.*, *17*(4), 477–480, doi:10.1029/GL017i004p00477. *[cited on pages 30 and 51.]*

Lovelock, J. E. (1971), Atmospheric Fluorine Compounds as Indicators of Air Movements, *Nature*, *230*(5293), 379–379, doi:10.1038/230379a0. *[cited on page 21.]*

Lowe, D., and A. R. MacKenzie (2008), Polar stratospheric cloud microphysics and chemistry, *J. Atmos. Terr. Phy.*, *70*(1), 13–40, doi:10.1016/j.jastp.2007.09.011. *[cited on pages 24, 26, 45, 57, 60, 64 and 67.]*

Manney, G. L., L. Froidevaux, J. W. Waters, and R. W. Zurek (1995), Evolution Of Microwave Limb Sounder Ozone And The Polar Vortex During Winter, *J. Geophys. Res.-Atmos.*, *100*(D2), 2953–2972. *[cited on pages 40, 61 and 75.]*

Manney, G. L., J. L. Sabutis, S. Pawson, M. L. Santee, B. Naujokat, R. Swinbank, M. E. Gelman, and W. Ebisuzaki (2003), Lower stratospheric temperature differences between meteorological analyses in two cold Arctic winters and their impact on polar processing studies, *J. Geophys. Res.-Atmos.*, *108*(D5), doi:10.1029/2001JD001149. *[cited on page 61.]*

Manney, G. L., M. L. Santee, L. Froidevaux, K. Hoppel, N. J. Livesey, and J. W. Waters (2006), EOS MLS observations of ozone loss in the 2004-2005 Arctic winter, *Geophys. Res. Lett.*, *33*(4), L04802, doi:10.1029/2005GL024494. *[cited on pages 38, 39, 40, 51, 52, 53, 62 and 68.]*

Manney, G. L., et al. (2011), Unprecedented Arctic ozone loss in 2011, *Nature*, *478*(7370), 469–475, doi:10.1038/nature10556. *[cited on pages 34, 36, 90, 93, 96, 97 and 99.]*

Matsuno, T. (1971), A Dynamical Model of the Stratospheric Sudden Warming, *J. Atmos. Sci.*, *28*(8), 1479–1494, doi:10.1175/1520-0469(1971)028⟨1479:ADMOTS⟩2.0.CO;2. *[cited on page 11.]*

McElroy, M. B., R. J. Salawitch, S. C. Wofsy, and J. A. Logan (1986), Reductions of Antarctic Ozone due to Synergistic Interactions of Chlorine and Bromine, *Nature*, *321*(6072), 759–762. *[cited on page 22.]*

McInturff, R. (1978), Stratospheric warmings: Synoptic, dynamic and general-circulation aspects, *25 tech. rep. nasa-rp-1017*, NASA Reference Publ., Washington, DC. *[cited on page 12.]*

Michelsen, H. A., G. L. Manney, M. R. Gunson, and R. Zander (1998), Correlations of stratospheric abundances of NOy , O3, N2O, and CH4 derived from ATMOS measurements, *J. Geophys. Res.*, *103(D21)*, 28,347–28,359, doi:doi:10.1029/98JD02850. *[cited on page 39.]*

Molina, L. T., and M. J. Molina (1987), Production of Cl2O2 from the Self-Reaction of the ClO Radical, *Journal Of Physical Chemistry*, *91*(2), 433–436. *[cited on page 21.]*

Molina, M. J., and F. S. Rowland (1974), Stratospheric Sink for Chlorofluoromethanes - Chlorine Atomic-Catalysed Destruction of Ozone, *Nature*, *249*(5460), 810–812. *[cited on page 21.]*

Moore, W. J. (1962), *Physical Chemistry*, 3rd ed., Prentice-Hall, Englewood Cliffs, NJ. *[cited on page 27.]*

Newman, P. e. a. (2010), *Stratospheric Ozone - An Electronic Textbook*, Goddard Space Flight Center Atmospheric Chemistry and Dynamics Branch (Code 916). *[cited on page 2.]*

Noxon, J. F., R. T. Norton, and W. R. Henderson (1978), Observations of Atmospheric NO3, *Geophys. Res. Lett*, *5*, 675–678. *[cited on page 23.]*

Pitts, M. C., L. R. Poole, and L. W. Thomason (2009), CALIPSO polar stratospheric cloud observations: second-generation detection algorithm and composition discrimination, *Atmos. Chem. Phys.*, *9*(19), 7577–7589, doi:10.5194/acp-9-7577-2009. *[cited on page 45.]*

Poole, L. R., and M. P. McCormick (1988), Airborne lidar observations of Arctic polar stratospheric clouds: Indications of two distinct growth stages, *Geophys. Res. Lett.*, *15*(1), 21–23, doi:10.1029/GL015i001p00021. *[cited on page 25.]*

Portmann, R. W., S. Solomon, R. R. Garcia, L. W. Thomason, L. R. Poole, and M. P. McCormick (1996), Role of aerosol variations in anthropogenic ozone depletion in the polar regions, *J. Geophys. Res.-Atmos.*, *101*(D17), 22,991–23,006. *[cited on page 56.]*

Poulet, G., M. Pirre, F. Maguin, R. Ramaroson, and G. Le Bras (1992), Role of the BRO + HO2 reaction in the stratospheric chemistry of bromine, *Geophys. Res. Lett.*, *19*(23), 2305–2308, doi:10.1029/92GL00781. *[cited on page 20.]*

Proffitt, M. H., S. Solomon, and M. Loewenstein (1992), Comparison of 2-D Model Simulations of Ozone and Nitrous Oxide at High Latitudes With Stratospheric Measurements, *J. Geophys. Res.-Atmos.*, *97*(D1), 939–944, doi:10.1029/91JD02756. *[cited on page 40.]*

Pundt, I., J.-P. Pommereau, C. Phillips, and E. Lateltin (1998), Upper Limit of Iodine Oxide in the Lower Stratosphere, *J. Atmos. Chem.*, *30*(1), 173–185, doi:10.1023/A:1006071612477. *[cited on page 20.]*

Randall, C., R. Bevilacqua, J. Lumpe, and K. Hoppel (2001), Validation of POAM III aerosols: Comparison to SAGE II and HALOE, *J. Geophys. Res.*, *106*(D21), 27,525–27,536. *[cited on pages 70 and 71.]*

Randall, C. E., D. W. Rusch, R. M. Bevilacqua, K. W. Hoppel, and J. D. Lumpe (1998), Polar Ozone and Aerosol Measurement (POAM) II stratospheric NO2, 1993-1996, *J. Geophys. Res.-Oc. Atm.*, *103*(D21), 28,361–28,371, doi:10.1029/98JD02092. *[cited on page 70.]*

Randall, C. E., V. L. Harvey, C. S. Singleton, P. F. Bernath, C. D. Boone, and J. U. Kozyra (2006), Enhanced NOx in 2006 linked to strong upper stratospheric Arctic vortex, *Geophys. Res. Lett.*, *33*(18), doi:10.1029/2006GL027160. *[cited on page 28.]*

Randall, C. E., V. L. Harvey, C. S. Singleton, S. M. Bailey, P. F. Bernath, M. Codrescu, H. Nakajima, and J. M. Russell III (2007), Energetic particle precipitation effects on the Southern Hemisphere stratosphere in 1992-2005, *J. Geophys. Res.*, *112*(D08308). *[cited on pages 70, 71, 72 and 85.]*

Reed, R. J. (1966), Zonal wind behavior in the equatorial stratosphere and lower mesosphere, *J. Geophys. Res.-Atmos.*, *71*(18), 4223–4233, doi:10.1029/JZ071i018p04223. *[cited on page 10.]*

Rex, M., et al. (1999), Chemical ozone loss in the Arctic winter 1994/95 as determined by the Match technique, *J. Atmos. Chem.*, *32*(1), 35–59. *[cited on page 39.]*

Rex, M., R. J. Salawitch, P. von der Gathen, N. R. P. Harris, M. P. Chipperfield, and B. Naujokat (2004), Arctic ozone loss and climate change, *Geophys. Res. Lett.*, *31*(4), doi:10.1029/2003GL018844. *[cited on pages 36 and 40.]*

Rex, M., et al. (2006), Arctic winter 2005: Implications for stratospheric ozone loss and climate change, *Geophys. Res. Lett.*, *33*(23), L23808, doi:10.1029/2006GL026731. *[cited on pages 36, 38, 39 and 68.]*

Richter, J. H., F. Sassi, and R. R. Garcia (2010), Toward a Physically Based Gravity Wave Source Parameterization in a General Circulation Model, *J. Atmos. Sci.*, *67*(1), 136–156, doi:10.1175/2009JAS3112.1. *[cited on page 41.]*

Rienecker, e. a., M. M. (2008), The GEOS-5 data assimilation system - Documentation of versions 5.0.1 and 5.1.0, *Tech. Rep. Tech. Rep. NASA/TM-2007-104606, Vol. 27*, NASA GSFC. *[cited on page 41.]*

Rienecker, M. M., et al. (2011), MERRA: NASA's Modern-Era Retrospective Analysis for Research and Applications, *J. Climate*, *24*(14), 3624–3648, doi:10.1175/JCLI-D-11-00015.1. *[cited on page 73.]*

Roble, R. G., and E. C. Ridley (1987), An auroral model for the NCAR thermospheric general-circulation model (TGCM), *Ann. Geophys.*, *5*(6), 369–382. *[cited on page 40.]*

Rösevall, J. D., D. P. Murtagh, J. Urban, W. Feng, P. Eriksson, and S. Brohede (2008), A study of ozone depletion in the 2004/2005 Arctic winter based on data from Odin/SMR and Aura/MLS, *J. Geophys. Res.*, *113*(D13301), D13301, doi:10.1029/2007JD009560. *[cited on pages 38, 40 and 68.]*

Rusch, D. W., J.-C. Gérard, S. Solomon, P. J. Crutzen, and G. C. Reid (1981), The effect of particle precipitation events on the neutral and ion chemistry of the middle atmosphere-I. Odd nitrogen , *Planet. Space Sci.*, *29*(7), 767–774, doi:10.1016/0032-0633(81)90048-9. *[cited on page 28.]*

Salawitch, R. J., et al. (2010), A new interpretation of total column BrO during Arctic spring, *Geophys. Res. Lett.*, *37*, L21805, doi:10.1029/2010GL043798. *[cited on pages 46 and 105.]*

Salby, M., F. Sassi, P. Callaghan, W. Read, and H. Pumphrey (2003), Fluctuations of Cloud, Humidity, and Thermal Structure near the Tropical Tropopause, *J. Climate*, *16*(21), 3428–3446, doi:10.1175/1520-0442(2003)016⟨3428:FOCHAT⟩2.0.CO;2. *[cited on page 18.]*

Santee, M. L., et al. (2008), Validation of the Aura Microwave Limb Sounder ClO measurements, *J. Geophys. Res.-Atmos.*, *113*(D15), D15S22, doi:10.1029/2007JD008762. *[cited on pages 38, 39, 56 and 99.]*

Schoeberl, M. R., et al. (2006), Chemical observations of a polar vortex intrusion, *J. Geophys. Res.-Atmos.*, *111*(D20), D20306, doi:10.1029/2006JD007134. *[cited on page 58.]*

Schwartz, M. J., et al. (2008), Validation of the aura microwave limb sounder temperature and geopotential height measurements, *J. Geophys. Res.-Atmos.*, *113*(D15), D15S11, doi:10.1029/2007JD008783. *[cited on page 49.]*

Seppälä, A., P. T. Verronen, E. Kyrölä, S. Hassinen, L. Backman, A. Hauchecorne, J. L. Bertaux, and D. Fussen (2004), Solar proton events of October-November 2003: Ozone depletion in the Northern Hemisphere polar winter as seen by GOMOS/Envisat, *Geophys. Res. Lett.*, *31*(19), L19107, doi:10.1029/2004GL021042. *[cited on page 109.]*

Shepherd, T. G. (2000), The middle atmosphere, *J. Atmos. Sol.-Terr. Phy.*, *62*(17-18), 1587–1601, doi:10.1016/S1364-6826(00)00114-0. *[cited on pages 11, 12, 35, 49 and 109.]*

Shi, Q., J. T. Jayne, C. E. Kolb, D. R. Worsnop, and P. Davidovits (2001), Kinetic model for reaction of ClONO2 with H2O and HCl and HOCl with HCl in sulfuric acid solutions, *J. Geophys. Res.-Atmos.*, *106*(D20), 24,259–24,274. *[cited on pages 27 and 64.]*

Singleton, C. S. (2006), Investigation of Arctic Ozone Loss using Solar Occultation and Microwave Limb Sounding Instruments, Ph.D. thesis, Graduate School of the University of Colorado. *[cited on page 75.]*

Singleton, C. S., et al. (2005), 2002-2003 Arctic ozone loss deduced from POAM III satellite observations and the SLIMCAT chemical transport model, *Atmos. Chem. Phys.*, *5*, 597–609. *[cited on pages 60, 61 and 75.]*

Singleton, C. S., et al. (2007), Quantifying Arctic ozone loss during the 2004-2005 winter using satellite observations and a chemical transport model, *J. Geophys. Res.-Atmos.*, *112*(D7), D07304, doi:10.1029/2006JD007463. *[cited on pages 38, 40, 61, 68 and 105.]*

Sinnhuber, B.-M., G. Stiller, R. Ruhnke, T. von Clarmann, S. Kellmann, and J. Aschmann (2011), Arctic winter 2010/2011 at the brink of an ozone hole, *Geophys. Res. Lett.*, *38*(24), L24814, doi:10.1029/2011GL049784. *[cited on pages 36 and 105.]*

Smith, A. K., R. R. Garcia, D. R. Marsh, and J. H. Richter (2011), WACCM simulations of the mean circulation and trace species transport in the winter mesosphere, *J. Geophys. Res.-Atmos.*, *116*(D20), D20115, doi:10.1029/2011JD016083. *[cited on page 109.]*

Sneader, W. (2005), *Systematic Medicine*, chap. 8, pp. 74–87, 1st ed., John Wiley & Sons, Ltd, Chichester, UK., doi:10.1002/0470015535.ch8. *[cited on page 20.]*

Solomon, S. (1999), Stratospheric ozone depletion: A review of concepts and history, *Rev. Geophys.*, *37*(3), 275–316. *[cited on pages 26, 38 and 57.]*

Solomon, S., P. J. Crutzen, and R. G. Roble (1982), Photochemical coupling between the thermosphere and the lower atmosphere: 1. Odd nitrogen from 50 to 120 km, *J. Geophys. Res.-Oceans*, *87*(C9), 7206–7220, doi:10.1029/JC087iC09p07206. *[cited on page 28.]*

Solomon, S., R. R. Garcia, F. S. Rowland, and D. J. Wuebbles (1986), On the Depletion of Antarctic Ozone, *Nature*, *321*(6072), 755–758. *[cited on pages 22 and 25.]*

SPARC CCMVal (2010), *SPARC Report on the Evaluation of Chemistry-Climate Models*, vol. WCRP-132, Report No. 5. *[cited on pages 1, 5, 38, 46 and 69.]*

Steele, H. M., P. Hamill, M. P. McCormick, and T. J. Swissler (1983), The Formation of Polar Stratospheric Clouds, *J. Atmos. Sci.*, *40*(8), 2055–2068, doi:10.1175/1520-0469(1983)040⟨2055:TFOPSC⟩2.0.CO;2. *[cited on page 25.]*

Stolarski, R. S., and R. J. Cicerone (1974), Stratospheric Chlorine: a Possible Sink for Ozone, *Can. J. Chem.*, *52*(8), 1610–1615, doi:10.1139/v74-233. *[cited on page 21.]*

Stolarski, R. S., and R. D. Rundel (1975), Fluorine photochemistry in the stratosphere, *Geophys. Res. Lett.*, *2*(10), 443–444, doi:10.1029/GL002i010p00443. *[cited on page 20.]*

Thorne, R. M. (1980), The importance of energetic particle precipitation on the chemical composition of the middle atmosphere, *Pure Appl, Geophys.*, *118*(1), 128–151, doi:10.1007/BF01586448. *[cited on page 27.]*

Tilmes, S., R. Müller, J. U. Grooß, and J. M. Russell III (2004), Ozone loss and chlorine activation in the Arctic winters 1991-2003 derived with the tracer-tracer correlations, *Atmos. Chem. Phys.*, *4*, 2181–2213. *[cited on page 40.]*

Tilmes, S., D. E. Kinnison, R. R. Garcia, R. Salawitch, T. Canty, J. Lee-Taylor, S. Madronich, and K. Chance (2012), Impact of very short-lived halogens on stratospheric ozone abundance and UV radiation in a geo-engineered atmosphere, *Atmos. Chem. Phys.*, *12*(22), 10,945–10,955, doi:10.5194/acp-12-10945-2012. *[cited on page 46.]*

Toon, O. B., P. Hamill, R. P. Turco, and J. Pinto (1986), Condensation of HNO3 and HCl in the Winter Polar Stratospheres, *Geophys. Res. Lett.*, *13*(12, Suppl. S), 1284–1287, doi:10.1029/GL013i012p01284. *[cited on page 25.]*

Toon, O. B., E. V. Browell, S. Kinne, and J. Jordan (1990), An analysis of lidar observations of polar stratospheric clouds, *Geophys. Res. Lett.*, *17*(4), 393–396, doi:10.1029/GL017i004p00393. *[cited on pages 24 and 25.]*

Tsvetkova, N. D., V. A. Yushkov, A. N. Luk'yanov, V. M. Dorokhov, and H. Nakane (2007), Record-breaking chemical destruction of ozone in the arctic during the winter of 2004/2005, *Izv. Atmos. Ocean Phy.*, *43*(5), 592–598, doi:10.1134/S0001433807050076. *[cited on pages 38, 39 and 68.]*

Tung, K. K., M. K. W. Ko, J. M. Rodriguez, and N. D. Sze (1986), Are Antarctic Ozone Variations a Manifestation of Dynamics or Chemistry, *Nature*, *322*(6082), 811–814. *[cited on page 22.]*

Turco, R. P., R. C. Whitten, and O. B. Toon (1982), Stratospheric aerosols: Observation and theory, *Rev. Geophys.*, *20*(2), 233–279, doi:10.1029/RG020i002p00233. *[cited on page 24.]*

van Dijk, A., et al. (2013), Skin Cancer Risks Avoided by the Montreal Protocol - Worldwide Modeling Integrating Coupled Climate-Chemistry Models with a Risk Model for UV, *Photochem Photobiol*, *89*(1), 234–246, doi:10.1111/j.1751-1097.2012.01223.x. *[cited on pages 2 and 4.]*

Voigt, C., et al. (2000), Nitric Acid Trihydrate (NAT) in Polar Stratospheric Clouds, *Science*, *290*(5497), 1756–1758, doi:10.1126/science.290.5497.1756. *[cited on page 25.]*

von Hobe, M., et al. (2006), Severe ozone depletion in the cold Arctic winter 2004-05, *Geophys. Res. Lett.*, *33*(17), doi:10.1029/2006GL026945. *[cited on pages 38, 40, 68 and 105.]*

Walker, S. J., R. F. Weiss, and P. K. Salameh (2000), Reconstructed histories of the annual mean atmospheric mole fractions for the halocarbons CFC-11 CFC-12, CFC-113, and carbon tetrachloride, *J. Geophys. Res.-Oceans*, *105*(C6), 14,285–14,296, doi:10.1029/1999JC900273. *[cited on page 21.]*

Wegner, T. (2012), Chlorine Activation and Heterogeneous Chemistry in the Polar Stratosphere: Model Simulations, In-Situ- and Satellite Observations, Ph.D. thesis, Bergische Universität Wuppertal. *[cited on page 27.]*

Wegner, T., et al. (2012), Heterogeneous chlorine activation on stratospheric aerosols and clouds in the Arctic polar vortex, *Atmos. Chem. Phys.*, *12*(22), 11,095–11,106, doi:10.5194/acp-12-11095-2012. *[cited on pages 45 and 79.]*

Wennberg, P. O., J. W. Brault, T. F. Hanisco, R. J. Salawitch, and G. H. Mount (1997), The atmospheric column abundance of IO: Implications for stratospheric ozone, *J. Geophys. Res.-Atmos.*, *102*(D7), 8887–8898, doi:10.1029/96JD03712. *[cited on page 20.]*

Wilcoxon, F. (1945), Individual Comparisons by Ranking Methods, *Biometrics Bull*, *1*(6), 80–83, doi:10.2307/3001968. *[cited on page 47.]*

Wilks, D. S. (2006), *Statistical methods in the atmospheric sciences*, *International Geophysics Series*, vol. 91, 2nd ed., Academic Press, San Diego. *[cited on page 47.]*

WMO (1995), *Scientific Assessment of Ozone Depletion: 1994*, Global Ozone Research and Monitoring Project - Report No. 37. *[cited on page 19.]*

WMO (2003), *Scientific Assessment of Ozone Depletion: 2002*, 498 pp. pp., Global Ozone Research and Monitoring Project - Report No. 47, Geneva, Switzerland. *[cited on pages 9 and 13.]*

WMO (2011a), *Scientific Assessment of Ozone Depletion: 2010*, 516 pp. pp., Global Ozone Research and Monitoring Project - Report No. 52, Geneva, Switzerland. *[cited on pages 1, 4, 5, 33, 36, 38, 46, 71 and 73.]*

WMO (2011b), *Twenty Questions and Answers About the Ozone Layer: 2010 Update*, Geneva, Switzerland, 72 pp. pp., Scientific Assessment of Ozone Depletion: 2010. *[cited on page 4.]*

Yung, Y. L., J. P. Pinto, R. T. Watson, and S. P. Sander (1980), Atmospheric Bromine and Ozone Perturbations in the Lower Stratosphere, *J. Atmos. Sci.*, *37*(2), 339–353, doi:10.1175/1520-0469(1980)037⟨0339:ABAOPI⟩2.0.CO;2. *[cited on page 20.]*

Appendix A

Gridding Method

The method described in this appendix is used to transform one day of irregularly spaced MLS data to the $1.9° \times 2.5°$ horizontal WACCM grid.

(1) Read one day of MLS data data screening according to recommendations from [*Livesey*, 2011] considering precision, status, convergence, quality, and pressure range. Also filtering values with errors greater than 100% (error $\equiv 100\% \times \frac{\|\text{precision}\|}{\|\text{value}\|}$)

(2) Logarithmically interpolate from MLS pressure levels to WACCM pressure levels. WACCM data at pressure levels which are not within the recommended MLS pressure range are set to NaN. The spatial interpolation is done for each pressure level separately.

(3) Carry out Delaunay triangulation [*Knuth*, 1992, and references therein] The entire sphere is exhaustively covered with the smallest possible non-overlapping triangles connecting all measurements. In IDL, the Delaunay triangulation is done using the `qhull` procedure.

(4) Interpolate to desired gridpoints For each grid point within a triangle, create a non-orthogonal 2D interpolation based on the triangle corners. Disadvantage: since each grid-point is calculated based on one triangle only, differentiability is not given and smoothing becomes necessary.

(5) Distance weighted smoothing on the "big array"

(a) A "big array" (Figure A.1) is an array combination of spatial geolocations that extends the original spatial geolocations in all directions in order to avoid boundaries during smoothing.

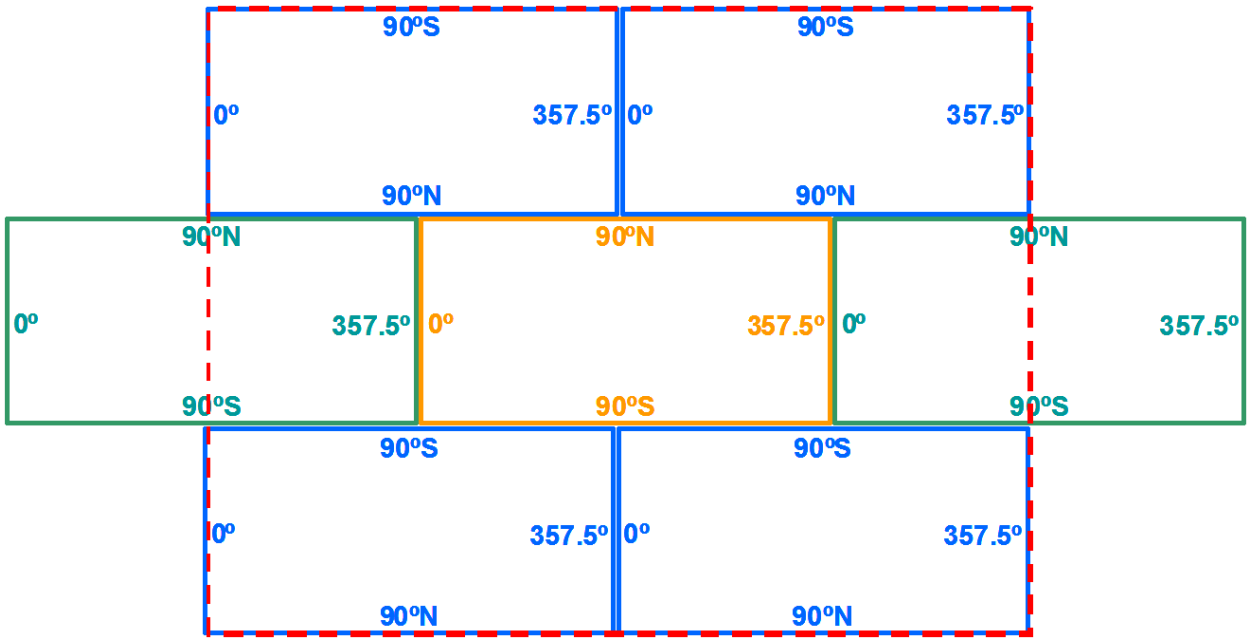

Figure A.1: Array combination in order to eliminate boundaries of the main data field (orange). Since the boundaries of the main data field are cyclic, copies of the main data field are appended in "zonal" direction (green) and in "meridional" direction (blue) including a phase shift of 90°W. For smoothing only the big array (red dashed) is used. After processing, the main array (orange) is extracted as the result.

(b) Create a kernel with the dimensions of 3 latitude gridpoints (which is a constant length) and the equivalent length in longitudes (which is a length depending on latitude).

(c) Fill the entire kernel with distance weights (e.g., inverse quadratic) around the center.

(d) Run convolution (smoothing) on red dashed field in Figure A.1: this removes artifacts created by step 4.

(6) Save center array of the big array (orange field in Figure A.1) as the result.

Appendix B

Initialization Method

This appendix describes how the climatological initialization from WACCM is updated with observations as described by *Brakebusch et al.* [2013].

(1) Choose date for initialization. For polar O_3 loss investigations, the ideal initialization date falls before the onset of O_3 loss, but after the polar vortex is developed.

(2) Choose species to initialize. For initialization observations with representative polar cap coverage are necessary. Initialization of species with diurnal variation is very difficult since the observational coverage of one instrument at the time of initialization cannot cover the entire polar cap. So for initialization of diurnally varying species, several instruments need to be combined.

(3) Check availability of observations (global coverage within the day of initialization), find/create initial condition model file from previous climatological run for subsequent initialization update.

(4) Use gridding method to create distribution of profiles on WACCM grid (Appendix A)

(5) For each profile create a linear combination of observations and model: outside the valid vertical range of the observations the linear combination consists of 100% climatological data. Within the valid vertical range, the numbers of levels used for the transition depth from 100% climatological data to 100% observation data back to 100% climatological data

depends on how similar the observations are to the model and how steep gradients are at the transition regions. Figure B.1 shows the SD-WACCM, MLS, and initialization O_3 profile on Dec 1, 2004 as used by *Brakebusch et al.* [2013]. Examples for this step can be found in Table 3.1 in Chapter 3.

(6) Double check profiles if unphysical structure was introduced in the transition regions (e.g., local maxima). If necessary, adjust transition region depths.

(7) In the initial conditions file replace each species with the profiles just created (keep in mind that the climatological initialization files from WACCM contain species in mass mixing ratio and not volume mixing ratio).

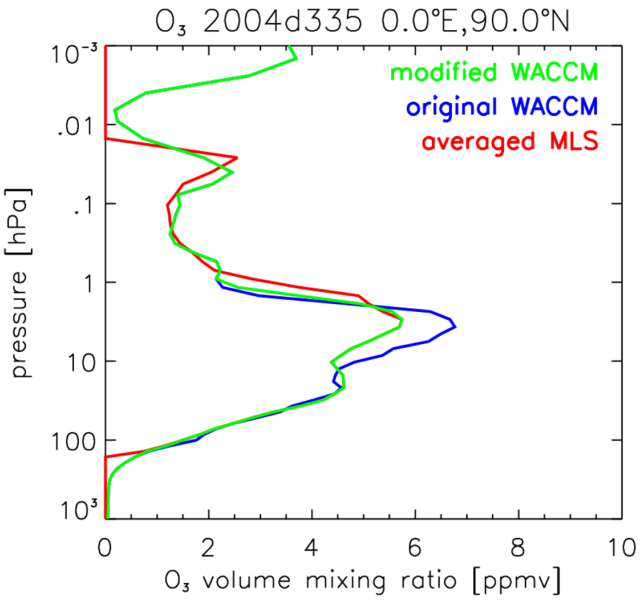

Figure B.1: Example profile (Dec 1, 2004 at 0°E 90°N) during initialization process: the original profile from the climatological WACCM initialization (blue), the observed profile from MLS (red), and the updated initialization profile (green). Here, O_3 is taken from the climatological profile for pressure $\geq$164 hPa, from MLS between 101-2.95 hPa, and from the climatological profile for pressure $\leq$0.91 hPa.

Appendix C

Averaging Method

The method described below can be used to produce a weighted average for, e.g., polar vortex averages. A reason to use this method is that the sampling of instruments and models is not equally spaced, i.e., the distance between individual observations or grid points is not constant. While this is not problematic for model/instrument comparisons, the illustration of an average representation of the real atmosphere requires an area weighting. In such a weighting, many spatially dense values in the area of interest are weighted less since each point individually represents a small area, while spaced-out values are weighted more since each point individually represents a larger area.

Each model or observation point represents an area that can be defined by means of a Voronoi diagram. The Voronoi diagram divides space into a number of regions around points of interest. Any part of an area representing one point of interest is closer to that point than any other point, see Figure C.1. The area of the closed polygons around each point represents the weight for the averaging relative to the whole area.

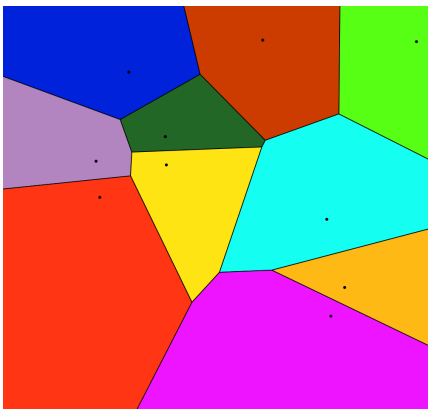

Figure C.1: Map of points and their Voronoi cells.[1]

When the appropriate averaging of a regular gridded model output (e.g., the standard $1.9° \times 2.5°$ WACCM grid) is of concern, a possible simplification is the multiplication of each grid point with the cosine of its latitude since the meridional distance between each grid point is constant.

[1] From http://commons.wikimedia.org/wiki/File:Voronoi_diagram_%2810_sites%29.svg, retrieved on 2013/06/02.

Appendix D

Satellite History File

When instrument and model data are compared, it is important to have a comparable sampling for both. While it is obvious for the spatial sampling that model output must occur near an observation, the temporal sampling is equally important, especially for diurnally varying species. For instance, MLS ClO observations in the NH polar region occur between 3 am and 1 pm local time (see Figure D.1) and thus no observations of this strongly varying species are made during afternoon and evening. Neither instantaneous nor daily averaged model output is suited for comparison to such a diurnally varying species.

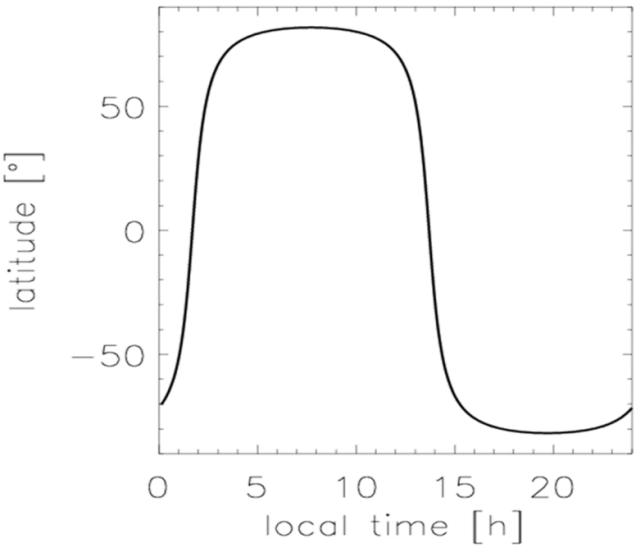

Figure D.1: Latitudes observed by MLS for each local time.

In order to address this issue, a new sampling of model output was developed for CESM, where CESM outputs vertical profiles of predefined species closest to prescribed locations and times (i.e., at latitude/longitude/time triples also called geolocations) into new model instrument

sampling output files. The resulting sampling error is less or equal to half the model grid size and half the model time step. This form of sampled output comes at no significant increase in computation time since the entire global field of each species is simulated at each time step anyway.

The list of geolocations provided to CESM is called satellite history file. This file contains one-dimensional variables of at least latitude, longitude, and time from the observations of interest. Any additional variable in the satellite history file, e.g., Julian day or SZA, is not considered for model sampling but carried over into the sampled output files.

Appendix E

Workflow

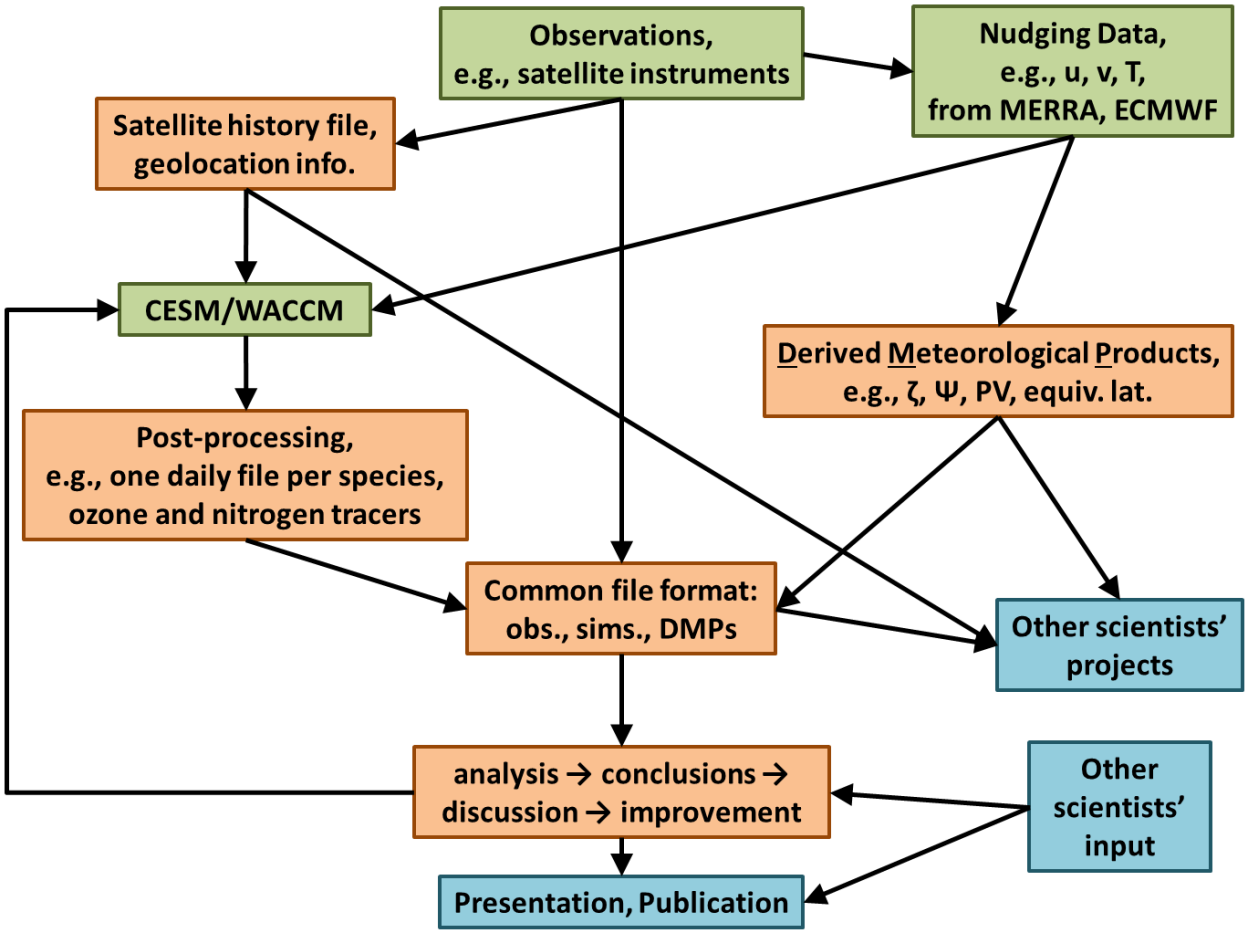

Figure E.1: Workflow diagram for the work presented in Chapter 3, Chapter 4, and Chapter 5. Green boxes depict parts of the workflow that are provided by the scientific community, orange boxes describe components of the workflow, and blue boxes indicate connections to the scientific community.

List of Acronyms

ACE-FTS	Atmospheric Chemistry Experiment Fourier Transform Spectrometer
BDC	Brewer Dobson circulation
CALIPSO	Cloud-Aerosol Lidar and Infrared Pathfinder Satellite Observation
CAM	Community Atmosphere Model
CARMA	Community Aerosol and Radiation Model for Atmospheres
CCM	chemistry climate model
CCMI	Chemistry-Climate Model Initiative
CCMVal	Chemistry-Climate Model Validation
CESM	Community Earth System Model
CTM	chemical transport model
DNA	deoxyribonucleic acid
DU	Dobson Units
EOS	Earth Observing System

EP	energetic particle
EPP	energetic particle precipitation
ESM	Earth System Model
ESMVal	Earth System Model Validation
GEOS5	Goddard Earth Observing System 5
GHG	greenhouse gas
GW	gravity wave
IL	inferred loss
IPCC	Intergovernmental Panel on Climate Change
MEE	medium energy electron
MERRA	Modern-Era Retrospective analysis for Research and Applications
MIPAS	Michelson Interferometer for Passive Atmospheric Sounding
ML	modeled loss
MLS	Microwave Limb Sounder
MOZART	Model for OZone And Related chemical Tracers
NASA	National Aeronautics and Space Administration
NCAR	National Center for Atmospheric Research
NH	northern hemisphere
NIR	near infrared

PNJ	polar night jet
PSC	polar stratospheric cloud
PV	potential vorticity
PW	planetary wave
SAD	surface area density
SD-WACCM	Specified Dynamics Whole Atmosphere Community Climate Model
SH	southern hemisphere
SLIMCAT	SLIMCAT 3-D chemical transport model
SP	solar proton
SPARC	Stratospheric Processes And Their Role in Climate
SPE	solar proton event
sPV	scaled potential vorticity
SSA	stratospheric sulfate aerosol
SSW	sudden stratospheric warming
STS	supercooled ternary solution
SZA	solar zenith angle
temperature	temperature (T)
TIME-GCM	Thermosphere-Ionosphere-Mesosphere Electrodynamics General Circulation Model
UV	ultra violet

VIS	visible
VMR	volume mixing ratio
VSL	very short-lived
WACCM	Whole Atmosphere Community Climate Model
WMO	World Meteorological Organization

List of Chemical Species

Br	bromine
BrCl	bromine chloride
BrO	bromine monoxide
$BrONO_2$	bromine nirate
BrO_X	reactive bromine
Br_Y	inorganic bromine
CFC	chlorofluorocarbon
CH_3Br	methyl bromide
CH_3Cl	methyl chloride
CH_4	methane
Cl	chlorine
Cl_2	molecular chlorine
ClO	chlorine monoxide
$ClONO_2$	chlorine nirate
ClOOCl	hypochlorite dimer (also Cl_2O_2)
ClOOCl	hypochlorite dimer (also Cl_2O_2)
ClO_X	total reactive chlorine
Cl_Y	inorganic chlorine
CO	carbon monoxide

CO_2	carbon dioxide
COS	carbonyl sulfide
F	fluorine
H	atomic hydrogen
H_2O	water vapor
HBr	hydrogen bromide
HCl	hydrogen chloride
HF	hydrogen fluoride
HNO_3	nitric acid
HNO_4	peroxynitric acid
HO_2	peroxyl radical
OH	hydroxyl radical
HO_2NO_2	peroxinitric acid
HOBr	hypobromous acid
HOCl	hypochlorous acid
HO_X	odd hydrogen
HSO_3^-	hydrogen sulfite ion
I	iodine
N_2	molecular nitrogen
N_2O	nitrous oxide
N_2O_5	nitrogen pentoxide
NAT	nitric acid trihydrate
NO	nitrogen oxide

NO_2	nitrogen dioxide
NO_3	nitrate radical
NO_X	nitrogen oxide, {NO+NO_2}
NO_Y	total reactive odd nitrogen {N + NO + NO_2 + NO_3 + $2N_2O_5$ + HO_2NO_2 + HNO_3 + $ClONO_2$}
O	atomic oxygen
$O(^1D)$	singlet D oxygen
O_2	molecular oxygen
O_3	ozone
O_3TRAC	ozone tracer
OClO	chlorine dioxide
O_X	odd oxygen, {O+O_3}
ppO_3	pseudo-passive ozone
H_2SO_4	sulfuric acid
S	sulfur
SO	sulfur monoxide
sulfate	sulfate ion, SO_4^{2-}